INTERNATIONAL ATOMIC ENERGY AGENCY
UNITED NATIONS EDUCATIONAL, SCIENTIFIC AND CULTURAL ORGANIZATION
INTERNATIONAL CENTRE FOR THEORETICAL PHYSICS
I.C.T.P., P.O. BOX 586, 34100 TRIESTE, ITALY, CABLE: CENTRATOM TRIESTE

H4.SMR/709-8

Second Workshop on Non-Linear Dynamics
and Earthquake Prediction

22 November - 10 December 1993

Magnetic Field Generation due to the Helical Flow of an Electrically Conducting Fluid

A. Soloviev
Russian Academy of Sciences
International Institute of Earthquake Prediction
Theory and Mathematical Geophysics
Moscow 113556
Russian Federation

MAGNETIC FIELD GENERATION DUE TO THE HELICAL FLOW OF AN ELECTRICALLY CONDUCTING FLUID

A.A.Soloviev

INTRODUCTION

The idea about the possibility of magnetic field generation due to movement of an electrically conducting medium belongs to Larmor (1919) and was used for the explanation of the Sun magnetic field existence.

Magnetic field generation due to movement of an electrically conducting medium (magnetic dynamo) is considered now as the basic mechanism of origin and existence of the magnetic fields of the Earth, the Sun, planets, stars, and other space objects. The reviews of the results of the numerous investigations in this field can be found for example in Roberts (1972), Moffatt (1978, 1983), Parker (1979), Krause and Rädler (1980), Busse (1981, 1983), Cowling (1981), Benton (1983), Gubbins (1984), and Childress (1985).

The first examples of magnetic dynamo were suggested by Parker (1955, 1957), Bullard and Gellman (1954), Backus (1958), Herzenberg (1958), and Rikitake (1958). In these investigations for the specified velocity fields of an electrically conducting medium the existence of magnetic dynamo was proved. The action of the magnetic field on the medium movement was not considered and such models are called kinematic dynamo.

The velocity field $\mathbf{V}$ of the moving medium is connected with the medium density ρ by the equation of conservation of mass

$$\frac{\partial \rho}{\partial t} + \mathbf{div}(\rho \mathbf{V}) = 0 \ . \qquad (1)$$

If the movement occurs inside of the some region then on the region boundary surface the following condition has to be valid

$$\mathbf{Vn} = 0 \ . \qquad (2)$$

Here the vector $\mathbf{n}$ is normal to the boundary surface. If the velocity field $\mathbf{V}$ and the density field ρ satisfy to equation (1) and the boundary condition (2) then the field $(\mathbf{V}, \rho)$ is called kinematically feasible. The field $(\mathbf{V}, \rho)$ is dynamically feasible if it also satisfies to the equations which describe the medium motion, for example the Navier-Stokes equation. As a rule in the known models of the magnetic dynamo the medium motion is kinematically feasible. But dynamical feasibility of the motion is not usual. Thus the investigation of dynamically feasible flows of an electrically conducting fluid as the cause of the magnetic field generation has a certain interest.

The Couette-Poiseuille flow (Joseph, 1976) is an example of a such flow. It is a fluid motion between two coaxial cylinders of infinite length. The flow satisfies to the Navier-Stokes equation and the proper boundary conditions. The magnetic dynamo problem for this flow is formulated and investigated below. The motion of an electrically conducting fluid between two cylinders was early considered (for example see Bathaiah and Venugopal, 1982, Busse, 1982, Tabeling, 1982, Childress, 1983, Chowdhury, 1983, and Sai, 1985). But in these investigations either the flow was not the Couette-Poiseuille flow or the magnetic dynamo problem was not considered.

Evolution of the magnetic field in the moving medium is described by the magnetic induction equation (Moffatt, 1978)

$$\frac{\partial \mathbf{H}}{\partial t} = \mathbf{rot}(\mathbf{V} \times \mathbf{H}) + \lambda \nabla^2 \mathbf{H} \ . \qquad (3)$$

Here $\mathbf{H}$ is a vector of the magnetic field, $\mathbf{V}$ is a vector of the

medium velocity; λ is the magnetic diffusivity of the medium the value of which is connected with the value of the electrical conductivity σ of the medium by the formula $\lambda = (\mu_0\sigma)^{-1}$ where the value of the constant μ_0 depends on the selected system of units (in SI $\mu_0 = 4\pi 10^{-7}$ Wb/A·m); by definition $\nabla^2\mathbf{H} = -\,\mathrm{rot}(\mathrm{rot}\mathbf{H})$.

Accordingly to the Maxwell's equations

$$\mathrm{div}\mathbf{H} = 0 \,, \tag{4}$$

that means the absence of isolated magnetic poles.

The electrically conducting fluid is supposed to be incompressible. Thus it has the constant density ρ and equation (1) has for it the following view

$$\mathrm{div}\mathbf{V} = 0 \,. \tag{5}$$

In the kinematic formulation of the magnetic dynamo problem the action of the magnetic field on the fluid velocity field is not considered and equations (3) and (4) are the equations for the vector-function $\mathbf{H}$ with the known vector-function $\mathbf{V}$.

The existence of the magnetic dynamo means that there are the initial magnetic field $\mathbf{H}_0$ and the values of the flow parameters for which the magnitude of the vector-function $\mathbf{H}$ which satisfies to equations (3) and (4) increases infinitely when $t \to \infty$.

The boundary conditions have to be formulated for the system of equations (3), (4). The following two cases are examined below: perfectly conducting boundaries and dielectric boundaries.

As the vector-function $\mathbf{V}$ has the axial symmetry the cylindrical coordinates r, φ, z with the z axis being the common axis of the cylinders are convenient to use. The system of equations (3), (4) is linear relatively to the vector-function $\mathbf{H}$. Therefore a harmonic $\mathcal{H}(r)\exp(in\varphi + i\alpha z)$ in the expansion of the initial magnetic field $\mathbf{H}_0$

can be examined. Here n is an integer and α a real number. The substitution of a single harmonic in equations (3) and (4) reduces the magnetic dynamo problem to the eigenvalue problem for the system of the two ordinary equations with the uniform boundary conditions. The magnetic field is generated if there exists an eigenvalue with a positive real part for this boundary problem. The magnetic dynamo problem for a spiral velocity field was investigated early by the same way (for example see Ponomarenko, 1973).

The magnetic dynamo problem for the Couette-Poiseuille flow of the electrically conducting fluid was analyzed numerically and by the asymptotic method developed by Ruzmaikin et al. (1987). The results of the both approaches are in good agreement. The main result lies in the evidence of the magnetic field generation by the Couette-Poiseuille flow of the electrically conducting fluid.

BASIC EQUATIONS

The magnetic induction equation (3) has the following view in the cylindrical coordinate system defined above

$$\begin{aligned}
\frac{\partial H_r}{\partial t} &= \frac{V_r}{r}\frac{\partial H_\varphi}{\partial \varphi} + \frac{H_\varphi}{r}\frac{\partial V_r}{\partial \varphi} - \frac{V_\varphi}{r}\frac{\partial H_r}{\partial \varphi} - \frac{H_r}{r}\frac{\partial V_\varphi}{\partial \varphi} + V_r\frac{\partial H_z}{\partial z} + \\
&+ H_z\frac{\partial V_r}{\partial z} - V_z\frac{\partial H_r}{\partial z} - H_r\frac{\partial V_z}{\partial z} + \\
&+ \lambda\left(\frac{\partial^2 H_r}{\partial z^2} + \frac{1}{r^2}\frac{\partial^2 H_r}{\partial \varphi^2} - \frac{\partial^2 H_z}{\partial r \partial z} - \frac{1}{r}\frac{\partial^2 H_\varphi}{\partial r \partial \varphi} - \frac{1}{r^2}\frac{\partial H_\varphi}{\partial \varphi}\right), \\
\frac{\partial H_\varphi}{\partial t} &= V_\varphi\left(\frac{\partial H_r}{\partial r} + \frac{\partial H_z}{\partial z}\right) - V_r\frac{\partial H_\varphi}{\partial r} - H_\varphi\frac{\partial V_r}{\partial r} + H_r\frac{\partial V_\varphi}{\partial r} + H_z\frac{\partial V_\varphi}{\partial z} - \\
&- V_z\frac{\partial H_\varphi}{\partial z} - H_\varphi\frac{\partial V_z}{\partial z} + \lambda\left(\frac{\partial^2 H_\varphi}{\partial r^2} + \frac{\partial^2 H_\varphi}{\partial z^2} - \frac{1}{r}\frac{\partial^2 H_r}{\partial r \partial \varphi} - \right.
\end{aligned} \tag{6}$$

$$- \frac{1}{r}\frac{\partial^2 H_z}{\partial\varphi\,\partial z} + \frac{1}{r}\frac{\partial H_\varphi}{\partial r} + \frac{1}{r^2}\frac{\partial H_r}{\partial\varphi} - \frac{H_\varphi}{r^2}\Bigg),$$

$$\frac{\partial H_z}{\partial t} = V_z\left(\frac{1}{r}\frac{\partial H_\varphi}{\partial\varphi} + \frac{\partial H_r}{\partial r} + \frac{H_r}{r}\right) - \frac{V_\varphi}{r}\frac{\partial H_z}{\partial\varphi} + \frac{H_\varphi}{r}\frac{\partial V_z}{\partial\varphi} -$$

$$- \frac{H_z}{r}\frac{\partial V_\varphi}{\partial\varphi} - V_r\frac{\partial H_z}{\partial r} - H_z\frac{\partial V_r}{\partial r} + H_r\frac{\partial V_z}{\partial r} - \frac{V_r H_z}{r} +$$

$$+ \lambda\left(\frac{\partial^2 H_z}{\partial r^2} + \frac{1}{r^2}\frac{\partial^2 H_z}{\partial\varphi^2} - \frac{\partial^2 H_r}{\partial r\,\partial z} - \frac{1}{r}\frac{\partial^2 H_\varphi}{\partial\varphi\,\partial z} + \frac{1}{r}\frac{\partial H_z}{\partial r} - \frac{1}{r}\frac{\partial H_r}{\partial z}\right).$$

Here H_r, H_φ, H_z and V_r, V_φ, V_z are the components in the cylindrical coordinate system of the vector-functions **H** and **V** respectively.

Equation (4) has in the cylindrical coordinate system the following view

$$\frac{H_r}{r} + \frac{\partial H_r}{\partial r} + \frac{1}{r}\frac{\partial H_\varphi}{\partial\varphi} + \frac{\partial H_z}{\partial z} = 0 . \qquad (7)$$

If the vector-function **H** satisfies to the induction equation (3) then

$$\frac{\partial}{\partial t}\mathbf{div}\mathbf{H} = \mathbf{div}\left(\frac{\partial \mathbf{H}}{\partial t}\right) = \mathbf{div}\left[\mathbf{rot}(\mathbf{V}\times\mathbf{H} - \lambda\,\mathbf{rot}\mathbf{H})\right] = 0 .$$

Thus if for the initial magnetic field $\mathbf{div}\mathbf{H}_0 = 0$ then the vector-function **H** which is the decision of equation (3) satisfies to the condition $\mathbf{div}\mathbf{H} = 0$. It means that four equations (6) and (7) are not independent and one of them can be ignored.

The Couette-Poiseuille flow is a helical flow with an axial symmetry (Joseph, 1976) and the components of the vector **V** of its velocity field have the following view

$$V_r = 0 , \quad V_\varphi(r,\varphi,z) = V_\varphi(r) , \quad V_z(r,\varphi,z) = V_z(r) . \qquad (8)$$

By using formulas (8) and equation (7) the first two equations of

(6) can be transformed to the form

$$\frac{\partial H_r}{\partial t} = -\frac{V_\varphi}{r}\frac{\partial H_r}{\partial\varphi} - V_z\frac{\partial H_r}{\partial z} + \lambda\left(\frac{\partial^2 H_r}{\partial r^2} + \frac{1}{r^2}\frac{\partial^2 H_r}{\partial\varphi^2} + \right.$$

$$\left. + \frac{\partial^2 H_r}{\partial z^2} - \frac{H_r}{r^2} + \frac{1}{r}\frac{\partial H_r}{\partial r} - \frac{2}{r^2}\frac{\partial H_\varphi}{\partial\varphi}\right),$$

$$\frac{\partial H_\varphi}{\partial t} = \left(\frac{\partial V_\varphi}{\partial r} - \frac{V_\varphi}{r}\right)H_r - \frac{V_\varphi}{r}\frac{\partial H_\varphi}{\partial\varphi} - V_z\frac{\partial H_\varphi}{\partial z} + \lambda\left(\frac{\partial^2 H_\varphi}{\partial r^2} + \right. \qquad (9)$$

$$\left. + \frac{1}{r^2}\frac{\partial^2 H_\varphi}{\partial\varphi^2} + \frac{\partial^2 H_\varphi}{\partial z^2} - \frac{H_\varphi}{r^2} + \frac{1}{r}\frac{\partial H_\varphi}{\partial r} + \frac{2}{r^2}\frac{\partial H_r}{\partial\varphi}\right).$$

Note that equations (9) contain the two unknown functions H_r and H_φ. If for these equations the boundary conditions which do not depend on the function H_z can be formulated then the functions H_r and H_φ can be obtained from them. Then the function H_z can be obtained from equation (7) or from the third equation of (6).

The Couette-Poiseuille flow results from the rotation of the cylinders around their common axis, the motion of the inner cylinder along this axis, and a constant pressure gradient along this axis.

Denote the radii of the inner and outer cylinders by a and b ($a < b$), their angular velocities by Ω_1 and Ω_2, the axial velocity of the inner cylinder by U_c.

The components of the velocity field for the Couette-Poiseuille flow are defined by the formulas (Joseph, 1976)

$$V_\varphi(r) = \frac{b^2\Omega_2 - a^2\Omega_1}{b^2 - a^2}\,r - \frac{a^2 b^2(\Omega_2 - \Omega_1)}{r(b^2 - a^2)} ,$$

$$V_z(r) = V_z^c(r) + V_z^p(r) , \qquad (10)$$

$$V_z^c(r) = U_c \frac{\ln\frac{r}{b}}{\ln\eta} ,$$

$$V_z^p(r) = U_p \frac{\left[1 - \left(\frac{r}{b}\right)^2\right]\ln\eta^2 + (\eta^2 - 1)\ln\left(\frac{r}{b}\right)^2}{d(\eta)} .$$

Here

$$\eta = \frac{a}{b} \quad , \quad d(\eta) = \ln\eta^2 + (\eta^2 - 1)\left[-1 + \ln\left(\frac{\eta^2-1}{\ln\eta^2}\right)\right] . \tag{11}$$

$V_z^c(r)$ results from the axial motion of the inner cylinder and $V_z^p(r)$ is due to the pressure gradient. U_p is the maximum modulus of $V_z^p(r)$. This value is attained at $r = b\sqrt{\frac{\eta^2 - 1}{\ln\eta^2}}$ and can be calculated by the formula

$$U_p = -\frac{b^2}{4\ln\eta^2}\frac{d(\eta)\,P}{\nu}$$

where P is the magnitude of the pressure gradient and ν is the kinematical viscosity of the fluid.

Let b be the typical length and b^2/λ the typical time.

Introduce the magnetic Reynolds number

$$R_m = \frac{U_m b(1 - \eta)}{\lambda} \tag{12}$$

where $U_m = \sqrt{a^2(\Omega_1 - \Omega_2)^2 + U_c^2 + U_p^2}$ is the typical value of the fluid velocity.

Consider a harmonic $\mathcal{H}(r)\exp(in\varphi + i\alpha z)$ in the expansion of the initial magnetic field distribution. It was shown by Zeldovich (1956) and Braginsky (1964) that the harmonic can be excited only if $n \neq 0$ and $\alpha \neq 0$. Thus it will be supposed below that $n \neq 0$ and $\alpha \neq 0$.

After substitution

$$H_r = \mathcal{H}_r(r)\exp(in\varphi + i\alpha z + pt), \quad H_\varphi = \mathcal{H}_\varphi(r)\exp(in\varphi + i\alpha z + pt) \tag{13}$$

where p is a complex number and formulas (10) for the components of the velocity field in equations (9) these equations are transformed to the following form

$$\frac{d^2\mathcal{H}_r}{dr^2} + \frac{1}{r}\frac{d\mathcal{H}_r}{dr} - \left(\frac{1}{r^2} + Q(r) + p\right)\mathcal{H}_r - \frac{2in}{r^2}\mathcal{H}_\varphi = 0 ,$$

$$\frac{d^2\mathcal{H}_\varphi}{dr^2} + \frac{1}{r}\frac{d\mathcal{H}_\varphi}{dr} - \left(\frac{1}{r^2} + Q(r) + p\right)\mathcal{H}_\varphi + \left(\frac{2in}{r^2} - \frac{2R_m B}{r^2}\right)\mathcal{H}_r = 0 . \tag{14}$$

Here

$$Q(r) = \frac{n^2}{r^2} + \alpha^2 + iR_m q(r) ,$$

$$q(r) = n\left[\frac{b\Omega_2}{(1 - \eta)U_m} - B + \frac{B}{r^2}\right] + \frac{\alpha}{(1 - \eta)\sqrt{1 + \kappa^2}\sqrt{U_c^2 + U_p^2}}\left[U_c\frac{\ln r}{\ln\eta} + U_p\frac{(1 - r^2)\ln\eta^2 + (\eta^2 - 1)\ln r^2}{d(\eta)}\right] , \tag{15}$$

$$B = \frac{\eta\kappa}{(1 - \eta^2)(1 - \eta)\sqrt{1 + \kappa^2}} , \quad \kappa = \frac{a(\Omega_1 - \Omega_2)}{\sqrt{U_c^2 + U_p^2}} .$$

Accordingly to the normalization accepted the independent variables r and t in formulas (13), (15) and equations (14) are measured in units of b and b^2/λ respectively.

The component $\mathcal{H}_z(r)$ of the vector-function $\mathcal{H}(r)$ can be obtained from equation (7)

$$\mathcal{H}_z(r) = \frac{i}{\alpha r}\mathcal{H}_r(r) + \frac{i}{\alpha}\frac{d\mathcal{H}_r}{dr} - \frac{n}{\alpha r}\mathcal{H}_\varphi(r) . \tag{16}$$

BOUNDARY CONDITIONS

The system of equations (15) is considered over the interval $[\eta, 1]$. Boundary conditions for (15) depend on the electrical properties of the cylinders. Two cases will be examined below:

1) the material of the cylinders is a perfect conductor;

2) the material of the cylinders is a dielectric.

Let the material of the cylinders be a perfect conductor. Inside and on a surface of a perfect conductor

$$\mathbf{H} = 0, \quad \mathbf{E} = 0 \tag{17}$$

where $\mathbf{E}$ is a vector of an electric field. A magnetic field vector component which is normal to a boundary surface is continuous when crossing the boundary. Therefore on the boundaries

$$\mathbf{H}_r|_{r=\eta} = \mathbf{H}_r|_{r=1} = 0 . \tag{18}$$

It follows from the Maxwell's equations and conditions (17) that the vector-function $\mathbf{rot H}$ is proportional to the vector-function $\mathbf{J}$ of a current density. For a moving electrically conducting fluid with the velocity field $\mathbf{V}$ the vector function $\mathbf{J}$ is proportional to the vector-function $\mathbf{E} + \mathbf{V} \times \mathbf{H}$. Because of the adhesion condition on the boundary the vector-function $\mathbf{V}$ lies in the plane which is tangent to the boundary surface and it follows from conditions (17), (18) that on the boundary the proportional vector-functions $\mathbf{E} + \mathbf{V} \times \mathbf{H}$ and $\mathbf{rotH}$ are normal to the boundary surface. Thus

$$\begin{aligned} (\mathrm{rot}\ \mathbf{H})_\varphi|_{r=\eta} &= (\mathrm{rot}\ \mathbf{H})_\varphi|_{r=1} = 0 , \\ (\mathrm{rot}\ \mathbf{H})_z|_{r=\eta} &= (\mathrm{rot}\ \mathbf{H})_z|_{r=1} = 0 . \end{aligned} \tag{19}$$

For the harmonic under consideration condition (18) has the following form

$$\mathcal{H}_r(\eta) = \mathcal{H}_r(1) = 0 . \tag{20}$$

By using (20) conditions (19) for the harmonic under consideration are transformed to the form

$$\left.\frac{d\mathcal{H}_z}{dr}\right|_{r=\eta} = \left.\frac{d\mathcal{H}_z}{dr}\right|_{r=1} = 0 , \tag{21}$$

$$\left.\left(\frac{\mathcal{H}_\varphi}{r} + \frac{d\mathcal{H}_\varphi}{dr}\right)\right|_{r=\eta} = \left.\left(\frac{\mathcal{H}_\varphi}{r} + \frac{d\mathcal{H}_\varphi}{dr}\right)\right|_{r=1} = 0 . \tag{22}$$

It follows from equation (16) that

$$\frac{d\mathcal{H}_z}{dr} = \frac{i}{\alpha}\left(\frac{d^2\mathcal{H}_r}{dr^2} + \frac{1}{r}\frac{d\mathcal{H}_r}{dr} - \frac{2in}{r^2}\mathcal{H}_\varphi\right) - \frac{n}{\alpha r}\left(\frac{d\mathcal{H}_\varphi}{dr} + \frac{\mathcal{H}_\varphi}{r}\right) - \frac{i}{\alpha r^2}\mathcal{H}_r .$$

This relationship shows that conditions (21) follow from the second equation of (14) and conditions (20), (22). Thus for the harmonic under consideration the boundary conditions (18), (19) are equivalent to the boundary conditions (20), (22).

Conditions (22) can be simplified by the following transformation

$$R(r) = r\mathcal{H}_r(r) , \quad \Phi(r) = r\mathcal{H}_\varphi(r) . \tag{23}$$

The system of equations (14) and the boundary conditions (20), (22) are transformed for the functions $R(r)$ and $\Phi(r)$ into the system of equations

$$\begin{aligned} &\frac{d^2R}{dr^2} - \frac{1}{r}\frac{dR}{dr} - (Q(r) + p)R - \frac{2in}{r^2}\Phi = 0 , \\ &\frac{d^2\Phi}{dr^2} - \frac{1}{r}\frac{d\Phi}{dr} - (Q(r) + p)\Phi + \left(\frac{2in}{r^2} - \frac{2R_m B}{r^2}\right)R = 0 . \end{aligned} \tag{24}$$

with the boundary conditions

$$R(\eta) = R(1) = 0 , \quad \left.\frac{d\Phi}{dr}\right|_{r=\eta} = \left.\frac{d\Phi}{dr}\right|_{r=1} = 0 . \qquad (25)$$

Thus, if the material of the cylinders is a perfect conductor then the harmonic under consideration is excited (the magnetic dynamo exists) if there exists an eigenvalue p with a positive real part for the system of equations (24) over the interval $[\eta, 1]$ with the homogeneous boundary conditions (25).

Let the material of the cylinders be a dielectric. Inside a dielectric currents are absent and the vector-function **rot H** which is proportional to the vector-function **J** of a current density equals zero. It means that in the regions where $r < \eta$ or $r > 1$ the vector-function **H** has to satisfy to the system of equations

$$\mathbf{rot\ H} = 0 , \quad \mathbf{div\ H} = 0 . \qquad (26)$$

It follows from the first equation (26) that

$$H_r = \frac{\partial F}{\partial r} , \quad H_\varphi = \frac{1}{r}\frac{\partial F}{\partial \varphi} , \quad H_z = \frac{\partial F}{\partial z} \qquad (27)$$

where $F(r,\varphi,z)$ is a scalar function. For the harmonic under consideration this function has the form

$$F(r,\varphi,z) = \Psi(r)\ \exp(in\varphi + i\alpha z + ipt).$$

Accordingly to the second equation of (26) and formulas (27) the function $\Psi(r)$ has to satisfy to the equation

$$\frac{d^2\Psi}{dr^2} + \frac{1}{r}\frac{d\Psi}{dr} - \left(\frac{n^2}{r^2} + \alpha^2\right)\Psi = 0 . \qquad (28)$$

The equation (28) has a solution $Z_n(i|\alpha|r)$ where $Z_n(w)$ is the circular cylindrical function of order n with the complex argument w (Korn,G. and T.Korn 1961). The general solution of equation (28) can be represented as a linear combination of two linearly independent circular cylindrical function of order n with the complex argument $i|\alpha|r$. The Bessel function of order n $J_n(i|\alpha|r)$ and

the first kind Hankel function of order n $H_n^{(1)}(i|\alpha|r)$ can be used as the such functions. In this case the general solution of equation (28) has the following form

$$\Psi(r) = K_1 J_n(i|\alpha|r) + K_2 H_n^{(1)}(i|\alpha|r) \qquad (29)$$

where K_1 and K_2 are arbitrary constants.

In the region where $r > 1$ the solution of equation (28) has to be finite when $r \to \infty$. It follows from the asymptotic representations for $|w| \to \infty$

$$J_n(w) \approx \frac{1}{\sqrt{2\pi w}}\left[\exp\left[i\left(w - \frac{n\pi}{2} - \frac{\pi}{4}\right)\right] + \exp\left[-i\left(w - \frac{n\pi}{2} - \frac{\pi}{4}\right)\right]\right] ,$$

$$H_n^{(1)}(w) \approx \sqrt{\frac{2}{\pi w}}\ \exp\left[i\left(w - \frac{n\pi}{2} - \frac{\pi}{4}\right)\right]$$

(Korn,G. and T.Korn, 1961) that the condition $K_1 = 0$ is the necessary and sufficient condition for the function $\Psi(r)$ (29) to be finite for $r \to \infty$. Thus in the region where $r > 1$

$$\Psi(r) = K_2 H_n^{(1)}(i|\alpha|r) . \qquad (30)$$

In the region where $r < \eta$ the solution of equation (28) has to be finite for $r \to 0$. It follows from the formulas

$$J_n(w) = \left(\frac{w}{2}\right)^n \sum_{k=0}^{\infty} \frac{(-1)^k}{k!\,(n+k)!}\left(\frac{w}{2}\right)^{2k} ,$$

$$H_n^{(1)}(w) = J_n(w)\left[1 + \frac{2i}{\pi}\left(\ln\frac{w}{2} + C\right)\right] - \frac{i}{\pi}\left[\left(\frac{w}{2}\right)^n \frac{1}{n!} + \right.$$

$$+ \left(\frac{w}{2}\right)^n \sum_{k=1}^{\infty} \frac{(-1)^k}{k!\,(n+k)!}\left(\frac{w}{2}\right)^{2k}\left(\sum_{j=1}^{k}\frac{1}{j} + \sum_{j=1}^{n+k}\frac{1}{j}\right) +$$

$$\left. + \left(\frac{w}{2}\right)^{-n} \sum_{k=0}^{n-1} \frac{(n-k-1)!}{k!}\left(\frac{w}{2}\right)^{2k}\right]$$

where $C = 0{,}57721566...$ is the Euler number (Korn,G. and T.Korn,

1961) that the condition $K_2 = 0$ is the necessary and sufficient condition for the function $\Psi(r)$ (29) to be finite for $r \to 0$. Thus in the region where $r < \eta$

$$\Psi(r) = K_1 J_n(i|\alpha|r) \ . \tag{31}$$

In accordance with formulas (27), (30) and (31) the components of the vector-function $\mathcal{H}(r)$ has to satisfy to the following boundary conditions

$$\begin{aligned} \frac{\mathcal{H}_r(\eta)}{\mathcal{H}_\varphi(\eta)} &= \frac{\eta|\alpha|}{nJ_n(w)} \frac{dJ_n(w)}{dw}\Big|_{w=i|\alpha|\eta} \ , \\ \frac{\mathcal{H}_r(1)}{\mathcal{H}_\varphi(1)} &= \frac{|\alpha|}{nH_n^{(1)}(w)} \frac{dH_n^{(1)}(w)}{dw}\Big|_{w=i|\alpha|} \ , \end{aligned} \tag{32}$$

It follows from formulas (27) that

$$\mathcal{H}_z(\eta) = \frac{\alpha\eta}{n} \mathcal{H}_\varphi(\eta) \ , \quad \mathcal{H}_z(1) = \frac{\alpha}{n} \mathcal{H}_\varphi(1) \ .$$

The last formulas and formula (16) lead to the following boundary conditions

$$\begin{aligned} \frac{1}{r} \mathcal{H}_r(\eta) + \frac{d\mathcal{H}_r}{dr}\Big|_{r=\eta} &= -i\left(\frac{\alpha^2\eta}{n} + \frac{n}{\eta}\right)\mathcal{H}_\varphi(\eta) \ , \\ \mathcal{H}_r(1) + \frac{d\mathcal{H}_r}{dr}\Big|_{r=1} &= -i\left(\frac{\alpha^2}{n} + n\right)\mathcal{H}_\varphi(1) \ . \end{aligned} \tag{33}$$

The boundary conditions (32), (33) for the functions $R(r)$ and $\Phi(r)$ (23) can be represented in the following form

$$\begin{aligned} \Phi(\eta) &= \frac{in}{\eta|\alpha|} Y_1 R(\eta) \ , \quad \Phi(1) = \frac{in}{|\alpha|} Y_2 R(1) \ , \\ \frac{dR}{dr}\Big|_{r=\eta} &= \left(|\alpha| + \frac{n^2}{\eta^2|\alpha|}\right) Y_1 R(\eta) \ , \quad \frac{dR}{dr}\Big|_{r=1} = \left(|\alpha| + \frac{n^2}{|\alpha|}\right) Y_2 R(1) \ . \end{aligned} \tag{34}$$

Here

$$Y_1 = \frac{1}{i} \frac{J_n(w)}{\frac{dJ_n(w)}{dw}}\Big|_{w=i|\alpha|\eta} \ , \quad Y_2 = \frac{1}{i} \frac{H_n^{(1)}(w)}{\frac{dH_n^{(1)}(w)}{dw}}\Big|_{w=i|\alpha|} \ .$$

Thus, if the material of the cylinders is a dielectric then the harmonic under consideration is excited (the magnetic dynamo exists) if there exists an eigenvalue p with a positive real part for the system of equations (24) over the interval $[\eta, 1]$ with the homogeneous boundary conditions (34).

NUMERICAL ANALYSIS

Denote the maximum of all real parts of the eigenvalues p of the boundary problem (24), (25) or of the boundary problem (24), (34) by γ.

The value of γ is estimated by the Galerkin method. When the boundary problem (24), (25) is considered the functions $R(r)$ and $\Phi(r)$ are represented in the form

$$R(r) = \sum_{j=1}^{J} C_{2j} f_{2j}(r) \ , \quad \Phi(r) = \sum_{j=0}^{J} C_{2j+1} f_{2j+1}(r) \tag{35}$$

where

$$\begin{aligned} f_1(r) &= \frac{1}{\sqrt{1-\eta}} \ , \\ f_{2j}(r) &= \sqrt{\frac{2}{1-\eta}} \sin\frac{j(r-\eta)\pi}{1-\eta} \ , \\ f_{2j+1}(r) &= \sqrt{\frac{2}{1-\eta}} \cos\frac{j(r-\eta)\pi}{1-\eta} \ , \quad j \neq 0 \ . \end{aligned} \tag{36}$$

It follows from formulas (36) that the functions $R(r)$ and $\Phi(r)$

(35) satisfy to the boundary conditions (25). Substitute sums (35) in equations (24), multiply the first equation by the functions $f_{2m}(r)$ $(m = 1, 2, \ldots, J)$ and the second equation by the functions $f_{2m+1}(r)$ $(m = 0, 1, \ldots, J)$, and integrate the $2J + 1$ equations obtained over the segment $[\eta, 1]$. As the result the following equations will be obtained

$$\sum_{j=1}^{J} C_{2j}\int_{\eta}^{1}\left[-\left[\left(\frac{\pi j}{1-\eta}\right)^2 + Q(r)\right]f_{2j}(r)f_{2m}(r) - \right.$$

$$\left. - \frac{\pi j f_{2j+1}(r)f_{2m}(r)}{(1-\eta)r}\right]dr - 2in\sum_{j=0}^{J} C_{2j+1}\int_{\eta}^{1}\frac{f_{2j+1}(r)f_{2m}(r)}{r^2}\,dr -$$

$$- p\sum_{j=1}^{J} C_{2j}\int_{\eta}^{1} f_{2j}(r)f_{2m}(r)dr = 0\ ,$$

$$m = 1, 2, \ldots, J\ ,$$

$$\sum_{j=1}^{J} C_{2j+1}\int_{\eta}^{1}\left[-\left(\frac{\pi j}{1-\eta}\right)^2 f_{2j+1}(r)f_{2m+1}(r) + \right.$$

$$\left. + \frac{\pi j f_{2j}(r)f_{2m+1}(r)}{(1-\eta)r}\right]dr - \sum_{j=0}^{J} C_{2j+1}\int_{\eta}^{1} f_{2j+1}(r)f_{2m+1}(r)Q(r)dr + \qquad (37)$$

$$+ (2in - 2R_m B)\sum_{j=1}^{J} C_{2j}\int_{\eta}^{1}\frac{f_{2j}(r)f_{2m+1}(r)}{r^2}\,dr -$$

$$- p\sum_{j=0}^{J} C_{2j+1}\int_{\eta}^{1} f_{2j+1}(r)f_{2m+1}(r)dr = 0\ ,$$

$$m = 0, 1, \ldots, J\ .$$

Equations (37) are the linear algebraic homogeneous system with the unknowns $C_1, C_2, \ldots, C_K$ $(K = 2J + 1)$.

It follows from formulas (36) that

$$\int_{\eta}^{1} f_{2j+1}(r)f_{2j+1}(r)dr = 1\ ,\quad \int_{\eta}^{1} f_{2j}(r)f_{2j}(r)dr = 1\ ,$$

and (38)

$$\int_{\eta}^{1} f_{2j+1}(r)f_{2m+1}(r)dr = 0\ ,\quad \int_{\eta}^{1} f_{2j}(r)f_{2m}(r)dr = 0\ ,$$

if $j \neq m$.

Therefore system (37) can be represented in the form

$$(A - pE)C = 0. \qquad (39)$$

Here A is the matrix of order $K\times K$, E - the unit matrix of the same order, and $C = (C_1, C_2, \ldots, C_K)$ - the vector of the unknowns. System (39) has a nontrivial (nonzero) solution only in the case when p is an eigenvalue of the matrix A. Thus the value of γ is estimated by the maximum γ_K^* of all real parts of the eigenvalues of the matrix A. The estimation is better when the value of J is greater.

When the boundary problem (24), (34) (the material of the cylinders is a dielectric) is considered the transformation of the unknown functions R, $\Phi \rightarrow S$, T is made before the application of the Galerkin method. This transformation has the form

$$S(r) = \exp(-D_1 r^2 - D_2 r)R(r)\ ,$$

$$T(r) = \exp(-D_1 r^2 - D_2 r)\left[\Phi(r) - i\left(E_1 + E_2 r\right)R(r)\right] \qquad (40)$$

where D_1, D_2, E_1, and E_2 are constants.

The inverse transformation has the form

$$R(r) = \exp(D_1 r^2 + D_2 r)S(r)\ ,$$

$$\Phi(r) = \exp(D_1 r^2 + D_2 r)\left[T(r) + i\left(E_1 + E_2 r\right)S(r)\right]\ . \qquad (41)$$

The values of the constants D_1, D_2, E_1, and E_2 in formulas (40) and (41) are selected to have the following simple boundary conditions for the functions $S(r)$ and $T(r)$

$$\frac{dS}{dr}\Big|_{r=\eta} = \frac{dS}{dr}\Big|_{r=1} = 0 , \quad T(\eta) = T(1) = 0 . \tag{42}$$

According to formulas (40) and (41) and the boundary conditions (34) and (42) these values of the constants are calculated by the formulas

$$D_1 = \frac{1}{2(1-\eta)}\left[-\left(|\alpha| + \frac{n^2}{|\alpha|\eta^2}\right)Y_1 + \left(|\alpha| + \frac{n^2}{|\alpha|}\right)Y_2\right] ,$$

$$D_2 = \frac{1}{1-\eta}\left[-\left(|\alpha| + \frac{n^2}{|\alpha|}\right)\eta Y_2 + \left(|\alpha| + \frac{n^2}{|\alpha|\eta^2}\right)Y_1\right] , \tag{43}$$

$$E_1 = \frac{n}{(1-\eta)|\alpha|}\left(\frac{Y_1}{\eta} - \eta Y_2\right) , \quad E_2 = \frac{n}{(1-\eta)|\alpha|}\left(Y_2 - \frac{Y_1}{\eta}\right) .$$

It follows from the general features of the cylindrical functions (Korn,G. and T.Korn, 1961) that Y_1 and Y_2 (see formulas (34)) have to be real numbers. Therefore according to formulas (43) the constants D_1, D_2, E_1, and E_2 are also real numbers.

It follows from formulas (41) that after the transformation of variables the system of equations (24) has the form

$$\frac{d^2S}{dr^2} - \left[\frac{1}{r} - 2\left(2D_1r + D_2\right)\right]\frac{dS}{dr} - \left[Q(r) + p + \frac{D_2}{r} - \right.$$

$$\left. - \left(2D_1r + D_2\right)^2 - \frac{2n}{r^2}\left(E_1 + E_2r\right)\right]S - \frac{2in}{r^2}T = 0 ,$$

$$\frac{d^2T}{dr^2} - \left[\frac{1}{r} - 2\left(2D_1r + D_2\right)\right]\frac{dT}{dr} - \left[Q(r) + p + \frac{D_2}{r} - \left(2D_1r + \right.\right. \tag{44}$$

$$\left. + D_2\right)^2 - \frac{2n}{r^2}\left(E_1 + E_2r\right)\right]T + 2iE_2\frac{dS}{dr} + \left[\frac{2in}{r^2} - \frac{2R_mB}{r^2} + \right.$$

$$\left. + 2iE_2\left(2D_1r + D_2\right) - \frac{iE_2}{r} - \frac{2in}{r^2}\left(E_1 + E_2r\right)^2\right]S = 0 .$$

Notations (15) are used here. The boundary problem (42), (44) is equivalent to the boundary problem (24), (34).

The maximum real part γ of the eigenvalues p of the boundary problem (42), (44) is estimated by the Galerkin method as in the case of the boundary problem (24), (25).

The functions $S(r)$ and $T(r)$ are represented in the form

$$S(r) = \sum_{j=0}^{J} C_{2j+1}f_{2j+1}(r) , \quad T(r) = \sum_{j=1}^{J} C_{2j}f_{2j}(r) \tag{45}$$

where the functions $f_{2m+1}(r)$ ($m = 0, 1, \ldots, J$) and $f_{2m}(r)$ ($m = 1, 2, \ldots, J$) are defined by formulas (36).

Substitute sums (45) in equations (42) and multiply the first equation by the functions $f_{2m+1}(r)$ ($m = 0, 1, \ldots, J$) and the second equation by the functions $f_{2m}(r)$ ($m = 1, 2, \ldots, J$). After integration of the $2J + 1$ equations obtained over the segment $[\eta, 1]$ the following equations will be obtained

$$\sum_{j=1}^{J} C_{2j+1}\int_{\eta}^{1}\left[-\left(\frac{\pi j}{1-\eta}\right)^2 f_{2j+1}(r)f_{2m+1}(r) + \right.$$

$$\left. + \frac{\pi j}{1-\eta}\left(\frac{1}{r} - 4D_1r - 2D_2\right)f_{2j}(r)f_{2m+1}(r)\right]dr +$$

$$+ \sum_{j=0}^{J} C_{2j+1}\int_{\eta}^{1}\left\{-Q(r) - \frac{D_2 - 2nE_2}{r} + 4D_1^2r^2 + 4D_1D_2r + D_2^2 + \right.$$

$$\left. + \frac{2nE_1}{r^2}\right\}f_{2j+1}(r)f_{2m+1}(r)dr -$$

$$- 2in\sum_{j=1}^{J} C_{2j}\int_{\eta}^{1}\frac{f_{2j}(r)f_{2m+1}(r)}{r^2}dr -$$

$$- p \sum_{j=0}^{J} C_{2j+1} \int_{\eta}^{1} f_{2j+1}(r) f_{2m+1}(r) dr = 0 ,$$

$$m = 0, 1, \ldots , J ,$$

$$\sum_{j=1}^{J} C_{2j} \int_{\eta}^{1} \left[\left[-\left(\frac{\pi j}{1-\eta} \right)^2 - Q(r) - \frac{D_2 - 2nE_2}{r} + 4D_1^2 r^2 + \right. \right. \qquad (46)$$

$$+ 4D_1 D_2 r + D_2^2 - \frac{2nE_1}{r^2} \Bigg] f_{2j}(r) f_{2m}(r) - \frac{\pi j}{1-\eta} \left(\frac{1}{r} - 4D_1 r - \right.$$

$$\left. - 2D_2 \right) f_{2j+1}(r) f_{2m}(r) \Bigg] dr -$$

$$- 2iE_2 \sum_{j=1}^{J} C_{2j+1} \left(\frac{\pi j}{1-\eta} \right) \int_{\eta}^{1} f_{2j}(r) f_{2m}(r) \, dr +$$

$$+ \sum_{j=0}^{J} C_{2j+1} \int_{\eta}^{1} \left[\frac{2in\left(1 - E_1^2\right) - 2R_m B}{r^2} + 4iD_1 E_2 r + \right.$$

$$\left. + 2i\left(E_2 D_2 - nE_2^2\right) - iE_2 \frac{1 + 4nE_1}{r} \right] f_{2j+1}(r) f_{2m}(r) dr -$$

$$- p \sum_{j=1}^{J} C_{2j} \int_{\eta}^{1} f_{2j}(r) \, f_{2m}(r) \, dr = 0 ,$$

$$m = 1, 2, \ldots , J .$$

It follows from formulas (38) that equations (46) are the linear algebraic homogeneous system having the form (39). The maximum of all real parts of the eigenvalues of the matrix A which corresponds to equations (46) is the estimation of the value of γ.

The modified LR-algorithm (Rutishauser, 1958) was used for calculation of eigenvalues of the complex matrix A and proved its efficiency.

It follows from formulas (15) and (43) that the maximum real

part γ of the eigenvalues of the boundary problem (24), (25) or (42), (44) and its estimation γ_K^* depend on the following parameters of the problem: η, R_m, n, α, κ, $\kappa_1 = U_p/U_c$. Thus while the possibility of the magnetic field generation is considered it is supposed that $\Omega_2 = 0$.

To find the values of the parameters which provide the possibility of the magnetic field generation the gradient method is used to minimize the functional $W(\eta, R_m, n, \alpha, \kappa, \kappa_1) = -\gamma_K^*$. The search of the minimum of the functional W gives possibility to find the values of the parameters for which $\gamma_K^* > 0$ if such values exist. The value of the integer parameter n as well as the values of η and R_m are fixed and the values of α, κ, and κ_1 are changed while the gradient method is applied. The partial derivatives of W with respect to α, κ, and κ_1 which used for calculation of the consecutive approximations when the gradient method is applied are calculated by using of the finite-difference method.

The direct numerical solving of the boundary problem (24), (25) or (24), (34) is used to test the eigenvalues obtained by the Galerkin method. The solution of the boundary problems under consideration is the eigenvalue p and the vector-function $\mathbf{f}(r) = (R(r), \Phi(r))$ which satisfy to the equations (24) and the boundary conditions (25) or (34). The solution is not unique because if the pair p, $\mathbf{f}(r)$ is a solution then the pair p, $C\mathbf{f}(r)$ where C is an arbitrary complex constant is a solution also. One more boundary condition is added to avoid the anuniqueness of the solution. This condition is $\Phi(\eta) = 1$ in the case of the boundary problem (24), (25) or $R(\eta) = 1$ in the case of the boundary problem (24), (34). The eigenvalue p_K^* ($\mathrm{Re}\, p_K^* = \gamma_K^*$) of the matrix A is used as the initial

approximation of the eigenvalue p for the solution of the boundary problem. The solution $C = (C_1, C_2, \ldots, C_K)$ of system (39) with $p = p_K^*$ is used to calculate the initial approximation

$$\left.\frac{dR}{dr}\right|_{r=\eta} = \frac{\pi}{(1-\eta)\left(\frac{C_1}{\sqrt{2}} + \sum_{j=1}^{J} C_{2j+1}\right)} \sum_{j=1}^{J} jC_{2j}$$

for the boundary problem (24), (25) or the initial approximation

$$\left.\frac{d\Phi}{dr}\right|_{r=\eta} = (2D_1\eta + D_2)\,\frac{in}{\eta|\alpha|}\,Y_1 + iE_2 + \frac{\pi}{(1-\eta)\left(\frac{C_1}{\sqrt{2}} + \sum_{j=1}^{J} C_{2j+1}\right)} \sum_{j=1}^{J} jC_{2j}$$

for the boundary problem (24), (34).

RESULTS OF NUMERICAL ANALYSIS

The numerical analysis has proved the existence of the values of the parameters for which the magnetic field is generated (the magnetic dynamo exists). The example of such values is: $\eta = 0.25$, $R_m = 150$, $n = 1$, $\alpha = -2$, $\kappa = 1$, $\kappa_1 = 0$, $\Omega_2 = 0$. Note that the condition $\kappa_1 = 0$ means that there is absent the action of the pressure gradient on the fluid. In this case the flow is called the helical Couette flow.

Table 1 contains the real (γ_K^*) and imaginary (δ_K^*) parts of the eigenvalue $p_K^* = \gamma_K^* + i\delta_K^*$ of the matrix A calculated for different values of K. The last line of the table contains the eigenvalues $p = \gamma + i\delta$ obtained by the direct numerical solving of the boundary problem.

TABLE 1

K	Perfect conductor boundaries		Dielectric boundaries	
	γ_K^*	δ_K^*	γ_K^*	δ_K^*
7	0.26431	44.585	0.10092	46.435
13	0.44081	44.594	0.78056	45.688
19	0.44112	44.560	0.77751	45.590
29	0.44166	44.555	0.80235	45.540
49	0.44246	44.553	0.80804	45.525
69	0.44263	44.552	0.80935	45.523
99	0.44270	44.552	0.80986	45.522
	The eigenvalue $p = \gamma + i\delta$ obtained by the direct numerical solving of the boundary problem (24), (25)		(24), (34)	
	γ	δ	γ	δ
	0.44273	44.552	0.81019	45.521

In the case of the perfect conductor boundaries the table shows that if $K = 13$ then for $R_m \sim 10^2$ the values of γ_K^* and δ_K^* approximate the real and imaginary parts of the eigenvalue p with the relative accuracy $0.5 \cdot 10^{-2}$ and 10^{-3} respectively.

In the case of the dielectric boundaries it necessary to take $K = 29$ to obtain the relative accuracy of the approximation 10^{-2} for the real part and $0.4 \cdot 10^{-3}$ for the imaginary part of the eigenvalue p.

The corresponding to the eigenvalue p solutions $R(r)$ and $\Phi(r)$ of the boundary problems are shown in Figures 1 and 2 (for the perfect conductor boundaries) and in Figures 3 and 4 (for the dielectric boundaries). These solutions satisfy to the additional boundary condition $\Phi(\eta) = 1$ in the case of the boundary problem (24), (25) or $R(\eta) = 1$ in the case of the boundary problem (24), (34).

The next result of the numerical analysis is the construction of the boundaries of the regions of the magnetic dynamo existence on planes corresponding to the chosen pairs of parameters and the other parameters to be fixed. These boundaries are the curves where $\gamma = 0$ ard are called neutral curves. The approximation of the neutral curve (the curve $\gamma_K^* = 0$) can be constructed by the Galerkin method.

For the perfect conductor boundaries the neutral curve approximations $\gamma_K^* = 0$ for different values of K and the neutral curve obtained by the direct numerical solving of the boundary problem (24), (25) a·e shown in Figure 5. The plane R_m, α is considered and the other parameters have the following values: $\eta = 0.25$, $n = 1$, $\kappa = 1$, $\kappa_1 = 0$. The analogous curves for the dielectric boundaries and for the same values of η, n, κ, and κ_1 are demonstrated in Figu e 6.

Figures 5 and 6 show that the curves $\gamma_K^* = 0$ well approximate the upper part of the curve $\gamma = 0$. For the lower part of the curve $\gamma = 0$ the approximation is satisfactory if the value of R_m is small enough: $R_m < 200$ if $K = 7$, $R_m < 300$ if $K = 9$, $R_m < 400$ if $K = 11$, and $R_m < 600$ if $K = 13$ in the case of the perfect conductor boundaries and $R_m < 300$ if $K = 9$, $R_m < 500$ if $K = 11$, and $R_m < 800$ if $K = 13$ in the case of the dielectric boundaries.

From the form o.. the neutral curves shown in Figures 5 and 6 the assumption follows that if $\kappa_1 = 0$ and $\kappa > 0$ then for any value of R_m the magnetic dynamo exists only if

$$\alpha < \alpha_1(\eta, n, \kappa) < 0. \qquad (47)$$

The minimal values of R_m for the neutral curves $\gamma = 0$ shown in Figures 5 and 6 are -129 and -125 respectively.

The neutral curves $\gamma_{13}^* = 0$ on the plane κ, α for $R_m = 200$,

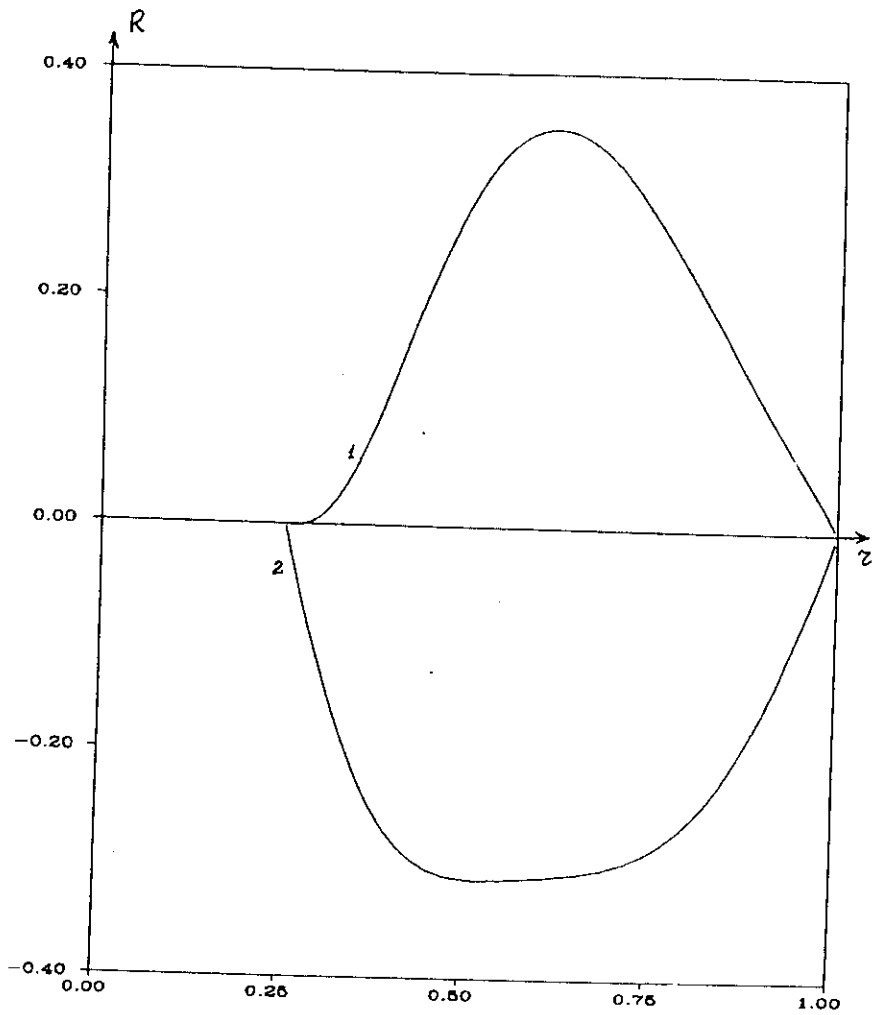

FIGURE 1. The real (1) and imaginary (2) parts of the function $R(r)$ in the case of the perfect conductor boundaries.

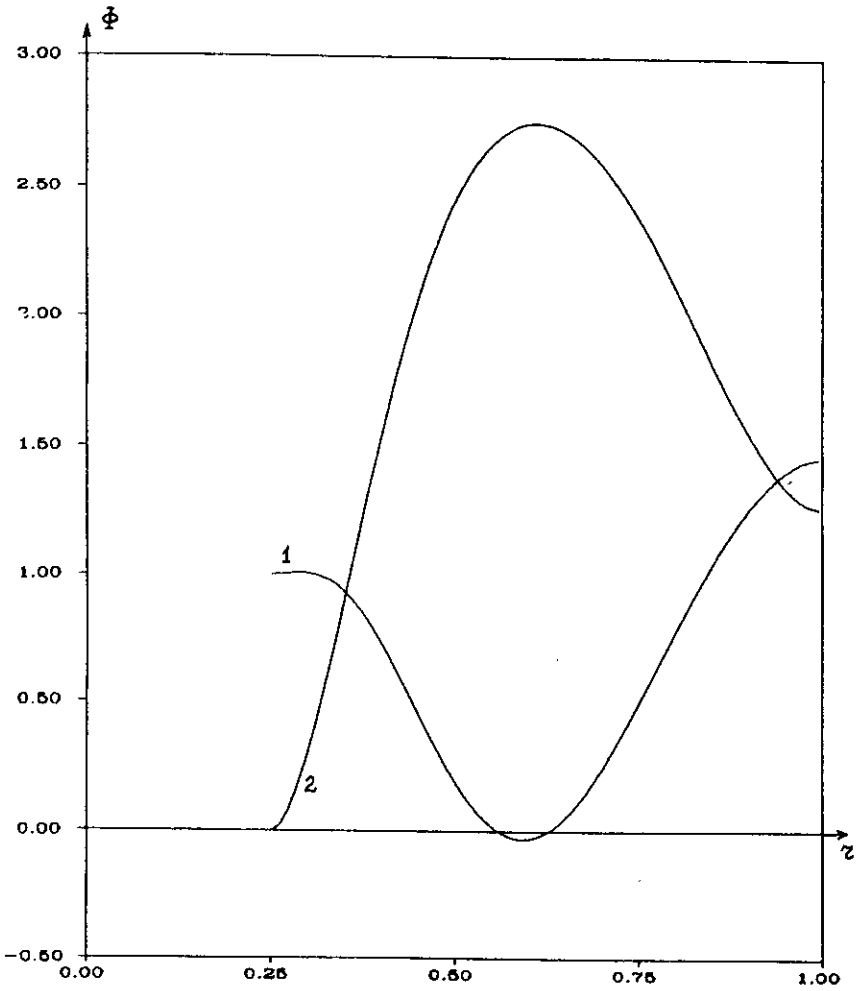

FIGURE 2. The real (1) and imaginary (2) parts of the function $\Phi(r)$ in the case of the perfect conductor boundaries.

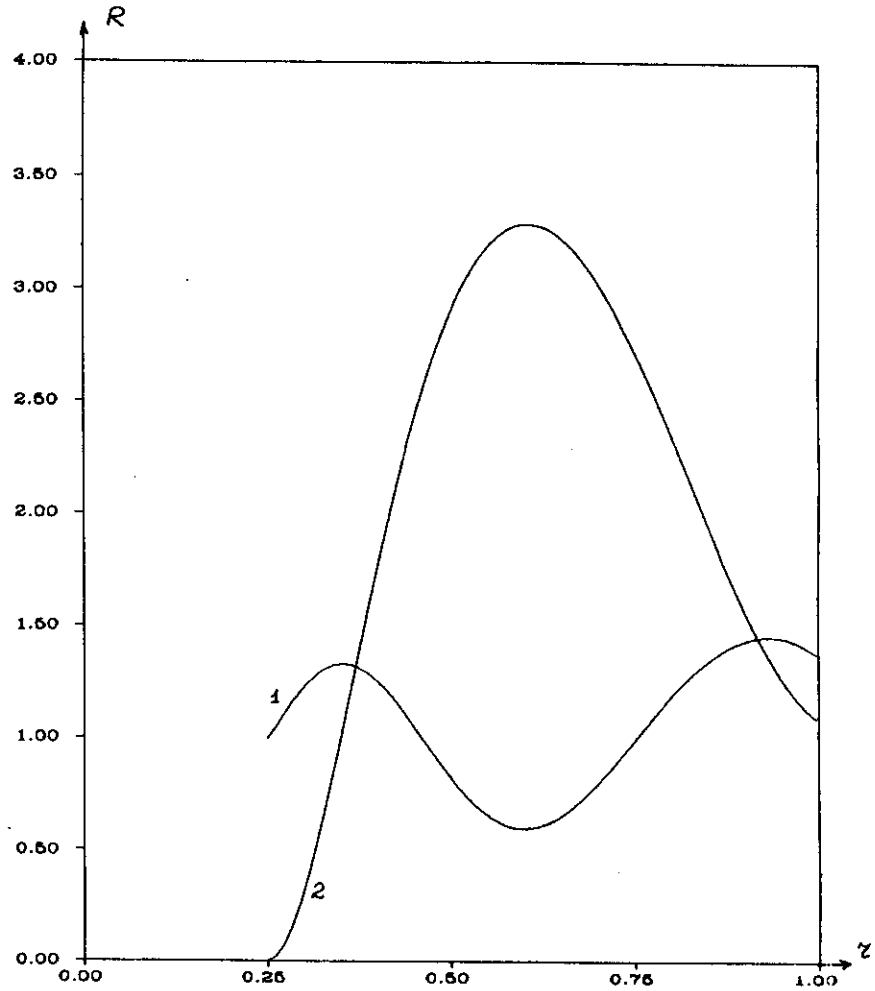

FIGURE 3. The real (1) and imaginary (2) parts of the function $R(r)$ in the case of the dielectric boundaries.

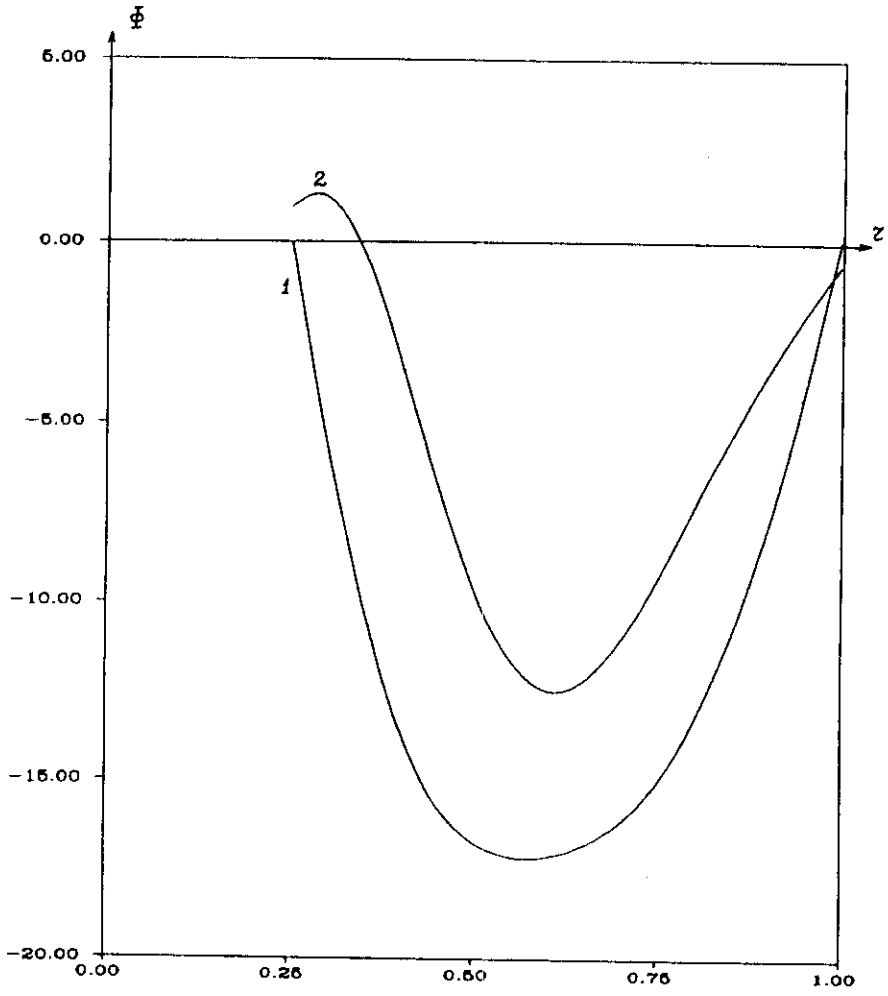

FIGURE 4. The real (1) and imaginary (2) parts of tne function $\Phi(r)$ in the case of the dielectric boundaries.

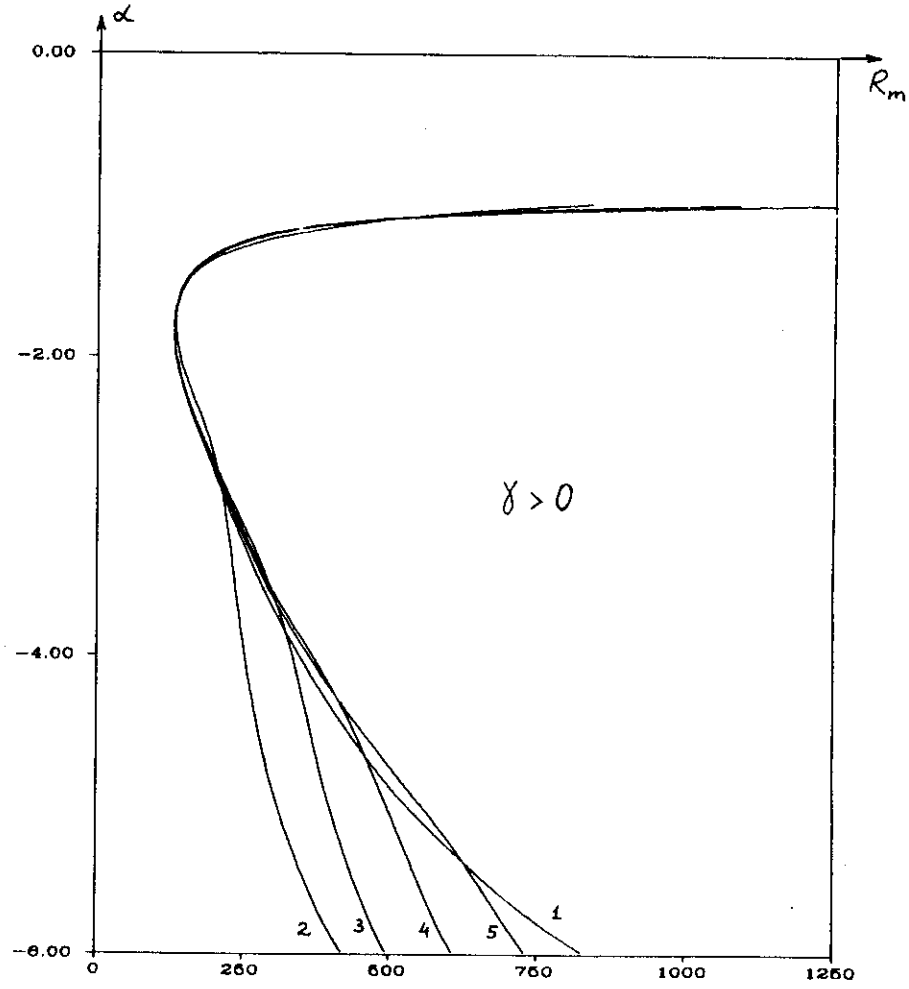

FIGURE 5. The neutral curves on the plane R_m, α for the perfect conductor boundaries: $\gamma = 0$ (1), $\gamma_7^* = 0$ (2), $\gamma_9^* = 0$ (3), $\gamma_{11}^* = 0$ (4), $\gamma_{13}^* = 0$ (5).

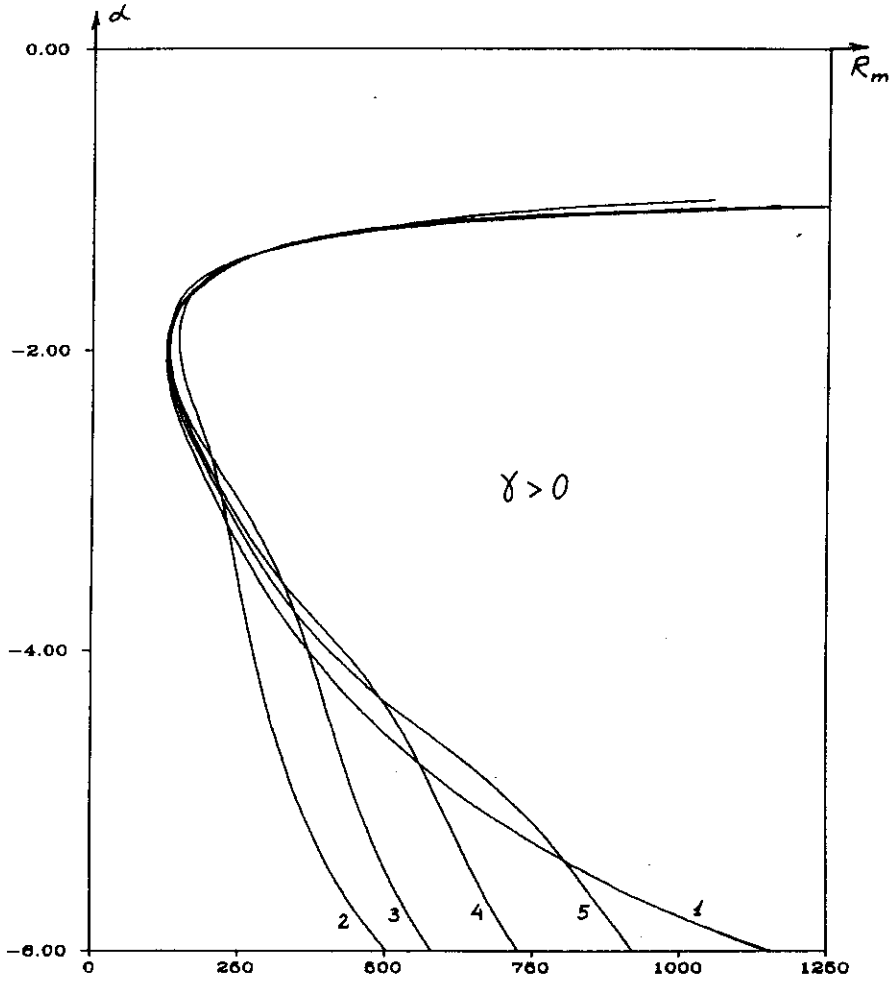

FIGURE 6. The neutral curves on the plane R_m, α for the dielectric boundaries: $\gamma = 0$ (1), $\gamma_7^* = 0$ (2), $\gamma_9^* = 0$ (3), $\gamma_{11}^* = 0$ (4), $\gamma_{13}^* = 0$ (5).

$n = 1$, $\kappa_1 = 0$ and different values of η are shown in Figures 7 and 8 for the perfect conductor boundaries and the dielectric boundaries respectively. In the both figures the region of the values of κ and α for which the magnetic dynamo exists has the maximum square when $\eta = 0.25$. If $\eta \to 0$ or $\eta \to 1$ then the size of this region decreases. For instance in the case of the dielectric boundaries if $\eta = 0.75$, $R_m = 200$, $n = 1$, and $\kappa_1 = 0$ then there are not any values of κ, α for which $\gamma \geq 0$ and the region of the magnetic dynamo existence is absent for $\eta = 0.75$ in Figure 8. The disappearance of the magnetic dynamo when $\eta \to 1$ can be explained by the fact that in this case the motion of the fluid between the cylindrical surfaces approaches to the motion between two planes and as proved by Zeldovich (1956) the plane motion of the electrically conducting fluid does not generate the magnetic field. The values of κ in the regions limited by the neutral curves shown in Figures 7 and 8 are close to 1. It means that the necessary condition for the magnetic field generation is that the magnitudes of the components V_φ and V_z of the fluid velocity have not to be different highly.

When $\Omega_2 = 0$ it follows from the form of system (24) and the boundary conditions (25) and (34) that if the values of κ and α are multiplied by -1 then the eigenvalues are transformed into the conjugate complex numbers and the value of γ does not change. It means that besides of the regions limited by the neutral curves presented in Figures 7 and 8 there are the symmetric to them about the coordinate origin regions of the magnetic dynamo existence on the plane κ, α (where $\kappa < 0$, $\alpha > 0$).

If the values of n and α are multiplied by -1 then the eigenvalues are also transformed into the conjugate complex numbers

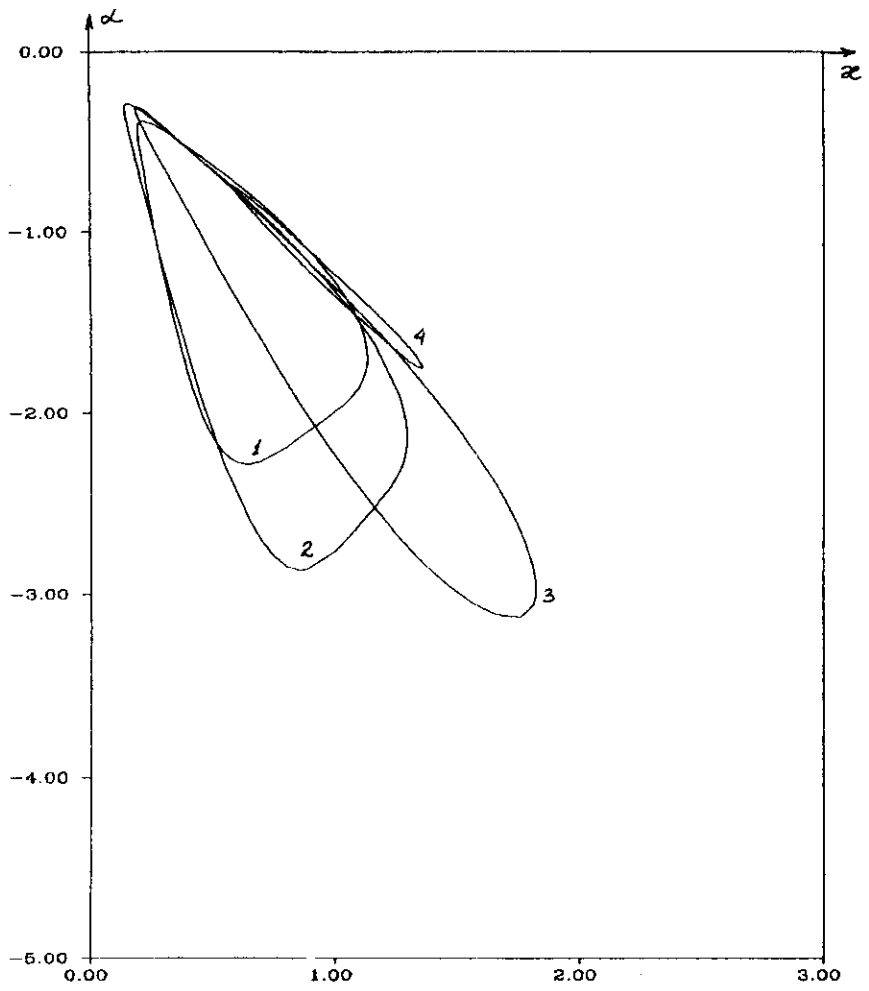

FIGURE 7. The curves $\gamma^{*}_{13} = 0$ on the plane κ, α for $R_{m} = 200$, $n = 1$, $\kappa_{1} = 0$, and $\eta = 0.15$ (1), 0.25 (2), 0.5 (3), 0.75 (4) in the case of the perfect conductor boundaries.

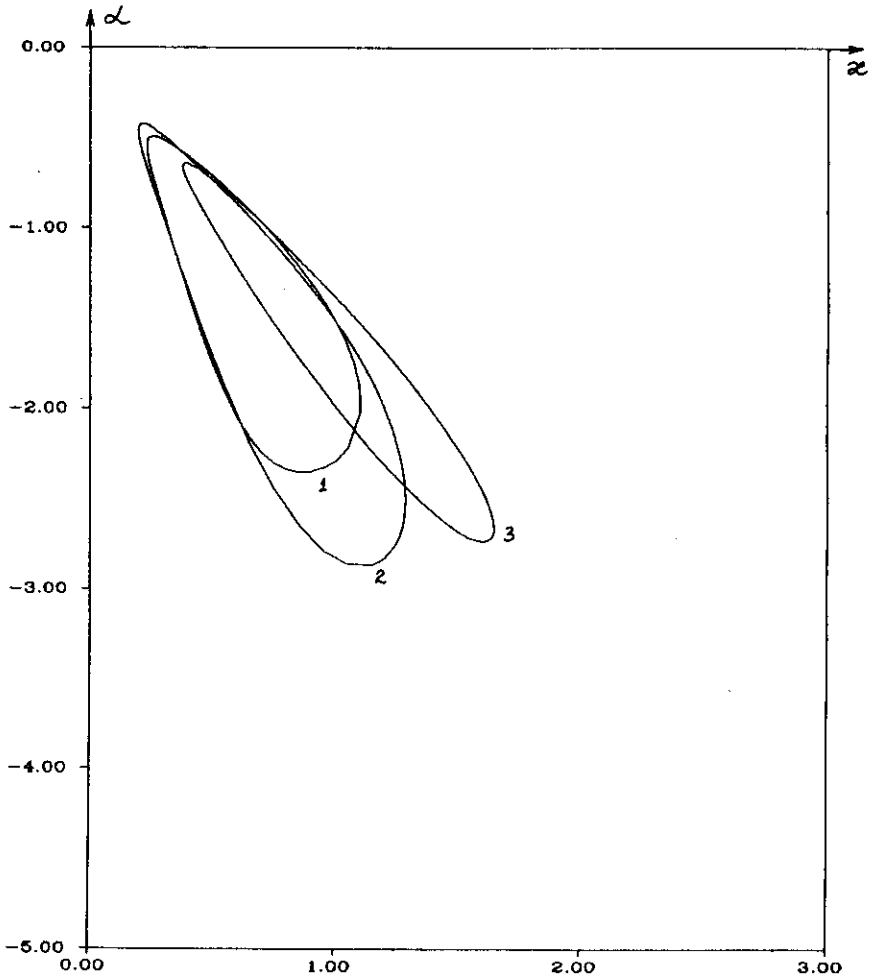

FIGURE 8. The curves $\gamma^{*}_{13} = 0$ on the plane κ, α for $R_{m} = 200$, $n = 1$, $\kappa_{1} = 0$, and $\eta = 0.15$ (1), 0.25 (2), 0.5 (3) in the case of the the dielectric boundaries.

and the value of γ does not change. Thus for $R_m = 200$, $n = -1$, $\kappa_1 = 0$ the regions of the magnetic dynamo existence on the plane κ, α are symmetric about the κ axis to those presented in Figures 7 and 8 for the same values of η.

The regions of the magnetic dynamo existence on the plane κ, α for the non-zero values of κ_1 in the case of the perfect conductor boundaries are shown in Figures 9-16. These regions were constructed for $R_m = 200$, $n = 1$, and $\eta = 0.25$, 0.5, and 0.75. The boundaries of the regions are the curves $\gamma^*_{13} = 0$. Thus Figures 9-16 show the evolution of the regions shown in Figure 7 when the value of κ_1 is changed.

When $\kappa_1 = -0.25$ (Figure 9) the sizes of the regions are greater than in the case of $\kappa_1 = 0$ (Figure 7). When the value of κ_1 is decreased to -0.5 (Figure 10) then the sizes of the regions for $\eta = 0.25$ and 0.5 are changed slightly but the size of the region for $\eta = 0.75$ is reduced sharply. For the smaller values of κ_1 (Figures 11-13) the region for $\eta = 0.75$ disappears and the size of the region for $\eta = 0.5$ is reduced when the value of κ_1 is decreased. When the value of κ_1 is changed from -0.5 to -1 then the size of the region for $\eta = 0.25$ is increased slightly. For the smaller values of κ_1 the size of this region practically is not changed.

The region of the magnetic dynamo existence for $U_c = 0$, $U_p > 0$, and $\eta = 0.25$ is shown in Figure 14. Note that if $U_c = 0$ than the simultaneous multiplication of α and U_p by -1 does not change the value of γ and the region of the magnetic dynamo existence for $U_c = 0$, $U_p < 0$, and $\eta = 0.25$ is symmetric about the κ axis to that presented in Figure 14. The regions for $\kappa_1 = 4$ and 2 and $\eta = 0.25$ are shown in the same figure. The size of the regions in Figure 14

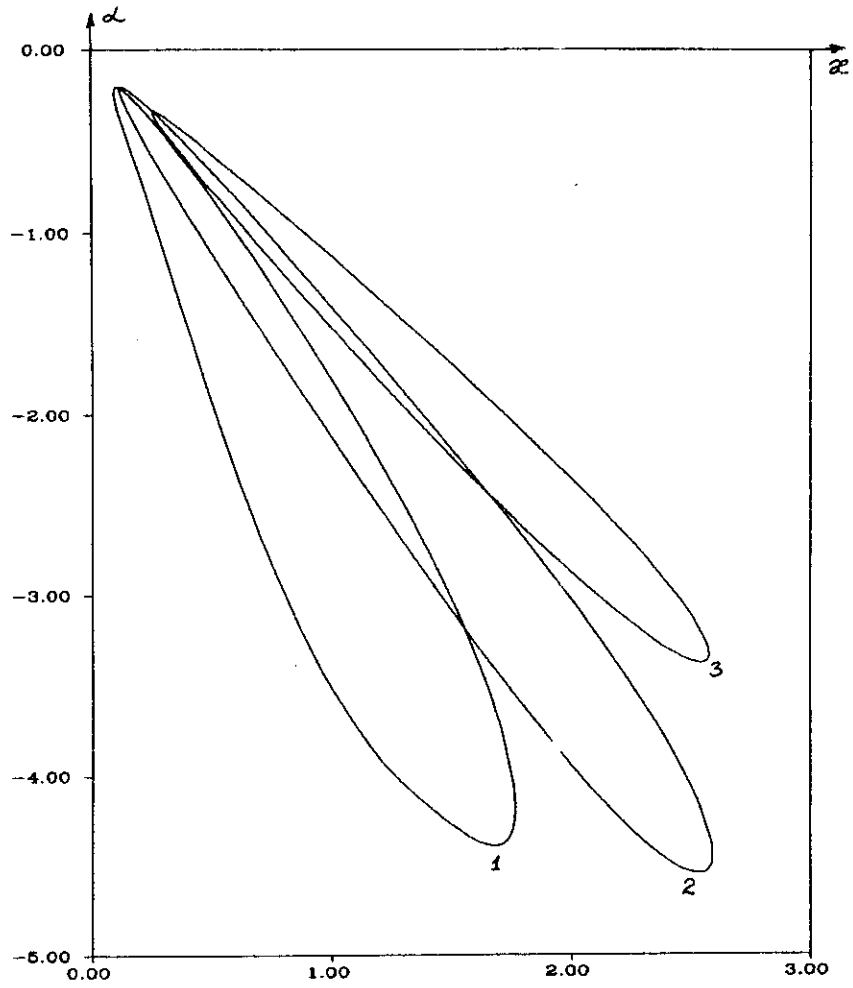

FIGURE 9. The curves $\gamma^*_{13} = 0$ on the plane κ, α for $R_m = 200$, $n = 1$, $\kappa_1 = -0.25$, and $\eta = 0.25$ (1), 0.5 (2), 0.75 (3) in the case of the perfect conductor boundaries.

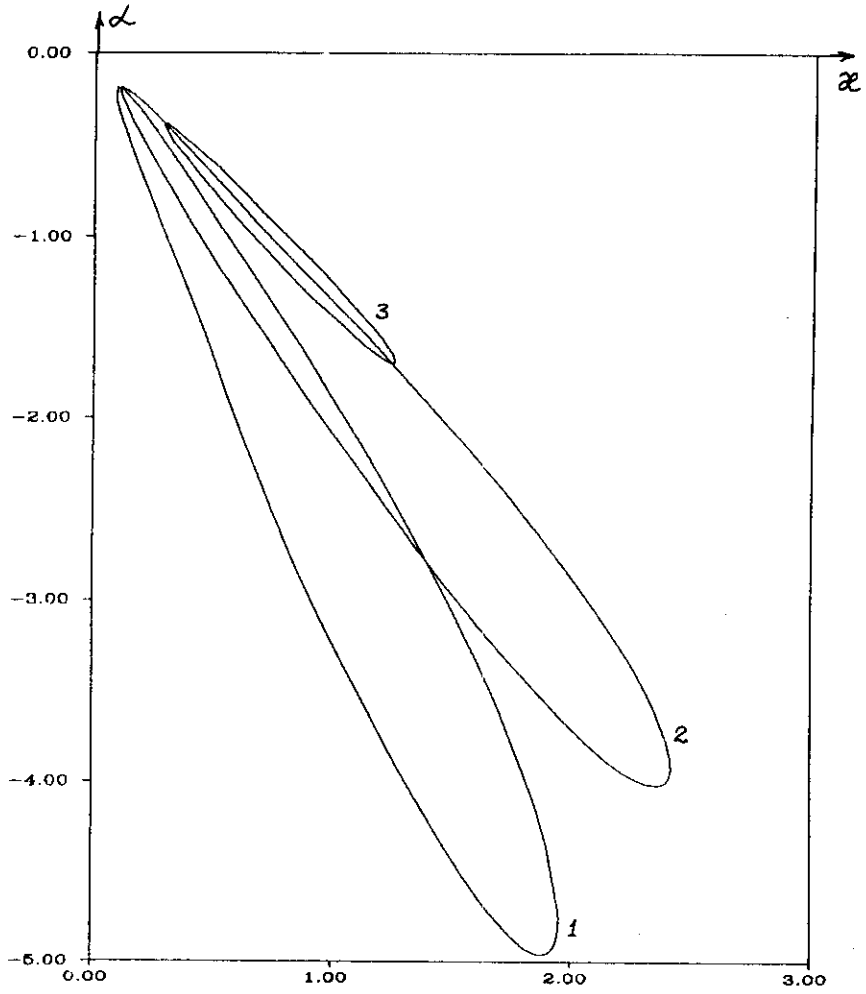

FIGURE 10. The curves $\gamma^{*}_{13} = 0$ on the plane κ, α for $R_m = 200$, $n = 1$, $\kappa_1 = -0.5$, and $\eta = 0.25$ (1), 0.5 (2), 0.75 (3) in the case of the perfect conductor boundaries.

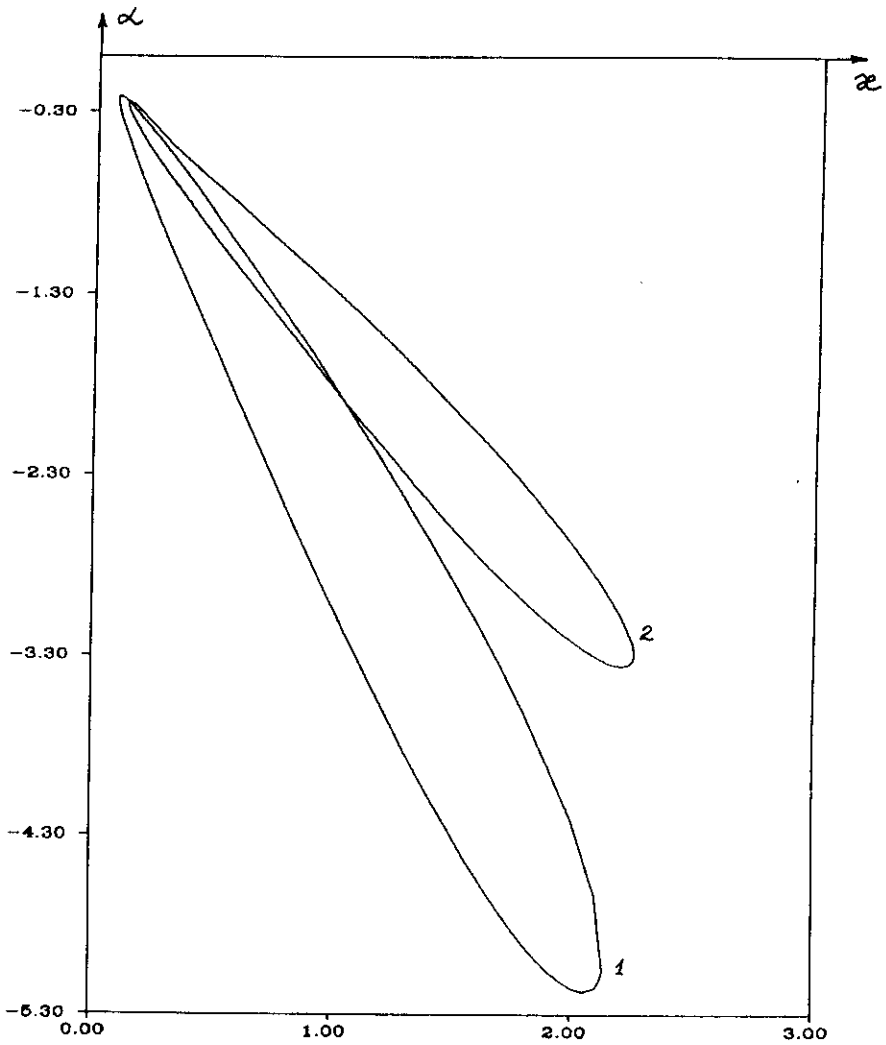

FIGURE 11. The curves $\gamma^{*}_{13} = 0$ on the plane κ, α for $R_m = 200$, $n = 1$, $\kappa_1 = -1$, and $\eta = 0.25$ (1), 0.5 (2) in the case of the perfect conductor boundaries.

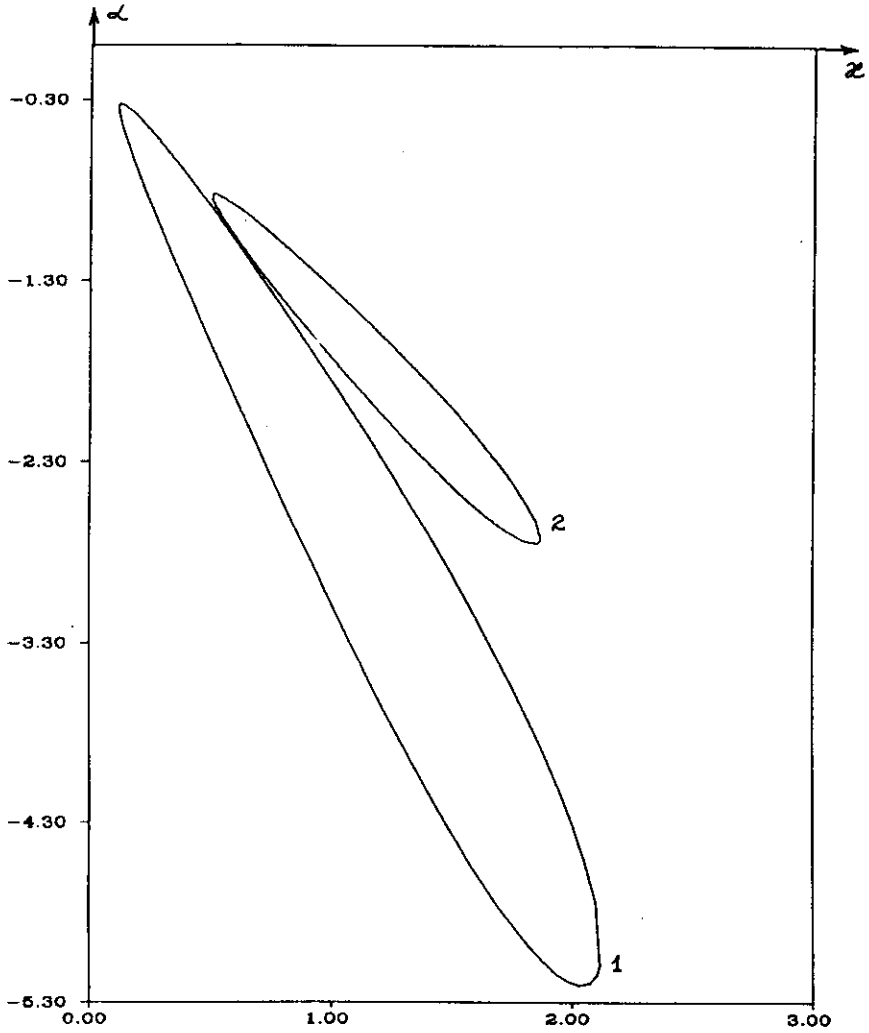

FIGURE 12. The curves $\gamma^*_{13} = 0$ on the plane κ, α for $R_m = 200$, $n = 1$, $\kappa_1 = -2$, and $\eta = 0.25$ (1), 0.5 (2) in the case of the perfect conductor boundaries.

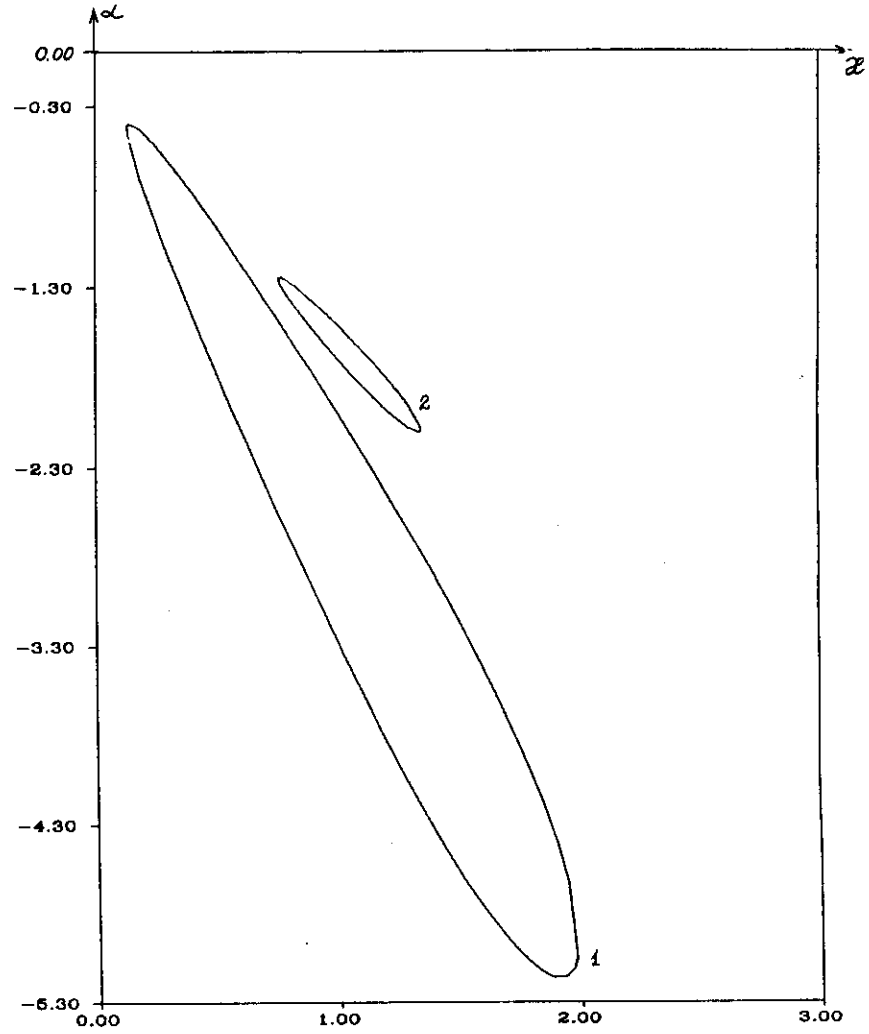

FIGURE 13. The curves $\gamma^*_{13} = 0$ on the plane κ, α for $R_m = 200$, $n = 1$, $\kappa_1 = -4$, and $\eta = 0.25$ (1), 0.5 (2) in the case of the perfect conductor boundaries.

is reduced when the value of κ_1 is decreased from ∞ to 2. In the case of the perfect conductor boundaries the region of the magnetic dynamo existence is absent on the plane κ, α for $\eta = 0.5$ or 0.75 if $R_m = 200$, $n = 1$, and $\kappa_1 > 1$.

The regions of the magnetic dynamo existence on the plane κ_1, α in the case of the perfect conductor boundaries are shown in Figure 15. The boundaries of these regions are the curves $\gamma^*_{13} = 0$ constructed for $\eta = 0.25$, $R_m = 200$, $n = 1$, and $\kappa = 1$. There are two regions in Figure 15: in one of them $\alpha > 0$ and $\kappa_1 > 0$, in the other $\alpha < 0$ and the values of κ_1 are negative or small positive. The region where $\alpha < 0$ has essential expansion for the small negative values of κ_1. The form of the regions allows to conclude that for the selected values of η, R_m, n, and κ the magnetic dynamo exists if $|\kappa_1| \to \infty$ and the value of α is close to -3 (if $\kappa_1 < 0$) or to 3 (if $\kappa_1 > 0$). This conclusion conforms to the forms of the regions of the magnetic dynamo existence presented in Figures 9-14: the point $\kappa = 1$, $\alpha = -3$ belongs to the regions constructed for $\eta = 0.25$ and $\kappa_1 < 0$ (Figures 9-13), and the point $\kappa = 1$, $\alpha = 3$ belongs to the regions constructed for $\eta = 0.25$ and $\kappa_1 > 0$ (Figure 14). Note that the region width with respect to α does not practically change when the values $|\kappa_1|$ are large. This correlates with slight changing of the size of the regions for $\eta = 0.25$ in Figures 10-14. The region for $\kappa_1 = 2$ in Figure 14 does not contain points with $\kappa = 1$. This conforms to the form of the region in Figure 15 for which $\alpha > 0$ because $\kappa_1 > 2$ for all points of this region.

The regions of the magnetic dynamo existence for $\eta = 0.5$ and 0.75 are shown in Figure 16. The values of R_m, n, and κ are the same as for the regions in Figure 15. The region with $\alpha < 0$ from Figure

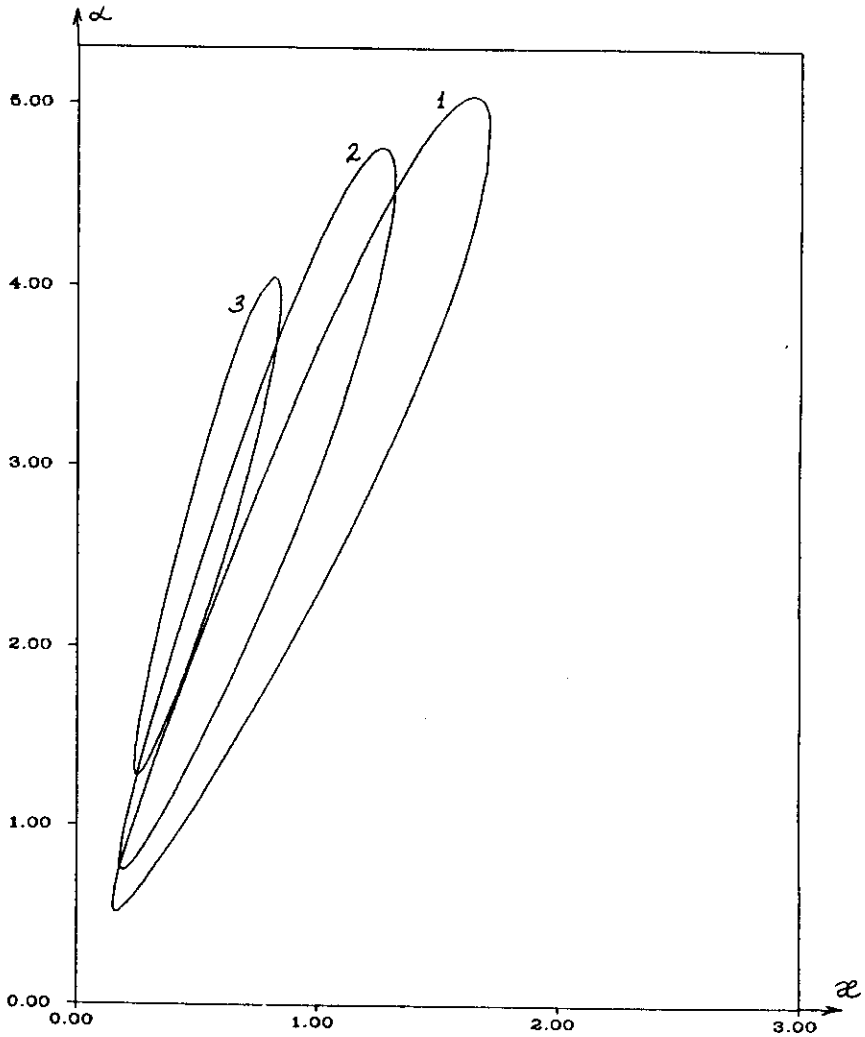

FIGURE 14. The curve $\gamma^*_{13} = 0$ on the plane κ, α for $R_m = 200$, $n = 1$, $\eta = 0.25$, and $\kappa_1 = \infty$ (1), 4 (2), 2 (3) in the case of the perfect conductor boundaries.

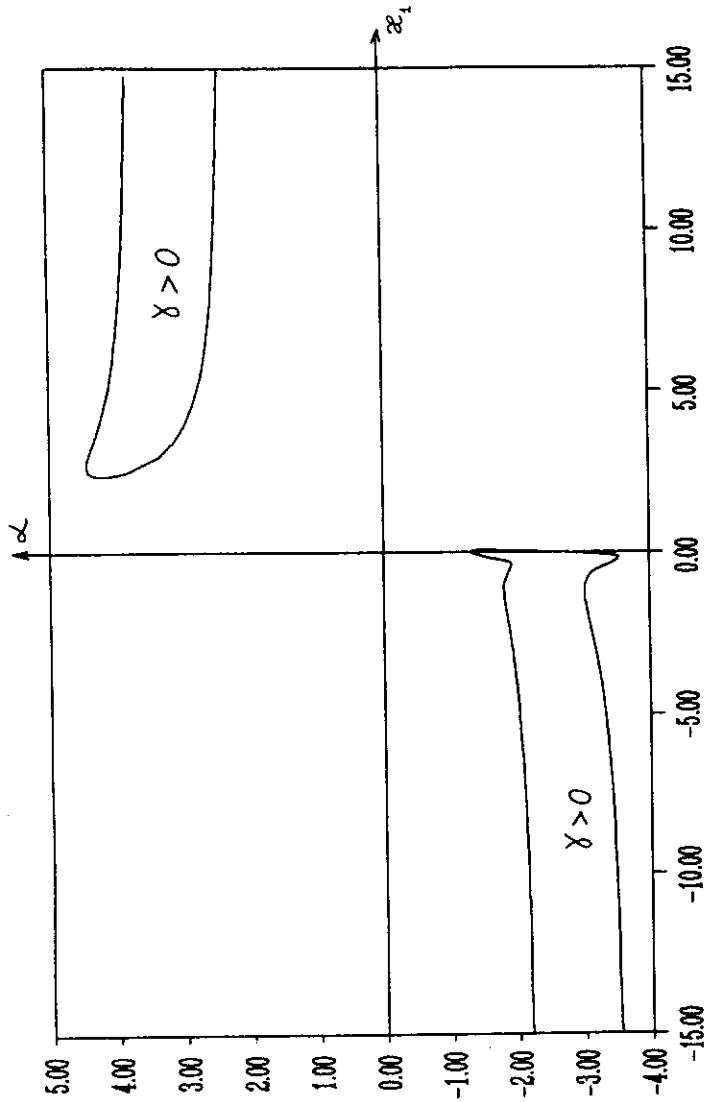

FIGURE 15. The curve $\gamma^*_{13} = 0$ on the plane κ_1, α for $R_m = 200$, $n = 1$, $\kappa = 1$, and $\eta = 0.25$ in the case of the perfect conductor boundaries.

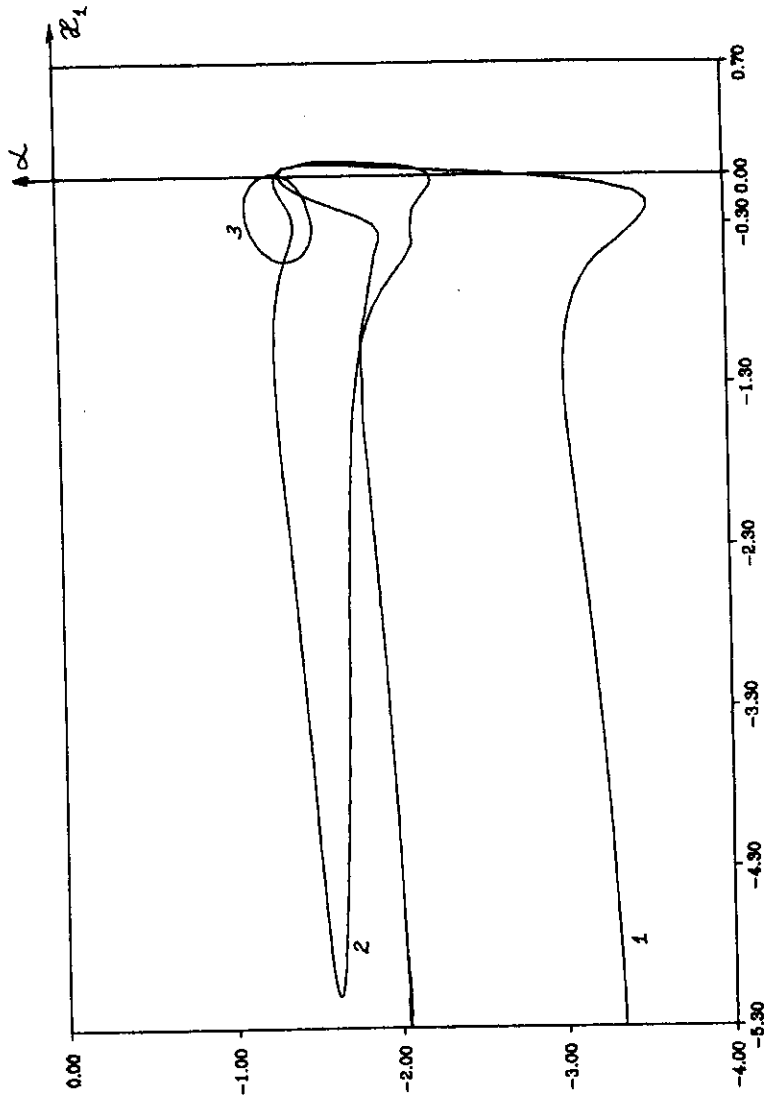

FIGURE 16. The curves $\gamma^*_{13} = 0$ on the plane κ_1, α for $R_m = 200$, $n = 1$, $\kappa = 1$, and $\eta = 0.25$ (1), 0.5 (2), and 0.75 (3) in the case of the perfect conductor boundaries.

15 is also shown here for comparison. For the considered values of R_m, n, and κ and $\eta = 0.5$ or 0.75 the regions of the magnetic dynamo existence were not found for $\alpha > 0$. Note that the size of the region is essentially reduced when the value of η is increased and the regions are limited with respect to κ_1 when $\eta = 0.5$ or 0.75.

The regions of the magnetic dynamo existence on the plane R_m, κ_1 give the additional information about dependence of the magnetic field generation process on the value of κ_1. Such regions are shown in Figures 17-20 for the case of the perfect conductor boundaries and in Figures 21-24 for the case of dielectric boundaries. The regions in these figures are constructed for the following values of the other parameters:

1) $\eta = 0.25$, $n = 1$, $\alpha = -1$, $\kappa = 0.5$ (Figures 17 and 21);

2) $\eta = 0.5$, $n = 1$, $\alpha = -1.25$, $\kappa = 0.75$ (Figures 18 and 22);

3) $\eta = 0.75$, $n = 1$, $\alpha = -1.14$, $\kappa = 0.88$ (Figures 19 and 23);

4) $\eta = 0.5$, $n = 1$, $\alpha = 1.25$, $\kappa = 0.75$ (Figures 20 and 24).

The boundaries of these regions are constructed by the Galerkin method with $K = 29$, i.e. the boundaries are the curves $\gamma^*_{29} = 0$.

Note that the region of the magnetic dynamo existence in Figure 15 extends for the smaller negative values of κ_1 than the region in Figure 17 which is constructed for the same value of η. This difference is explained by the evidence that these regions are constructed for the different value of κ and the region in Figure 17 is constructed for the value of α which is other than the values of α within the region of magnetic dynamo existence in Figure 15.

The regions of magnetic dynamo existence presented in Figures 17-24 show that there are the values of κ_1 for which the magnetic dynamo exists only for the values of R_m within some segment

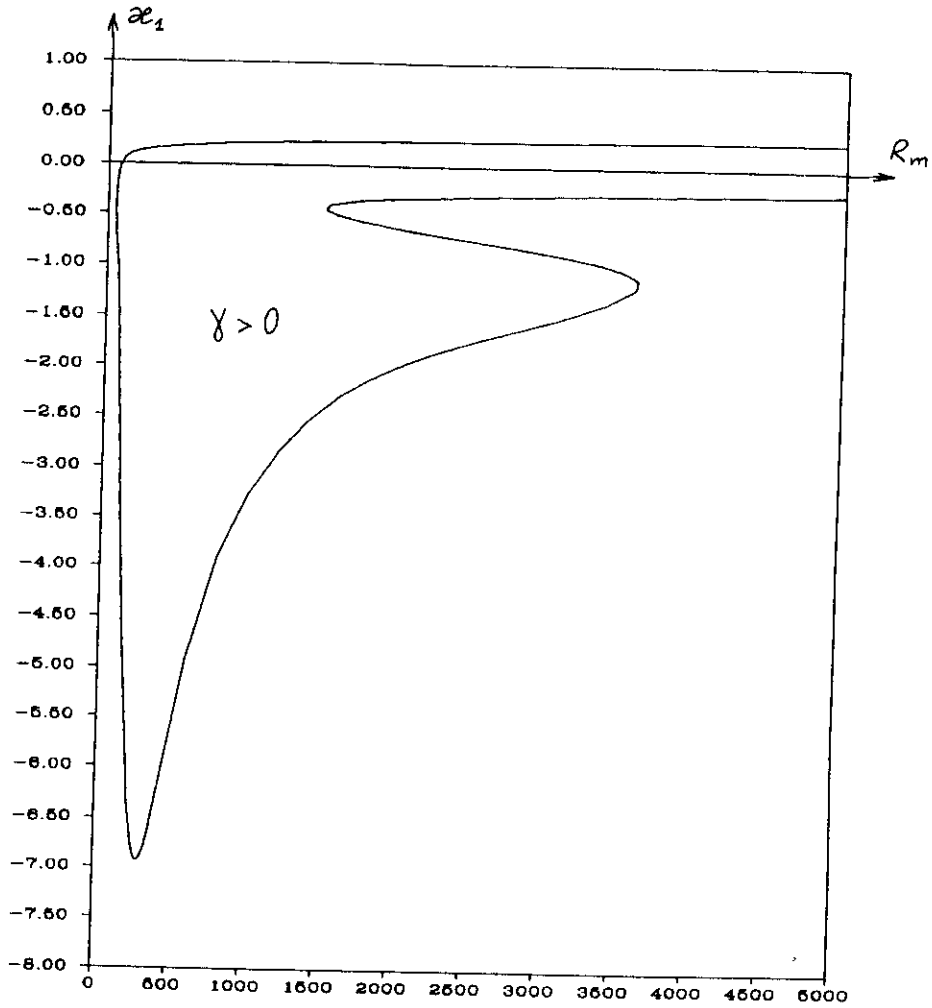

FIGURE 17. The curve $\gamma^*_{29} = 0$ on the plane R_m, κ_1 for $\eta = 0.25$, $n = 1$, $\kappa = 0.5$, $\alpha = -1$ in the case of the perfect conductor boundaries.

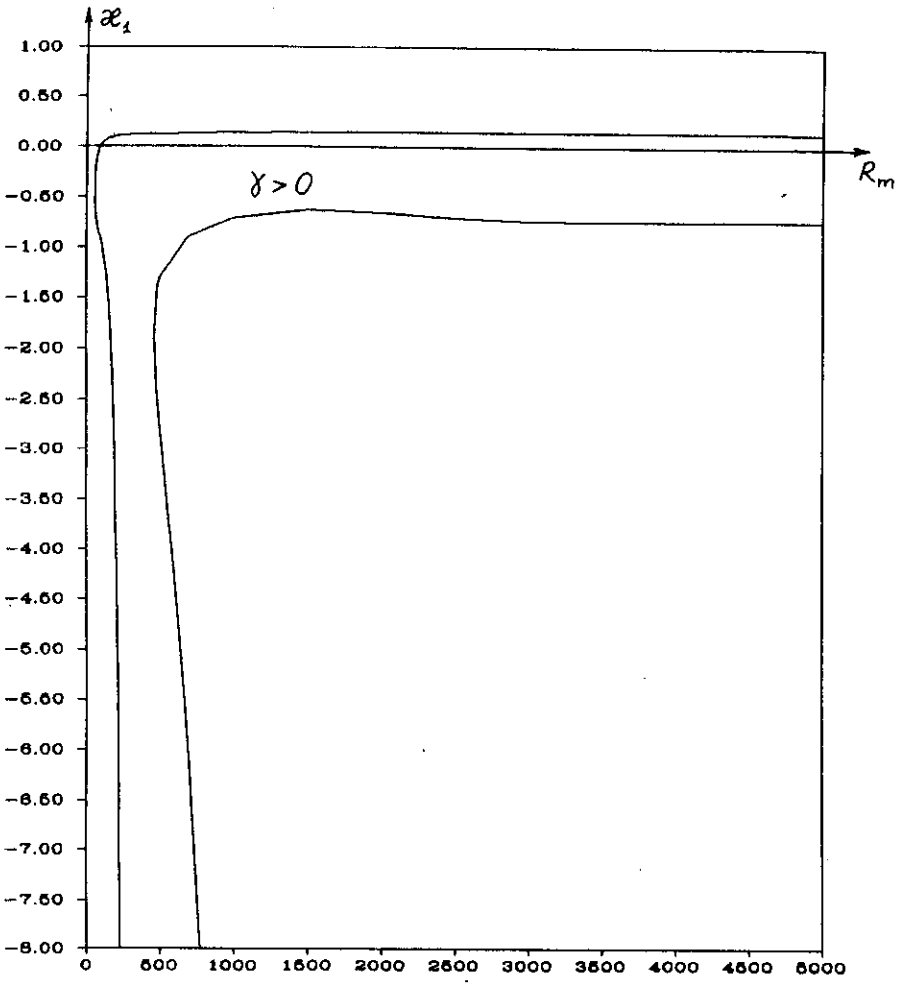

FIGURE 18. The curves $\gamma^*_{29} = 0$ on the plane R_m, κ_1 for $\eta = 0.5$, $n = 1$, $\kappa = 0.75$, $\alpha = -1.25$ in the case of the perfect conductor boundaries.

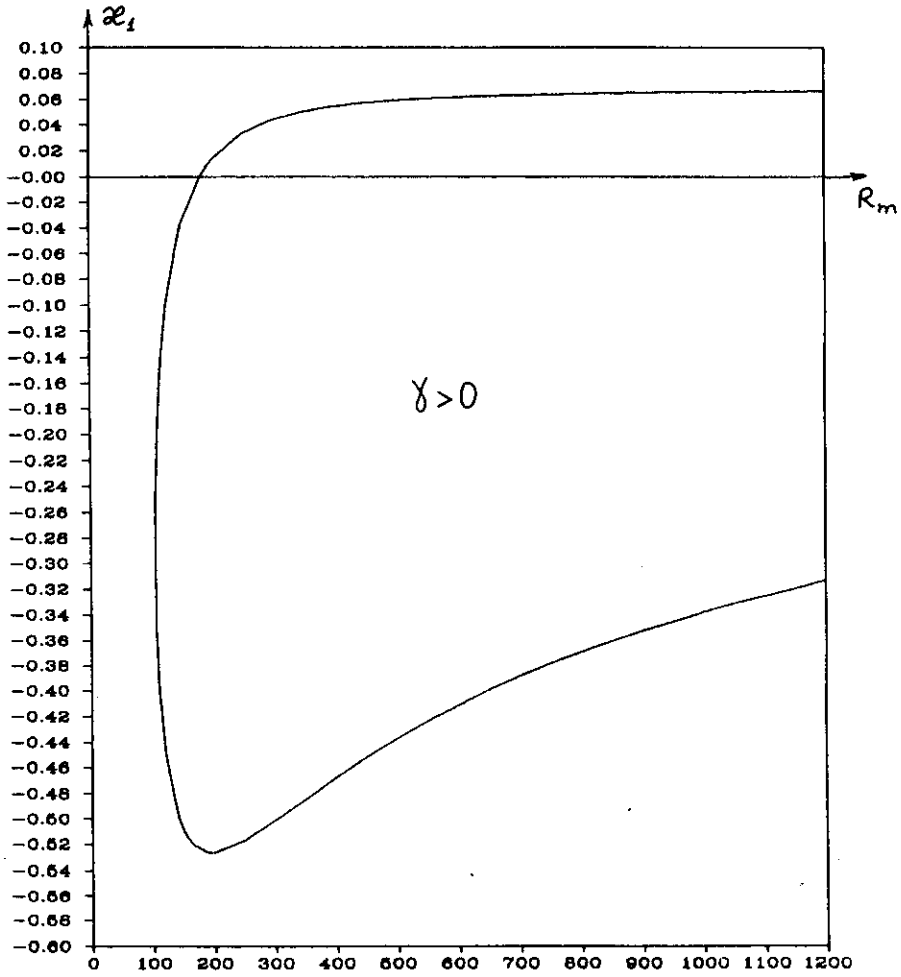

FIGURE 19. The curve $\gamma^*_{29} = 0$ on the plane R_m, κ_1 for $\eta = 0.75$, $n = 1$, $\kappa = 0.88$, $\alpha = -1.14$ in the case of the perfect conductor bound ries.

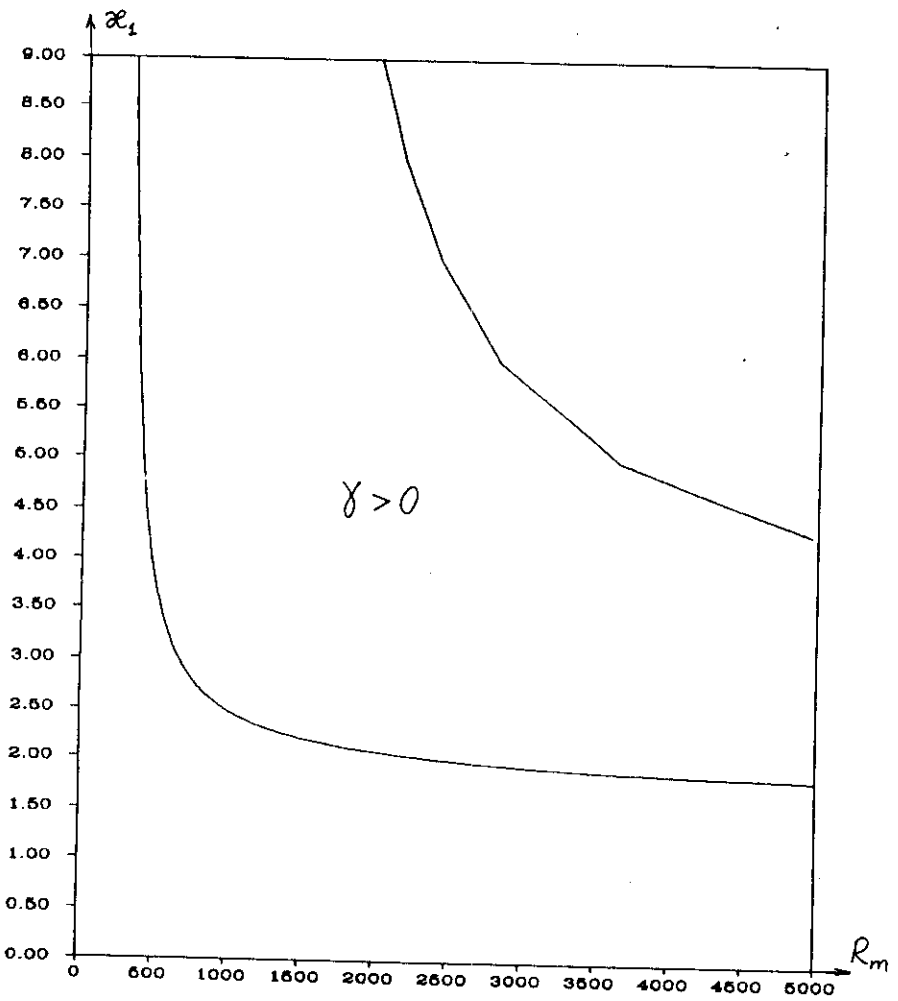

FIGURE 20. The curves $\gamma^*_{29} = 0$ on the plane R_m, κ_1 for $\eta = 0.5$, $n = 1$, $\kappa = 0.75$, $\alpha = 1.25$ in the case of the perfect conductor boundaries.

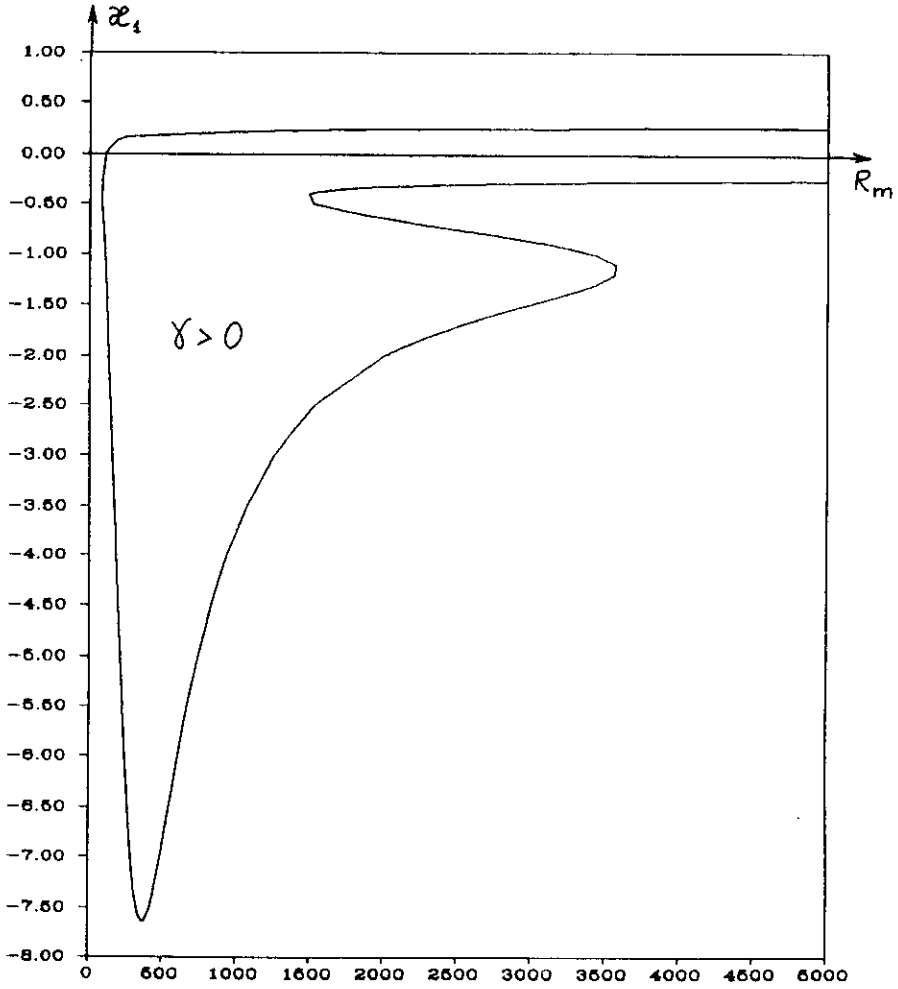

FIGURE 21. The curve $\gamma^*_{29} = 0$ on the plane R_m, κ_1 for $\eta = 0.25$, $n = 1$, $\kappa = 0.5$, $\alpha = -1$ in the case of the dielectric boundaries.

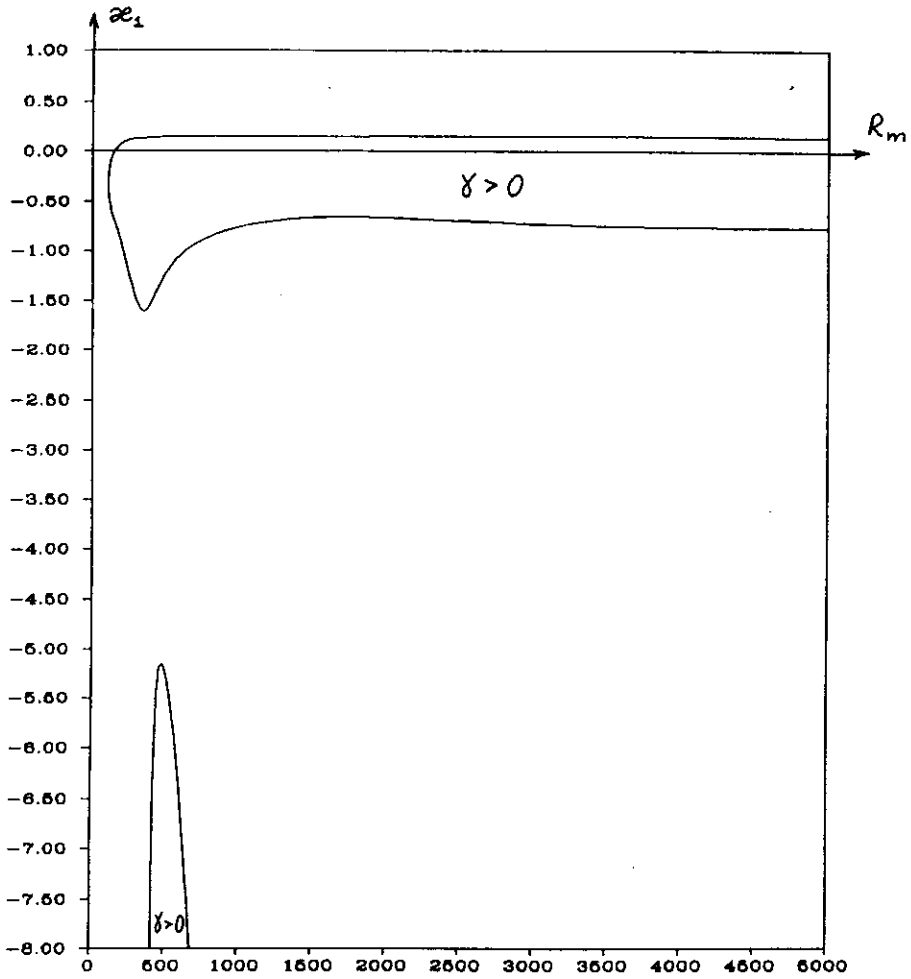

FIGURE 22. The curves $\gamma^*_{29} = 0$ on the plane R_m, κ_1 for $\eta = 0.5$, $n = 1$, $\kappa = 0.75$, $\alpha = -1.25$ in the case of the dielectric boundaries.

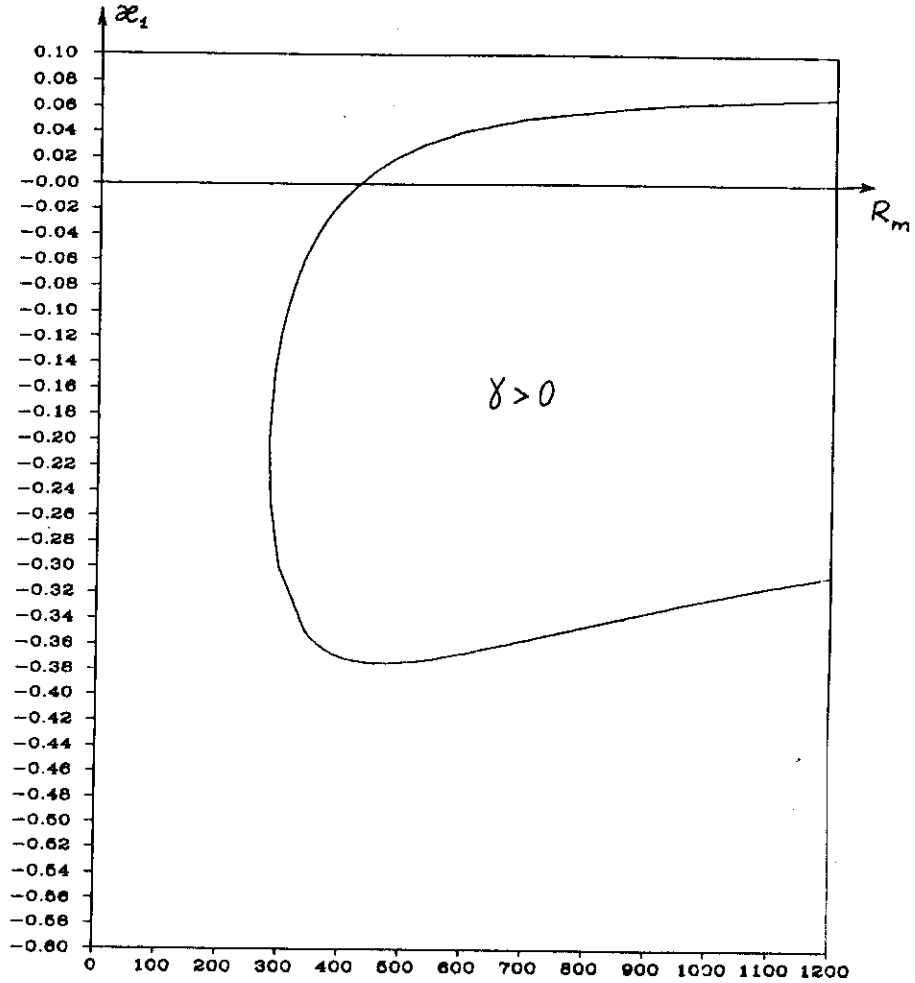

FIGURE 23. The curve $\gamma^*_{29} = 0$ on the plane R_m, κ_1 for $\eta = 0.75$, $n = 1$, $\kappa = 0.88$, $\alpha = -1.14$ in the case of the dielectric boundaries.

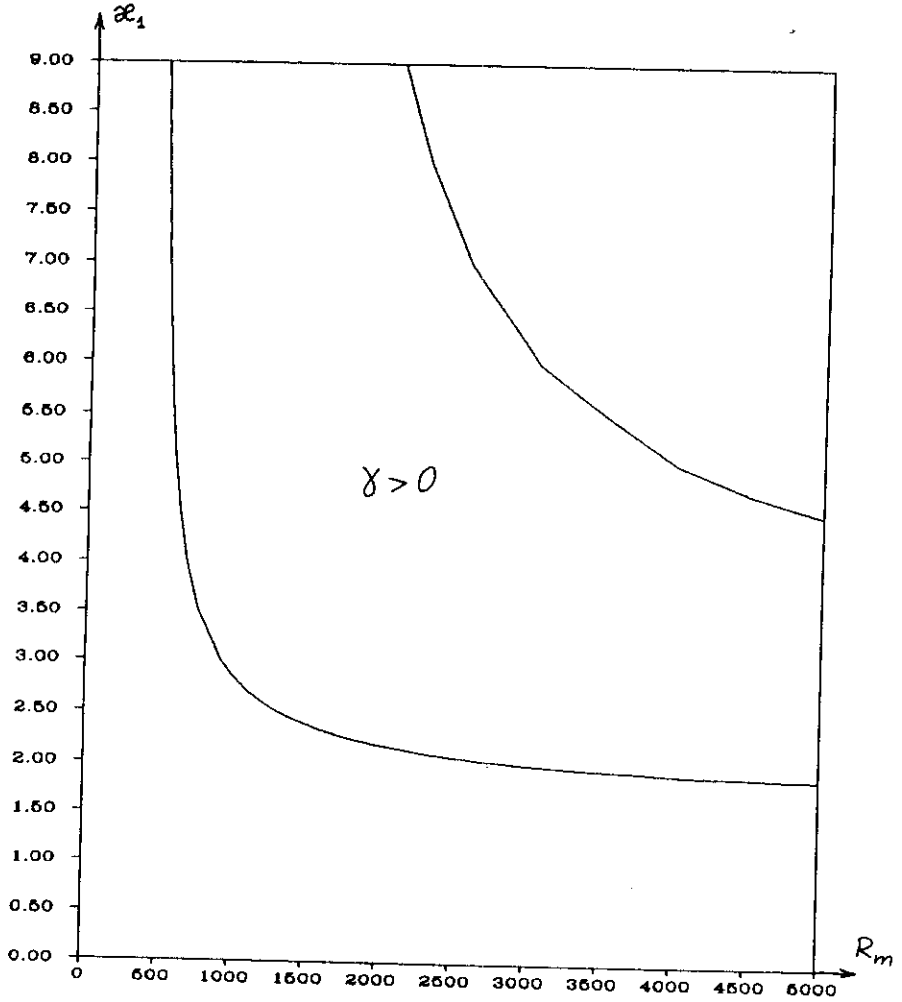

FIGURE 24. The curves $\gamma^*_{29} = 0$ on the plane R_m, κ_1 for $\eta = 0.5$, $n = 1$, $\kappa = 0.75$, $\alpha = 1.25$ in the case of the dielectric boundaries.

$R^1_m < R_m < R^2_m$, i.e. the magnetic dynamo does not exist for the values of R_m which are great enough but exists for the smaller values of R_m. Tables 2-4 contain the dependence on R_m of the values of γ^*_K obtained by the Galerkin method with the different values of K. The values of γ^*_K presented in Tables 2-4 estimate the maximums γ of the real parts of the eigenvalues of the boundary problem (24), (25) for $\kappa_1 = -6.5$ (Table 2), $\kappa_1 = -2$ (Table 3), $\kappa_1 = -0.525$ (Table 4) and the same values of η, n, α, and κ for which the regions in Figures 17, 18, and 19 were constructed respectively.

Table 2 shows that the using of the value of γ^*_{13} does not offer to detect the magnetic dynamo existence for $\kappa_1 = -6.5$. This was a reason of using of the curves $\gamma^*_{29} = 0$ (instead of $\gamma^*_{13} = 0$) as the boundaries of the regions of the magnetic dynamo existence in Figures 17-24.

The form of the region of the magnetic dynamo existence shown in Figure 18 permit to make an assumption that if the value of κ_1 is close to -0.7 then the magnetic dynamo exists for $R^1_m < R_m < R^2_m$ and for $R_m > R^3_m$ ($R^3_m > R^2_m$). This assumption is confirmed by the results of the calculation of the values of γ^*_K presented in Table 5. These results were obtained for $\kappa_1 = -0.7$ and the same values of η, n, α,

TABLE 2

R_m	γ^*_{13}	γ^*_{29}	γ^*_{69}
225	-0.41626	-0.05311	
250	-0.20585	-0.19673	0.23767
275	-0.08839	0.34910	
300	-0.05706	0.41017	
325	-0.10567	0.38563	
350	-0.22859	0.28067	
375	-0.42074	0.10003	
400	-0.67750	-0.15188	-0.09606

TABLE 3

R_m	γ^*_{13}	γ^*_{29}	γ^*_{69}
130	-1.95262	-1.96603	
180	0.61885	0.57667	
230	2.40275	2.32295	2.31804
280	3.35634	3.23110	
330	3.48607	3.30952	
380	2.79659	2.56597	
430	1.29104	1.00877	
480	-1.01571	-1.33881	-1.36620

TABLE 4

R_m	γ^*_{13}	γ^*_{29}	γ^*_{69}
175	-0.02160	-0.02501	
180	0.00562	0.00192	
185	0.02550	0.02149	
190	0.03792	0.03359	
195	0.04279	0.03812	0.03818
200	0.04004	0.03501	
205	0.02961	0.02419	
210	0.01145	0.00564	
215	-0.01444	-0.02067	-0.02066

TABLE 5

R_m	γ^*_{13}	γ^*_{29}	γ^*_{69}
900	6.71632	6.38460	6.34603
1200	-4.04723	-3.81965	
1500	-5.44053	-5.18908	
1800	-4.04538	-3.87839	-3.85894
2100	-2.17842	-2.05597	
2400	-0.46492	-0.30902	
2700	0.91169	1.19453	1.20510

and κ for which the regions in Figure 18 was constructed.

The fact that the dynamo action vanishes with increase of R_m was noted earlier for other flows of a conducting fluid by Arnold and Korkina (1983), Arnold (1984), and Galloway and Frisch (1984).

Note that the region of magnetic dynamo existence is reduced when the value of η is close to 1 (Figures 19 and 23).

The forms of the regions in Figures 18, 20, 22, and 24 furnish an assumption that if $\eta = 0.5$, $n = 1$, $\alpha = -1.25$ (or 1.25), $\kappa = 0.75$, the value of $|\kappa_1|$ is great enough, and the value of R_m belongs to some segment then the magnetic dynamo exists. Note that in the case of the dielectric boundaries the region of the magnetic dynamo existence for $\eta = 0.5$, $n = 1$, $\alpha = -1.25$, and $\kappa = 0.75$ (Figure 22) consists of the two separate subregions.

The results of the construction of the regions of the magnetic dynamo existence furnish the following general conclusions:

1. For $\kappa_1 < 0$ and $n = 1$ magnetic field generation is possible if $\alpha\kappa > 0$. If the value of $|\kappa_1|$ is great enough then the magnetic dynamo exists only for the values of R_m which belong to some segment. In some cases the dynamo action vanishes with increase of R_m and appears again for the greater values of R_m.
2. For the small positive values of κ_1 and $n = 1$ the magnetic dynamo exists if $\alpha\kappa < 0$ and the value of R_m exceeds some threshold.
3. There is the segment of the positive values of κ_1 between 0.25 and 1 for which the magnetic dynamo is not possible if $n = 1$.
4. For the greater positive values of κ_1 and $n = 1$ the magnetic dynamo exists if $\alpha\kappa > 0$. If the value of κ_1 is not too great then magnetic field generation is possible for the all values of R_m exceeding some threshold. For the greater values of κ_1 the magnetic dynamo exists only if the value of R_m belongs to some segment.
5. In the case of the perfect conductor boundaries magnetic field generation is possible for the smaller values of R_m than in the case of dielectric boundaries. This is particularly pronounced for the

values of η which are close to 1 (Figures 19 and 23).

The calculations were made to find the minimal values of R_m for which the magnetic dynamo exists. Let $\Omega_2 = 0$ and the values of η, n, and κ_1 are fixed. Let also there are the values of α and γ and $R_m = R_m^c$ for which $\gamma(R_m^c, \alpha, \kappa) \geq 0$. Then in the case of the perfect conductor boundaries (the boundary problem (24), (25)) the minimal value R_m^{min} of R_m for which $\gamma \geq 0$ for some values of α and κ is defined by the formula

$$R_m^{min} = R_m^c \sqrt{1 - \left[\min_{\alpha,\kappa}\left[(1+\kappa^2)\left(1 + \frac{\alpha^2}{\gamma(R_m^c,\alpha,\kappa)}\right)\right]\right]^{-1}} \qquad (48)$$

where the minimum is taken with respect to those pairs α, κ for which $\gamma(R_m^c, \alpha, \kappa) > 0$.

Table 6 contains the minimal values R_m^{min} of R_m for which the magnetic dynamo exists. These values were obtained for $\Omega_2 = 0$, $n = 1$, $\kappa_1 = 0$, and different values of η. Instead of γ its approximation γ_{13}^* calculated by the Galerkin method was used. In the case of the perfect conductor boundaries formula (48) with $R_m^c = 200$ was applied to obtain the values of $R_m^{min}(\eta)$. In the case of the dielectric boundaries this formula cannot be applied and for the values of R_m changing with the step 1 the attempt was made to find by the gradient method the values of κ and α for which $\gamma \geq 0$. The minimum value of R_m for which this attempt was successful was taken as $R_m^{min}(\eta)$. Table 6 contains also the values $\kappa(\eta)$ and $\alpha(\eta)$ for which $\gamma(R_m^{min}(\eta), \kappa(\eta), \alpha(\eta)) \geq 0$ and the values of the ratio $\alpha(\eta)/\kappa(\eta)$.

Table 6 shows that in the case of the perfect conductor boundaries the minimal with respect to η value of $R_m^{min}(\eta)$ is reached when $\eta = 0.3$. In the case of the dielectric boundaries the value of

TABLE 6

η	Perfect conductor boundaries				Dielectric boundaries			
	$R_m^{min}(\eta)$	$\kappa(\eta)$	$\alpha(\eta)$	$\frac{\alpha(\eta)}{\kappa(\eta)}$	$R_m^{min}(\eta)$	$\kappa(\eta)$	$\alpha(\eta)$	$\frac{\alpha(\eta)}{\kappa(\eta)}$
0.15	119.8	0.5250	-1.0319	-1.97	124	0.6324	-1.303	-2.06
0.20	98.3	0.5127	-1.0924					
0.25	87.4	0.5333	-1.1173	-2.10	104	0.6300	-1.313	-2.08
0.30	82.3	0.5892	-1.1987					
0.50	91.2	0.7330	-1.2304	-1.68	145	0.8186	-1.358	-1.66
0.75	181.7	0.8796	-1.1377	-1.29	415	1.0355	-1.333	-1.29

$R_m^{min}(\eta)$ obtained for $\eta = 0.75$ confirms the fact noted above that for $\eta = 0.75$, $R_m = 200$, $n = 1$, and $\kappa_1 = 0$ there are not any values of κ, α for which $\gamma \geq 0$. The comparison of the values of $R_m^{min}(\eta)$ obtained for different boundary conditions shows that the magnetic field can be generated for the smaller values of R_m in the case of the perfect conductor boundaries than in the case of the dielectric boundaries. The values of the ratio $\alpha(\eta)/\kappa(\eta)$ for the different boundary conditions are close. For the both boundary conditions the value of $\alpha(\eta)$ changes slightly as a function of η and the value of $\kappa(\eta)$ is minimal when $\eta = 0.20 \div 0.25$ and increases when the value of η increases.

Formula (48) was also used for the search of the minimal values R_m^{min} of R_m for which the magnetic dynamo exists for $\kappa_1 \neq 0$ in the case of the perfect conductor boundaries. The calculations were carried out for $n = 1$ and various values of κ_1. For fixed κ_1 the value of η increased by increments of 0.01 and formula (48) was used to compute R_m^{min}. Denote $R_m^{min}(\kappa_1)$ the minimal value of R_m^{min} over all these steps and by $\eta^{min}(\kappa_1)$ the value of η at which $R_m^{min}(\kappa_1)$ is attained. Denote also

$$\alpha^{min}(\kappa_1) = \frac{\alpha'}{\sqrt{\xi^2(1+(\kappa')^2) - (\kappa')^2}}$$

and

$$\kappa^{min}(\kappa_1) = \frac{\kappa'}{\sqrt{\xi^2(1 + (\kappa')^2) - (\kappa')^2}}$$

where $\xi = \frac{R_m^c}{R_m^{min}(\kappa_1)}$ and α' and κ' are the values of α and κ at which the minimum in (48) is attained when $\eta = \eta^{min}(\kappa_1)$. If $\eta = \eta^{min}(\kappa_1)$, $\kappa = \kappa^{min}(\kappa_1)$, $\alpha = \alpha^{min}(\kappa_1)$, and $R_m > R_m^{min}(\kappa_1)$ then the magnetic dynamo exists. The results of the calculations are listed in Table 7. Instead of γ its approximations calculated by the Galerkin method were used (γ_{15}^* for $\kappa_1 = 0.25$ and γ_{13}^* for other values of κ_1).

Table 7 shows that the minimal threshold value $R_m \sim 48$ is

TABLE 7

κ_1	$R_m^{min}(\kappa_1)$	$\eta^{min}(\kappa_1)$	$\kappa^{min}(\kappa_1)$	$\alpha^{min}(\kappa_1)$
$U_c = 0$, $U_p > 0$	88.3	0.20	0.5596	1.9774
10	96.0	0.20	0.5415	2.0644
8	98.3	0.20	0.5448	2.1132
4	111.7	0.20	0.5109	2.2280
2	153.8	0.19	0.4127	2.5006
1	380.4	0.20	0.2573	3.2000
0.25	897.2	0.13	0.2560	-1.4848
0.125	181.7	0.32	0.4595	-0.8854
0.1	139.0	0.34	0.5053	-0.9954
0	80.9	0.35	0.6035	-1.1862
-0.1	63.6	0.35	0.6598	-1.2922
-0.125	61.0	0.35	0.6603	-1.2919
-0.25	53.0	0.34	0.6665	-1.3329
-0.4	49.1	0.33	0.6442	-1.3243
-0.5	48.3	0.32	0.6104	-1.2926
-0.6	48.4	0.32	0.6086	-1.3247
-1	55.7	0.29	0.5424	-1.3258
-1.5	64.4	0.23	0.6116	-1.6220
-2	68.0	0.22	0.6338	-1.7240
-4	75.2	0.21	0.6084	-1.8253
-8	80.8	0.21	0.6045	-1.9176
-10	82.1	0.21	0.5911	-1.9161
$U_c = 0$, $U_p < 0$	88.3	0.20	0.5596	-1.9774

TABLE 8

R_m	γ_{13}^*	γ_{29}^*
48.0	-0.0255	-0.0157
48.1	-0.0153	-0.0056
48.2	-0.0052	0.0046
48.3	0.0049	0.0147

reached when $\kappa_1 \sim -0.5$. This value of κ_1 means that the pressure gradient has an opposite direction to the velocity of the axial motion of the inner cylinder and the value of U_p is half that of U_c. The situation is less suitable for the magnetic field generation if $U_c/10 < U_p < 2U_c$ and the direction of the pressure gradient is the same as the axial velocity of the inner cylinder. Table 8 shows the dependence of γ on R_m near $R_m = 48$ when $n = 1$, $\kappa_1 = -0.5$, $\eta = 0.32$, $\kappa = 0.6104$, and $\alpha = -1.2926$. For the same values of parameters the boundaries (the curves $\gamma_{29}^* = 0$) of the region of the magnetic dynamo existence on the plane R_m, κ_1 are shown in Figure 25. The comparison of Figure 25 with Figures 17-24 shows that the region of the magnetic dynamo existence is considerably larger in the case of the parameter values for which the minimal threshold value of R_m is attained.

ASYMPTOTIC ANALYSIS

The change of variables

$$S(r) = -\frac{i\Phi(r)}{\sqrt{1 + \frac{iR_m B}{n}}} \qquad (49)$$

is convenient for analysis of dynamo action for $R_m \to \infty$. If the value of the square root with the positive real part is chosen in (49)

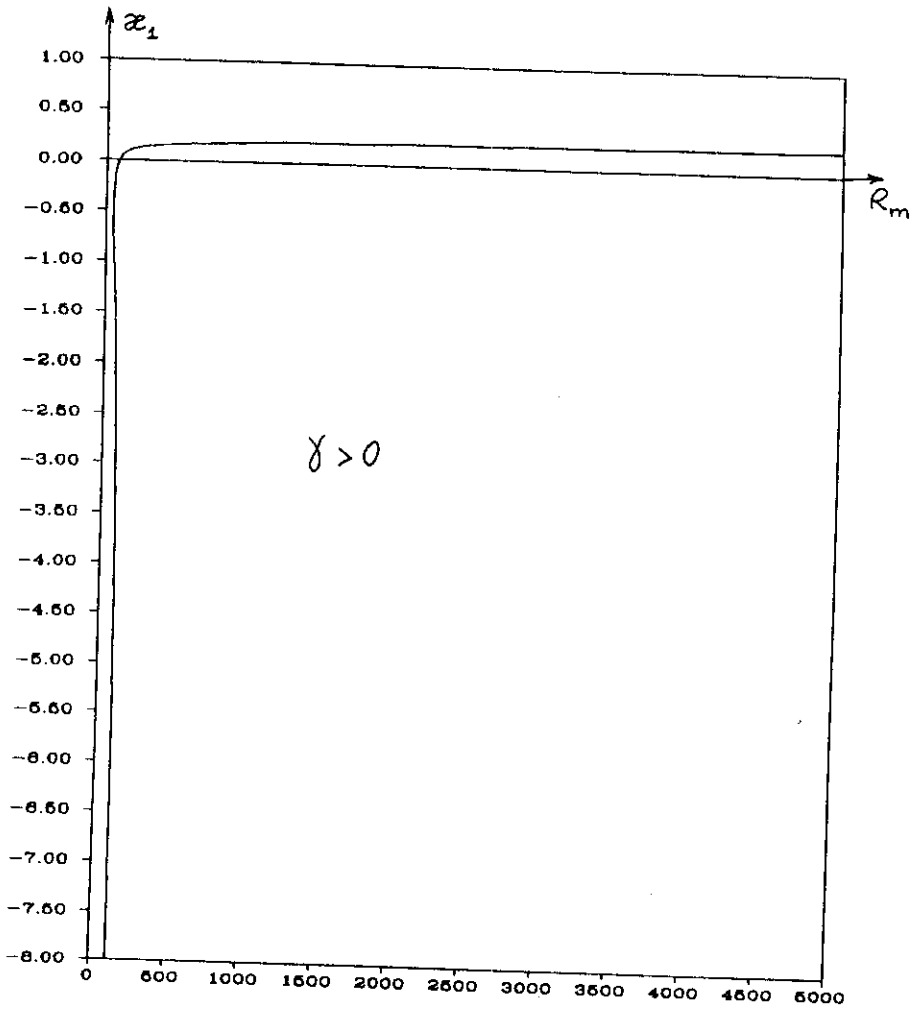

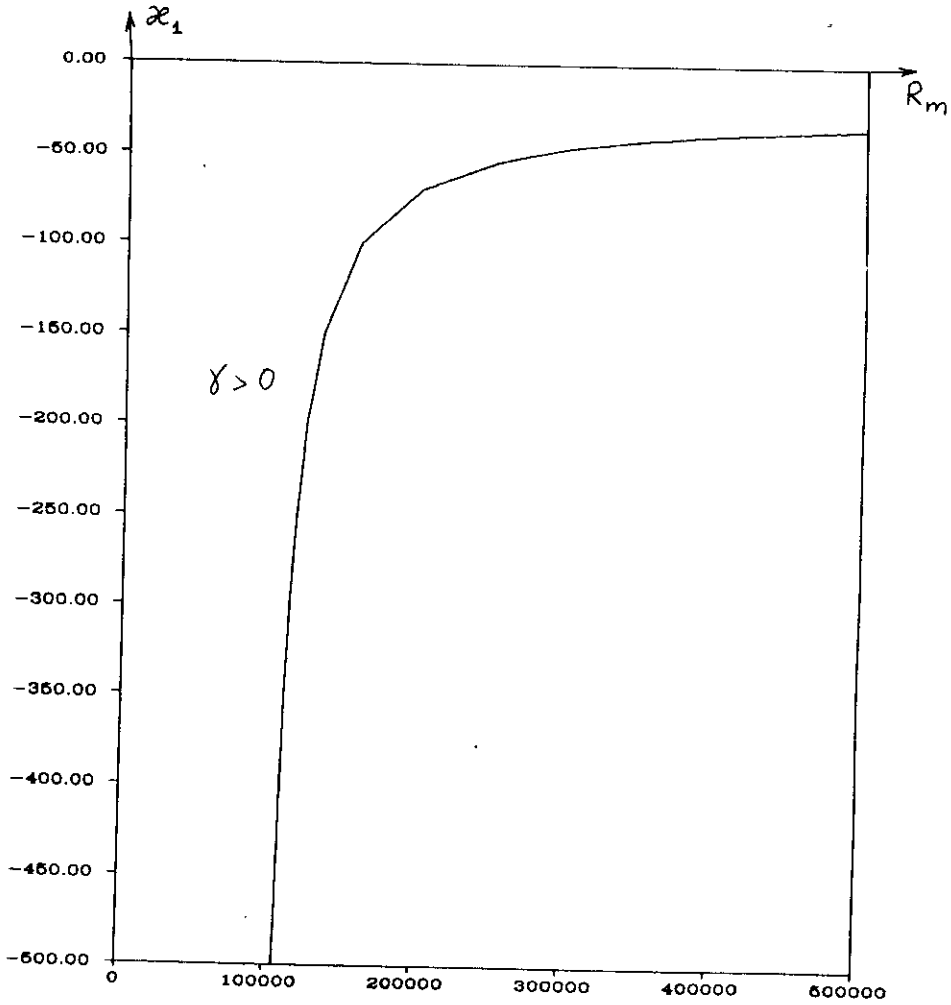

FIGURE 25. The curves $\gamma^{\circ}_{29} = 0$ on the plane R_m, κ_1 for $\eta = 0.32$, $n = 1$, $\kappa = 0.6104$, $\alpha = -1.2926$ in the case of the perfect conductor boundaries.

then equations (24) take the form

$$\frac{d^2R}{dr^2} - \frac{1}{r}\frac{dR}{dr} - (Q(r) + p)R + \frac{2n}{r^2}\sqrt{1 + \frac{iR_mB}{n}}\,S = 0\,,$$
$$\frac{d^2S}{dr^2} - \frac{1}{r}\frac{dS}{dr} - (Q(r) + p)S + \frac{2n}{r^2}\sqrt{1 + \frac{iR_mB}{n}}\,R = 0\,. \qquad (50)$$

After the change of the independent variable $x = r^2$ the first derivatives are excluded and equations (50) take the form

$$\frac{d^2R}{dx^2} - \frac{Q(\sqrt{x}) + p}{4x}R + \frac{n}{4x^2}\sqrt{1 + \frac{iR_mB}{n}}\,S = 0\,,$$
$$\frac{d^2S}{dx^2} - \frac{Q(\sqrt{x}) + p}{4x}S + \frac{n}{4x^2}\sqrt{1 + \frac{iR_mB}{n}}\,R = 0\,. \qquad (51)$$

System (51) is considered over the interval $[\eta^2, 1]$. The boundary conditions (25) for system (51) take the form

$$R(\eta^2) = R(1) = 0, \quad S'(\eta^2) = S'(1) = 0. \qquad (52)$$

Multiply the first equation (51) by the function $\overline{R(x)}$ which is conjugate complex to the function $R(x)$ and the second equation (51) by the function $\overline{S(x)}$ which is conjugate complex to the function $S(x)$. After integration of the sum of these equations over the segment $[\eta^2, 1]$ with regard for formulas (15) and the boundary conditions (52) the following equation for the real part will be obtained

$$\left\|\frac{df}{dx}\right\|^2 + \frac{n^2}{4}\left\|\frac{f(x)}{x}\right\|^2 + \frac{\alpha^2 + u}{4}\left\|\frac{f(x)}{\sqrt{x}}\right\|^2 + n\mathrm{Re}\sqrt{1 + \frac{iR_mB}{n}}\,\mathrm{Re}\int_{\eta^2}^{1}\frac{\overline{SR}}{x^2}dx = 0\,. \qquad (53)$$

Here $u = \mathrm{Re}p$, $v = \mathrm{Im}p$, and the magnitude of the vector-function

$f(x) = (R(x), S(x))$ is defined as follows

$$\|f(x)\| = \sqrt{\int_{\eta^2}^{1}\overline{RR}dx + \int_{\eta^2}^{1}\overline{SS}dx}\,.$$

By definition of the change of variables $\mathrm{Re}\sqrt{1 + \frac{iR_mB}{n}} > 0$ and the following inequality follows from (53)

$$(\alpha^2 + u)\left\|\frac{f(x)}{\sqrt{x}}\right\|^2 \le -n^2\left\|\frac{f(x)}{x}\right\|^2 + 4|n|\mathrm{Re}\sqrt{1 + \frac{iR_mB}{n}}\left|\mathrm{Re}\int_{\eta^2}^{1}\frac{\overline{SR}}{x^2}dx\right|\,. \qquad (54)$$

By using the inequalities

$$\left|\mathrm{Re}\int_{\eta^2}^{1}\frac{\overline{SR}}{x^2}dx\right| \le \int_{\eta^2}^{1}\frac{|S||R|}{x^2}dx \le \frac{1}{2}\int_{\eta^2}^{1}\frac{\overline{SS} + \overline{RR}}{x^2}dx \le \frac{1}{2}\left\|\frac{f(x)}{x}\right\|^2$$

and

$$\left\|\frac{f(x)}{x}\right\|^2 = \int_{\eta^2}^{1}\frac{\overline{SS} + \overline{RR}}{x^2}dx \le \frac{1}{\eta^2}\int_{\eta^2}^{1}\frac{\overline{SS} + \overline{RR}}{x}dx = \frac{1}{\eta^2}\left\|\frac{f(x)}{\sqrt{x}}\right\|^2$$

and the formula

$$\mathrm{Re}\sqrt{1 + \frac{iR_mB}{n}} = \frac{1}{\sqrt{2}}\sqrt{1 + \sqrt{1 + \frac{R_m^2B^2}{n^2}}}$$

the inequality

$$u \le -\alpha^2 + \frac{|n|}{\eta^2}\left(\sqrt{2}\sqrt{1 + \sqrt{1 + \frac{R_m^2B^2}{n^2}}} - |n|\right) \qquad (55)$$

is obtained from (54).

It follows from inequality (55) that the considered harmonic in the expansion of the initial magnetic field distribution is excited ($u > 0$) only if $n \neq 0$. This corresponds to the known fact (Cowling, 1934; Braginsky, 1964) that the axially symmetrical magnetic field ($n = 0$) cannot be excited by the axially symmetrical motion of an

electrically conducting fluid, as the helical Couette-Poiseuille flow. Note that if

$$n^6 - 4n^4 \geq 4R_m^2B^2$$

then

$$\sqrt{2}\sqrt{1 + \sqrt{1 + \frac{R_m^2B^2}{n^2}}} - |n| \leq 0$$

and the harmonic is not excited also. If

$$n^6 - 4n^4 < 4R_m^2B^2$$

the harmonic is not excited for the large values of α^2 for which the right part of inequality (55) is negative.

It follows from (55) that if the harmonic is excited for $R_m \to \infty$ then the growth rate of γ is limited by $\sqrt{R_m}$. With regard for the typical time accepted and the definition of R_m (12) it means that there is not a fast dynamo for the considered flow of an electrically conducting fluid. It follows from the analysis of the imaginary part of the integrated sum of equations (51) multiplied by the functions $\overline{R(x)}$ and $\overline{S(x)}$ that $|v| = O(R_m)$ for $R_m \to \infty$.

The detailed analysis of the asymptotic behavior of the magnetic field generation process in the Couette-Poiseuille flow of an electrically conducting fluid is carried out by using the methods developed by Ruzmaikin et al. (1987). These methods are based on the theory of singular perturbations.

It was shown by Ruzmaikin et al. (1987) that in the case of dynamo action for $R_m \to \infty$ the following asymptotic relations must be satisfied:

$$\frac{1}{R}\frac{dR}{dr} \sim R_m^{1/4}, \quad \frac{1}{R}\frac{d^2R}{dr^2} \sim R_m^{1/2}, \quad \frac{1}{\Phi}\frac{d\Phi}{dr} \sim R_m^{1/4},$$
$$\frac{1}{\Phi}\frac{d^2\Phi}{dr^2} \sim R_m^{1/2}, \quad Q(r) + p \sim R_m^{1/2}, \quad \frac{\Phi}{R} \sim R_m^{1/2}. \tag{56}$$

It follows from (15) that the relation $Q(r) + p \sim R_m^{1/2}$ cannot be true over the entire interval $[\eta, 1]$. However, it can be satisfied in the vicinity of some point $r_0 \in [\eta, 1]$. Then the eigenvalue takes the form

$$p = -iR_m q(r_0) + p', \quad p' \sim R_m^{1/2}. \tag{57}$$

The magnetic field concentrates in this vicinity in the process of excitation. This means that the eigenfunctions $R(r)$ and $\Phi(r)$ of the boundary problem (24), (25) (or (24), (34)) associated with an eigenvalue having a positive real part are essentially nonzero in the vicinity of r_0. According to Ruzmaikin et al. (1987), the asymptotic relation $Q(r) + p \sim R_m^{1/2}$ holds in the vicinity of r_0 of size $r - r_0 = O(R_m^{-1/4})$. By (15) this can only happen if

$$\left.\frac{dq}{dr}\right|_{r=r_0} = 0 . \tag{58}$$

Then it is possible to find r_0 from (58).

The system of differential equations (24) is defined on the interval $[\eta, 1]$. Consequently the point of concentration must fall into this range. This means that the magnetic field concentrates between the cylinders. Thus a necessary condition of magnetic dynamo action may be obtained from (58) for the Couette-Poiseuille flow. This condition states that at least one root of this equation must fall into the interval $[\eta, 1]$.

The analysis of equation (58) is easier for a helical Couette flow of a conducting fluid, that is, in the absence of an axial pressure gradient ($U_p = 0$). In that case equation (58) reduces to

$$-\frac{2\eta\kappa n}{1 - \eta^2} + \frac{\alpha}{\ln\eta}r_0^2 = 0 . \tag{59}$$

Equation (59) has one and only one root

$$r_0 = \sqrt{\frac{2\eta\kappa n \ln\eta}{\alpha(1 - \eta^2)}} \tag{60}$$

belonging to the interval $[\eta, 1]$, if and only if the following inequalities are true

$$\frac{1-\eta^2}{2\eta\ln\eta} < \frac{\kappa n}{\alpha} < \frac{\eta(1-\eta^2)}{2\ln\eta} \quad . \tag{61}$$

Inequalities (61) are necessary conditions for magnetic field excitation. They relate the values of η and κ specifying the helical Couette flow configuration to the values of n and α specifying the harmonic of the initial magnetic field. It follows from inequalities (61) that no magnetic field excited if $n > 0$ and the signs of κ and α are the same. This was noted above as a result of the numerical analysis for $n = 1$.

For $U_p \neq 0$, (15) leads to

$$\frac{dq}{dr} = -\frac{2nB}{\sigma}\left(r - 2\tau\frac{1}{r} + \sigma\frac{1}{r^3}\right) \tag{62}$$

where

$$\sigma = \frac{n\kappa\eta d(\eta)\sqrt{U_c^2 + U_p^2}}{2(1-\eta^2)\alpha U_p \ln\eta} \quad , \quad \tau = -\frac{1-\eta^2}{4\ln\eta} + \frac{U_c d(\eta)}{8U_p \ln^2\eta} \quad . \tag{63}$$

Equation (58) now reduces to the following equation in r_0:

$$r_0^4 - 2\tau r_0^2 + \sigma = 0 \tag{64}$$

whence $r_0^2 = \tau \mp \sqrt{\tau^2 - \sigma}$. The root of equation (64)

$$r_0 = \sqrt{\tau - \sqrt{\tau^2 - \sigma}} \tag{65}$$

is real and falls into the interval $[\eta, 1]$, if one of the following systems of inequalities is true:

$$\tau \geq 1 \ , \quad \eta^2(2\tau - \eta^2) < \sigma < 2\tau - 1 \tag{66}$$

or

$$\eta^2 < \tau < 1 \ , \quad \eta^2(2\tau - \eta^2) < \sigma < \tau^2. \tag{67}$$

The root

$$r_0 = \sqrt{\tau + \sqrt{\tau^2 - \sigma}} \tag{68}$$

is real and falls into the interval $[\eta, 1]$, if one of the following systems of inequalities is satisfied:

$$\tau \leq \eta^2, \quad 2\tau - 1 < \sigma < \eta^2(2\tau - \eta^2) \tag{69}$$

or

$$\eta^2 < \tau < 1 \ , \quad 2\tau - 1 < \sigma < \tau^2. \tag{70}$$

Note that there are values of σ and τ which satisfy to both systems of inequalities (67) and (70) simultaneously. In this case both roots, (65) and (68), of equation (64) fall into the interval $[\eta, 1]$. Thus if $U_p \neq 0$ then it is possible that there are two points of magnetic field concentration.

Make in (24) the change of variables (49). The inverse change of variables has the form

$$\Phi(r) = i\sqrt{1 + \frac{iR_m B}{n}}\, S(r) \quad . \tag{71}$$

Equations (24) are transformed into (50). Let there is at least one point of magnetic field concentration r_0 which falls into the interval $[\eta, 1]$. The eigenfunctions $R(r)$ and $S(r)$ associated with an eigenvalue having a positive real part concentrate in a vicinity of r_0 when $R_m \to \infty$ and it follows from (15), (56), and (71) that $R(r) = S(r)$.

Introduce the new independent variable $x = \varepsilon^{-1}(r - r_0)$ where $\varepsilon = R_m^{-1/4}$. Equations (50) now reduces to

$$\frac{1}{\varepsilon^2}\frac{d^2R}{dx^2} - \frac{1}{\varepsilon(r_0 + \varepsilon x)}\frac{dR}{dx} - \left[\frac{n^2}{(r_0 + \varepsilon x)^2} + \alpha^2 + p + \right.$$

$$+\frac{iq(r_0+\varepsilon x)}{\varepsilon^4}\Bigg]R+\frac{2n}{(r_0+\varepsilon x)^2}\sqrt{1+\frac{iB}{\varepsilon^4 n}}\,S=0\ ,$$

$$\frac{1}{\varepsilon^2}\frac{d^2S}{dx^2}-\frac{1}{\varepsilon(r_0+\varepsilon x)}\frac{dS}{dx}-\Bigg[\frac{n^2}{(r_0+\varepsilon x)^2}+\alpha^2+p+ \tag{72}$$

$$+\frac{iq(r_0+\varepsilon x)}{\varepsilon^4}\Bigg]S+\frac{2n}{(r_0+\varepsilon x)^2}\sqrt{1+\frac{iB}{\varepsilon^4 n}}\,R=0\ .$$

The end points of the interval $[\eta, 1]$ for the variable x are transformed into $x_1=\varepsilon^{-1}(\eta-r_0)$ and $x_2=\varepsilon^{-1}(1-r_0)$. If $R_m\to\infty$ then $\varepsilon\to 0$, $x_1\to-\infty$, and $x_2\to\infty$. Therefore the boundary conditions are naturally replaced by the following: $R(x)\to 0$ and $S(x)\to 0$ together with their derivatives for $x\to\pm\infty$. These boundary conditions agree with the given above definition of the magnetic field concentration in a vicinity of r_0 and do not depend on the assumed boundary conditions ((25) or (34)) for the functions $R(r)$ and $\Phi(r)$.

Consider now the equation

$$\frac{1}{\varepsilon^2}\frac{d^2R}{dx^2}-\frac{1}{\varepsilon(r_0+\varepsilon x)}\frac{dR}{dx}-\Bigg[\frac{n^2}{(r_0+\varepsilon x)^2}+\alpha^2+p+$$

$$+\frac{iq(r_0+\varepsilon x)}{\varepsilon^4}\Bigg]R+\frac{2n\psi}{(r_0+\varepsilon x)^2}\sqrt{1+\frac{iB}{\varepsilon^4 n}}\,S=0 \tag{73}$$

where $\psi=\pm 1$. If $R(x)$ is a solution of (73) and $R(x)\to 0$ together with its derivatives for $x\to\pm\infty$ then the pair $R(x)$, $S(x)=\psi R(x)$ is a solution of (72) with the boundary conditions formulated.

In accordance with (57) p' and $R(x)$ are represented below in the form of the asymptotic series

$$p'=\varepsilon^{-2}(p_0+\varepsilon p_1+\varepsilon^2 p_2+\ldots)\ ,$$

$$R(x)=R_0(x)+\varepsilon R_1(x)+\varepsilon^2 R_2(x)+\ldots\ . \tag{74}$$

Write the function $q(r_0+\varepsilon x)$ in the form of an asymptotic series,

$$q(r_0+\varepsilon x)=q_0+\varepsilon q_1 x+\varepsilon^2 q_2 x^2+\varepsilon q_3^3 x+\ldots\ . \tag{75}$$

It follows from (58) that

$$q_1=0\ . \tag{76}$$

The successive coefficients in (75) are defined by the formulas

$$q_2=\frac{1}{2}\frac{d^2q}{dr^2}\Big|_{r=r_0}\ ,\quad q_3=\frac{1}{6}\frac{d^3q}{dr^3}\Big|_{r=r_0}\ . \tag{77}$$

Substitute series (74), (75) into equation (73). Expand the coefficients on the left side of (73) in powers of ε and use relations (15), (57), and (76). Then the following equation is derived for the zero order approximation:

$$\frac{d^2R_0}{dx^2}-\left(iq_2x^2+p_0-\frac{2n\psi}{r_0^2}\sqrt{\frac{iB}{n}}\right)R_0=0 \tag{78}$$

where q_2 is defined by (77).

In accordance with the definition of change of variables (49), (71) the square root in (78) has the positive real part and it follows from (15) that

$$\sqrt{\frac{iB}{n}}=\sqrt{\frac{1}{2}\left|\frac{\beta}{n}\right|}(1+i\,\mathrm{sign}(\kappa n))\ . \tag{79}$$

To solve equation (78), make the change of variable (according to Ruzmaikin et al., 1987) $y=(iq_2)^{1/4}x$ and introduce the notation

$$s=\frac{1}{\sqrt{iq_2}}p_0 \tag{80}$$

where $\mathrm{Re}\sqrt{iq_2}>0$, that is,

$$\sqrt{iq_2}=\sqrt{\frac{|q_2|}{2}}(1+i\,\mathrm{sign}q_2)\ . \tag{81}$$

After the change of variable equation (78) takes the form

$$\frac{d^2R_0}{dy^2} - (s - \psi C\zeta + y^2)R_0 = 0 \tag{82}$$

where

$$C = \frac{2}{r_0^2}\sqrt{\left|\frac{nB}{q_2}\right|} ,$$

$$\zeta = \begin{cases} \text{sign}n, & \text{if } \kappa n q_2 > 0, \\ i\text{sign}, & \text{if } \kappa n q_2 < 0. \end{cases} \tag{83}$$

It was noted by Ruzmaikin et al. (1987) that equation (82) has the solution which vanishes for $x \to \pm\infty$, if

$$s = -(2m + 1) + \psi C\zeta \tag{84}$$

where $m = 0, 1, 2, \ldots$. This solution has the form

$$R_0(y) = \mathcal{K}H_m(y)\exp\left(-\frac{y^2}{2}\right) , \tag{85}$$

where $\mathcal{K}$ is an arbitrary complex constant and $H_m(y)$ is the Hermite polynomial of degree m.

If inequalities (61) are true for a helical Couette flow ($\kappa_1 = 0$), then (15), (77), and (83) yield

$$q_2 = \frac{2nB}{r_0^4} , \quad C = \sqrt{2} \tag{86}$$

where r_0 is defined by (60). It follows from (15) and (86) that $\kappa n q_2 > 0$. Therefore in accordance with (83)

$$\zeta = \text{sign}n . \tag{87}$$

By substituting (86) and (87) in (84) obtain

$$s = -(2m + 1) + \sqrt{2}\psi\text{sign}n . \tag{88}$$

As the real part of the square root in (80) is positive so $\text{Re}p_0 > 0$, if and only if $m = 0$ and $\psi = \text{sign}n$ in (88). Therefore if inequalities (61) are true then a helical Couette flow excites the considered harmonic of the magnetic field for $R_m \to \infty$.

Formulas (80), (81), (85), (86), and (88) lead for $m = 0$ and $\psi = \text{sign}n$ to the following form of the zero order approximation for a helical Couette flow:

$$p_0 = (\sqrt{2} - 1)\frac{\sqrt{|nB|}}{r_0^2}(1 + i\text{sign}(\kappa n)) ,$$

$$R_0(r) = \mathcal{K}\exp\left[-\frac{\sqrt{|nB|R_m}}{2r_0^2}(1 + i\text{sign}(\kappa n))(r - r_0)^2\right] . \tag{89}$$

In consequence of relations (56) and expansions (74), the function $\Phi(r)$ is represented by an asymptotic series in ε:

$$\Phi(x) = \varepsilon^{-2}(\Phi_0(x) + \varepsilon\Phi_1(x) + \varepsilon^2\Phi_2(x) + \ldots) . \tag{90}$$

Since $S(x) = \psi R(x)$, formula (71) leads to

$$\Phi_0(r) = \psi\sqrt{\frac{1}{2}\left|\frac{B}{n}\right|}(-\text{sign}(\kappa n) + i)R_0(r) . \tag{91}$$

By substituting (89) in formula (91) obtain for a helical Couette flow

$$\Phi_0(r) = \mathcal{K}\sqrt{\frac{1}{2}\left|\frac{B}{n}\right|}(-\text{sign}\kappa + i\text{sign}n)\times$$
$$\times\exp\left[\frac{\sqrt{|nB|R_m}}{2r_0^2}(1 + i\text{sign}(\kappa n))(r - r_0)^2\right] . \tag{92}$$

Note that in view of the analysis of Ruzmaikin et al. (1987), $p_1 = 0$ in expansions (74). This is proved by the following considerations. Denote by L the differentiation operator from the left part of equation (78)

$$L = \frac{d^2}{dx^2} - \left(iq_2x^2 + p_0 - \frac{2n\psi}{r_0^2}\sqrt{\frac{iB}{n}}\right) . \tag{93}$$

Substitute series (74) and (75) in equation (73). By using formulas (15) and (76) the following equation is derived for the first order

approximation:

$$LR_1 = \frac{1}{r_0}\frac{dR_0}{dx} + (iq_3x^3 + p_1)R_0 + \frac{4n\psi}{r_0^3}\sqrt{\frac{IB}{n}}xR_0 \ , \qquad (94)$$

where q_3 is defined by (77). Consider the scalar product (f,g) in L_2 of two functions $f(x)$ and $g(x)$ which assume complex values:

$$(f,g) = \int_{-\infty}^{\infty} f(x)\overline{g(x)}dx \ .$$

It follows from the second formula of (89), the boundary conditions for the function $R_1(x)$, and formula (93) that there is the scalar product (LR_1,R_0) and

$$(LR_1,\bar{R}_0) = (R_1,\bar{\bar{L}}R_0) \qquad (95)$$

where $\bar{R}_0(x)$ is conjugate complex to the function $R(x)$ and $\bar{L}$ is conjugate to the operator L. As $R_0(x)$ is a solution of equation (78) so $LR_0 = 0$ and $\bar{\bar{L}}R_0 = 0$. Therefore formula (95) leads to

$$(LR_1,\bar{R}_0) = 0 \ .$$

As the function $R_1(x)$ is a solution of equation (94) so the last quality leads the scalar product of the right part of equation (94) by the function $\bar{R}_0(x)$ to be equal to zero. Note that the second formula of (89) leads to

$$(x^{2k+1}R_0,\bar{R}_0) = 0$$

for every value of k and

$$(\frac{dR_0}{dx},\bar{R}_0) = 0 \ .$$

Therefore

$$p_1(R_0,\bar{R}_0) = 0 \ . \qquad (96)$$

As

$$\int_{-\infty}^{\infty} R_0^2(x)dx \neq 0$$

so (96) leads to

$$p_1 = 0 \ .$$

In the case of a helical Couette flow the formulas for $R_1(x)$ and p_2 can be obtained by the following way. It follows from equation (73), expansions (74) and (75), and formulas (15) that the equation for the l-th order approximation has the form

$$LR_l = G_l(x) \ , \qquad (97)$$

where the operator L is defined by (93) and the function $G_l(x)$ depends on the approximations of the lower orders than l. As the function $R_0(x)$ is the solution of equation (78) ($LR_0 = 0$) so if the function $R_l(x)$ is a solution of equation (97) then any function having the form $R_l(x) + CR_0(x)$ where C is an arbitrary complex constant is also a solution of equation (97). Therefore the boundary conditions that $R_l(x) \to 0$ together with its derivatives for $x \to \pm\infty$ is not sufficient for unambiguous determination of the function $R_l(x)$ from equation (97). To avoid this the following condition is formulated:

$$R_l(0) = 0 \ . \qquad (98)$$

Represent the function $R_l(x)$ in the form

$$R_l(x) = U_l(x)R_0(x) \ . \qquad (99)$$

If all functions $R_j(x)$ for $j = 1, 2, \ldots, l-1$ are presented in the the form (99) then the right part of equation (97) has the form

$$G_l(x) = g_l(x)R_0(x) \qquad (100)$$

where the function $g_l(x)$ depends on the functions $U_1(x)$, $U_2(x)$, ..., $U_{l-1}(x)$.

Substitute (99) in equation (97). It follows from formulas (85), (89), and (93) that the equation for the function $U_l(x)$ takes the form

$$\frac{d^2U_l}{dx^2} - 2\sqrt{iq_2}x\frac{dU_l}{dx} = g_l(x) \ . \qquad (101)$$

The general solution of equation (101) has the form

$$U_1(x) = \int\left(\int g_1(x)\exp(-\sqrt{iq_2}x^2)dx\right)dx \ . \qquad (102)$$

For a helical Couette flow formulas (15), (60), and (77) lead to

$$q_3 = -\frac{10}{3}\frac{nB}{r_0^5} \ . \qquad (103)$$

Formula (102) for $l = 1$, the form of the right part of equation (94), formulas (86), (100), and (103), and the relation $\psi = \mathrm{sign} n$ lead to

$$R_1(x) = \left[\frac{1}{r_0}\left(\frac{4}{3} - \sqrt{2}\right)x + \frac{5\sqrt{|\kappa n|}}{18r_0^3}(1 + i\,\mathrm{sign}(\kappa n))x^3\right]R_0(x) \ . \qquad (104)$$

The condition that $R_1(x) \to 0$ together with its derivatives for $x \to \pm\infty$ and condition (98) were used for determining of the values of arbitrary constants. The function $R_0(x)$ is defined by formulas (89).

The right part of equation (97) for the second order approximation has the form

$$G_2(x) = -\frac{x}{r_0^2}\frac{dR_0}{dx} + \left(iq_4x^4 + p_2 + \frac{n^2}{r_0^2} + \alpha^2 - \frac{6n\psi}{r_0^4}\sqrt{\frac{iB}{n}}x^2\right)R_0(x) +$$

$$+ \frac{1}{r_0}\frac{dR_1}{dx} + \left(iq_3x^3 + \frac{4n\psi}{r_0^3}\sqrt{\frac{iB}{n}}x\right)R_1(x) \qquad (105)$$

where in accordance with formulas (15) and (60)

$$q_4 = \frac{1}{24}\frac{d^4q}{dr^4}\Big|_{r=r_0} = \frac{9nB}{2r_0^6} \ . \qquad (106)$$

It was proved above that $(G_1, \bar{R}_0) = (LR_1, \bar{R}_0) = 0$. This proof can be applied for an equation for an approximation of any order. Therefore $(G_2, \bar{R}_0) = 0$. This equality and formulas (104)-(106) lead to the formula for coefficient p_2:

$$p_2 = -\left(n^2 - \frac{53}{36} + \sqrt{2}\right)\frac{1}{r_0^2} - \alpha^2 \ . \qquad (107)$$

Note that p_2 is a real number here.

Consider now the Couette-Poiseuille flow in the presence of an axial pressure gradient ($U_p \neq 0$).

Let equation (64) has a root which is real and falls into interval $[\eta, 1]$. Then formulas (62) and (77) yield

$$q_2 = -\frac{4nB}{\sigma r_0^4}(\tau r_0^2 - \sigma) \ . \qquad (108)$$

Expressions (83) and (108) lead to

$$C = \sqrt{\frac{1}{\left|1 - \frac{\tau}{\sigma}r_0^2\right|}} \ . \qquad (109)$$

It follows from formulas (80), (81), (83), and (84) that there exists an eigenvalue p_0 with $\mathrm{Re}p_0 > 0$ if and only if $C > 1$, which by (109) is equivalent to the inequalities

$$0 < \frac{\tau}{\sigma}r_0^2 < 2 \ . \qquad (110)$$

Inequalities (110) are satisfied only if $\frac{\tau}{\sigma} > 0$. If the value of r_0 is derived from (65), then

$$\frac{\tau}{\sigma}r_0^2 = 1 - \frac{\sqrt{\tau^2 - \sigma}}{\tau + \sqrt{\tau^2 - \sigma}} \ . \qquad (111)$$

If the value of r_0 is derived from (68), then

$$\frac{\tau}{\sigma}r_0^2 = 1 + \frac{\sqrt{\tau^2 - \sigma}}{\tau - \sqrt{\tau^2 - \sigma}} \ . \qquad (112)$$

Formula (111) shows that if the value of r_0 is derived from (65), then inequalities (110) follow both from (66) and from (67). Therefore if the value of r_0 derived from (65) is real and falls into the interval $[\eta, 1]$, then inequalities (110) are true.

If the value of r_0 is derived from (68), then it follows from (69), (70), and (112) that inequalities (110) are true for any

negative value of τ. For positive values of τ inequalities (110) are true if

$$\sigma > \frac{3}{4}\tau^2 . \qquad (113)$$

The results given above can be formulated geometrically. Denote the regions on the plane τ, σ where inequalities (66), (67), (69), and (70) are satisfied by O_1, O_2, O_3, and O_4 respectively. The regions O_2 and O_4 have a nonempty intersection O_5 (if a point occurs in O_5 then both roots, (65) and (68) belong to the interval $[\eta, 1]$). It follows from (110) and expressions (111) and (112) that an eigenvalue p_0 with $\mathrm{Re}p_0 > 0$ can be obtained in one of the following cases.

1. The point (τ, σ) belongs to the region O_1 or to the region O_2.
2. The point (τ, σ) belongs to the region $O_4 \setminus O_5$ and inequality (113) is true.
3. The point (τ, σ) belongs to the region O_3, $\tau > 0$, and inequality (113) is true.
4. The point (τ, σ) belongs to the region O_3 and $\tau < 0$.

Note that in cases 2-4 only one root (68) of equation (64) belongs to the interval $[\eta, 1]$ and $C > 1$ for this root. In case 1 only one root (65) belongs to the interval $[\eta, 1]$ if $(\tau,\sigma) \in O_1 \cup (O_2 \setminus O_5)$, and both roots (65) and (68) belongs to the interval $[\eta, 1]$ if $(\tau,\sigma) \in O_5$. Inequality $C > 1$ is always true for root (65). For root (68) $C > 1$, if inequality (113) is true. If $\eta > \frac{1}{\sqrt{3}}$ then inequality (113) is true for all points belonging to the region O_5. If $0 \le \tau \le \frac{2}{3}\eta^2$ then inequalities (113) and (69) cannot be true simultaneously. It means that no τ from the range $0 \le \tau \le \frac{2}{3}\eta^2$ will lead to an eigenvalue p_0 with $\mathrm{Re}p_0 > 0$.

Introduce the parameter $\xi = \frac{\kappa n}{\alpha}$. Then in accordance with

formulas (63) the values of σ and τ depend on three parameters: ξ, κ_1, and η. The regions of the magnetic dynamo existence for $R_m \to \infty$ ($\mathrm{Re}p_0 > 0$) can be constructed on the plane ξ, κ_1 for fixed values of η. Define the following regions on the plane ξ, κ_1: the region D_1 contains the points (ξ, κ_1) for which root (65) belongs to the interval $[\eta, 1]$ and either root (68) does not belong to the interval $[\eta, 1]$ or inequality (113) is not true; the region D_2 contains the points (ξ, κ_1) for which both roots (65) and (68) belong to the interval $[\eta, 1]$ and inequality (113) is true; the region D_3 contains the points (ξ, κ_1) for which root (68) belongs to the interval $[\eta, 1]$, inequality (113) is true, and root (65) does not belong to the interval $[\eta, 1]$; the region D_4 contains the points (ξ, κ_1) for which $\tau < 0$ and root (68) belongs to the interval $[\eta, 1]$; the region E contains the points (ξ, κ_1) for which root (65) does not belong to the interval $[\eta, 1]$ and root (68) belongs to the interval $[\eta, 1]$ but either $\frac{\tau}{\sigma} \le 0$ or inequality (113) is not true. These regions for $\eta = 0.05, 0.15, 0.25, 0.35, 0.5, 0.75$, and 0.9 are shown in Figures 26-32. An eigenvalue p_0 with $\mathrm{Re}p_0 > 0$ exists, if and only if the point (ξ,κ_1) belongs to the conjugation of the regions D_1, D_2, D_3, and D_4. In each of Figures 26-32 there is an interval of values of κ_1 covered by none of the regions D_1, D_2, D_3, and D_4. It means that it is impossible to obtain an eigenvalue p_0 with $\mathrm{Re}p_0 > 0$ for values of κ_1 from this interval. It follows from the definition of the regions D_1, D_2, D_3, and D_4 that values of κ_1 which are impossible in the conjugation of these regions are defined by the inequalities $0 \le \tau \le \frac{2}{3}\eta^2$. If $-\frac{1-\eta^2}{4\ln\eta} > \frac{2}{3}\eta^2$ then in accordance with (63) the interval of such values of κ_1 is limited, belongs to the region $\kappa_1 > 0$, and is defined by the inequalities

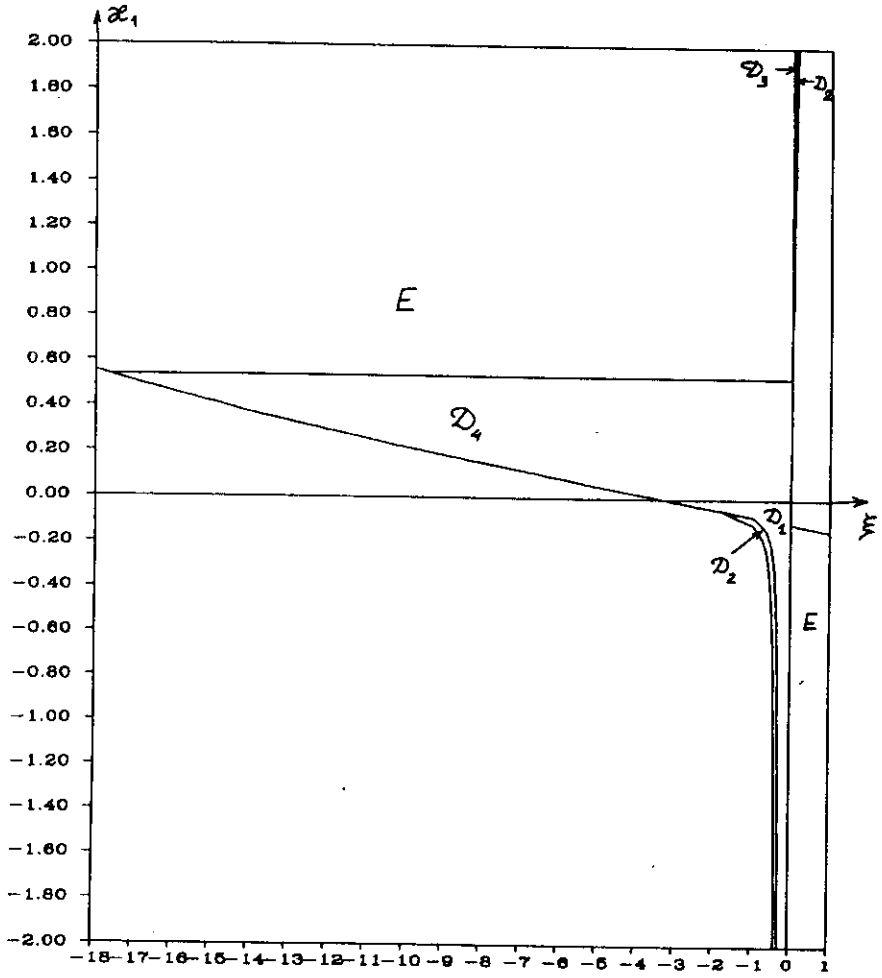

FIGURE 26. The regions D_1, D_2, D_3, D_4 and E on the plane ξ, κ_1 for $\eta = 0.05$.

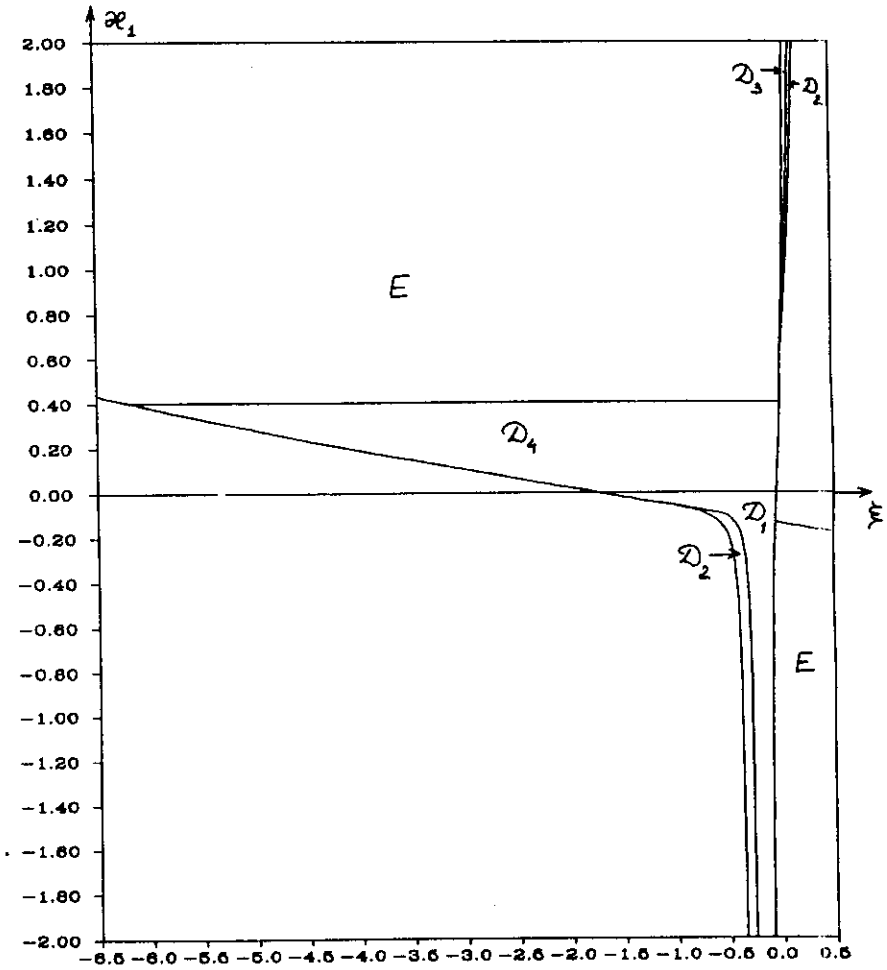

FIGURE 27. The regions D_1, D_2, D , D_4 and E on the plane ξ, κ_1 for $\eta = 0.15$.

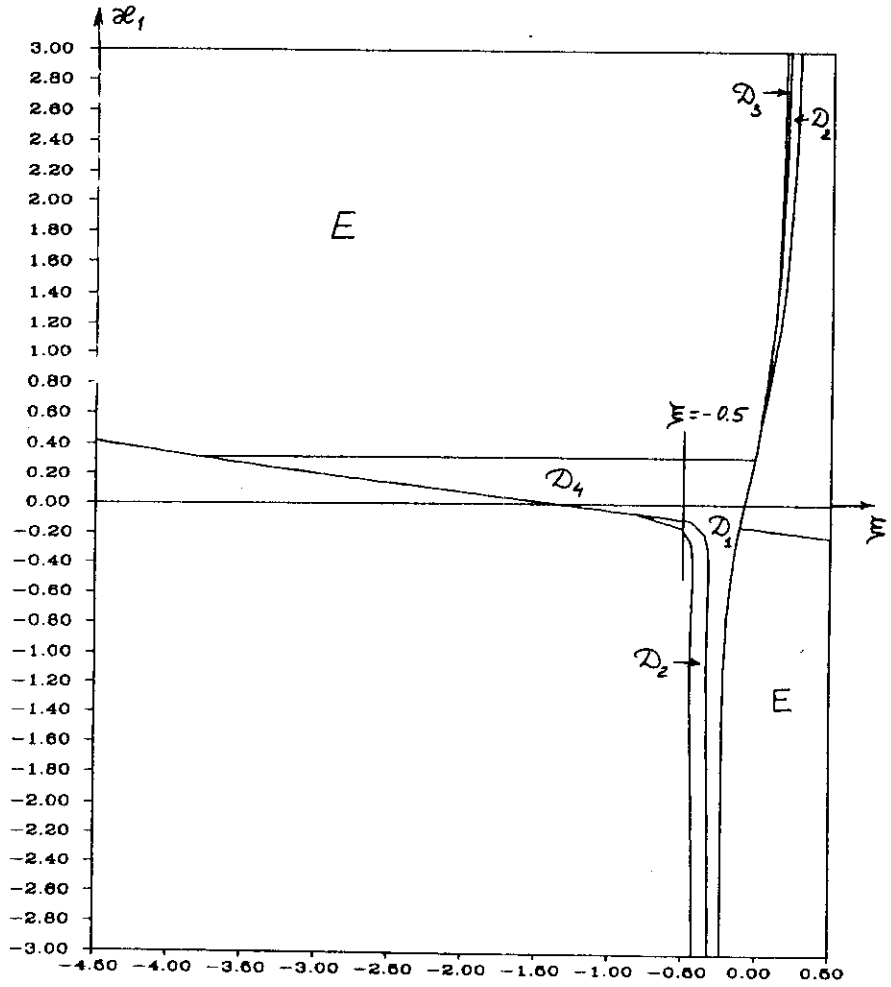

FIGURE 28. The regions D_1, D_2, D_3, D_4 and E on the plane ξ, κ_1 for $\eta = 0.25$.

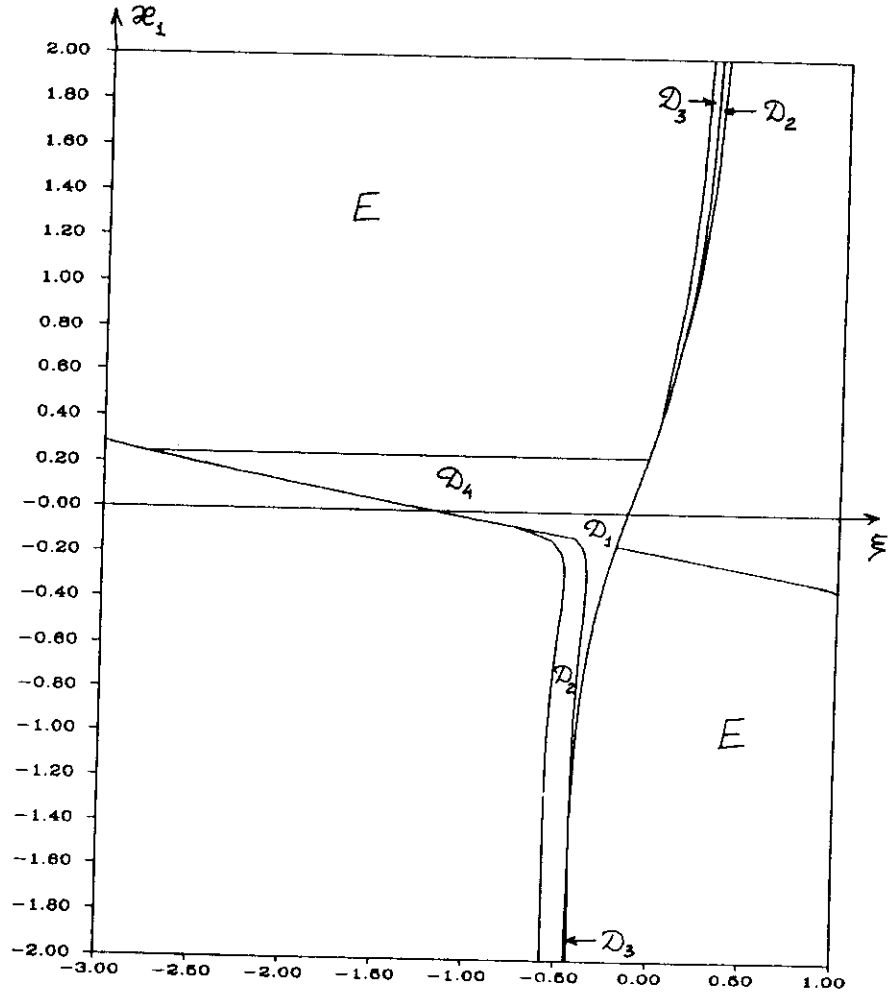

FIGURE 29. The regions D_1, D_2, D_3, D_4 and E on the plane ξ, κ_1 for $\eta = 0.35$.

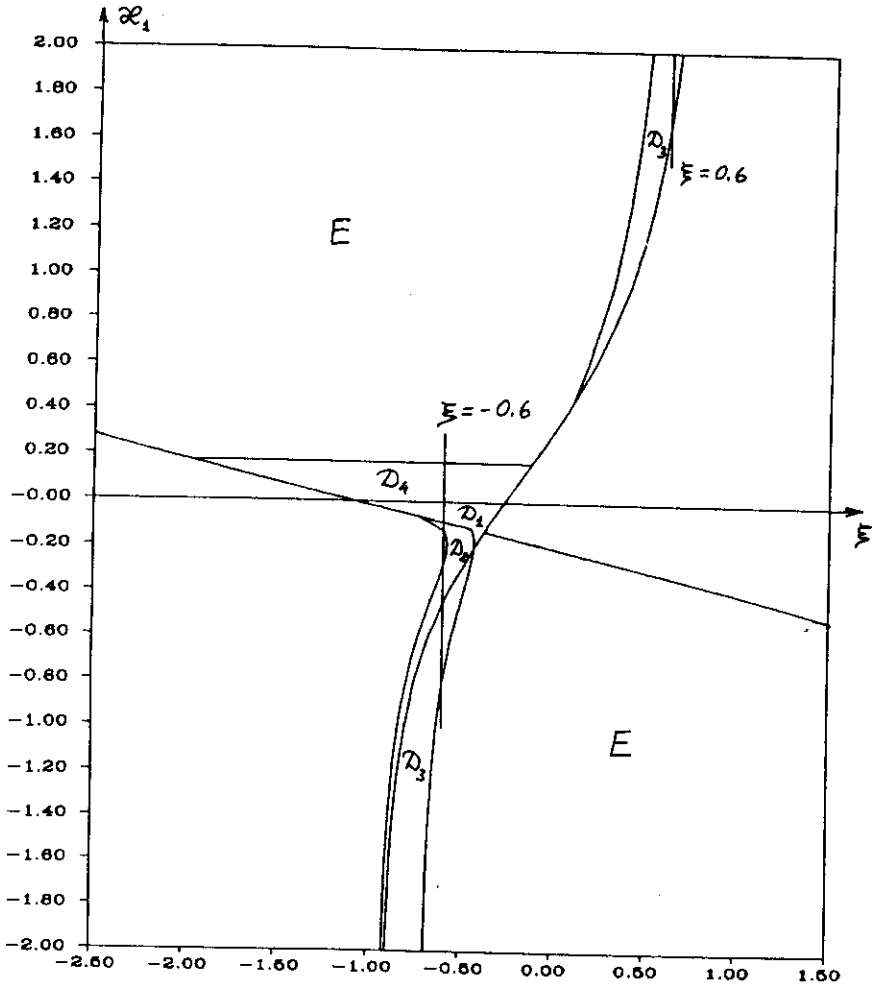

FIGURE 30. The regions D_1, D_2, D_3, D_4 and E on the plane ξ, κ_1 for $\eta = 0.5$.

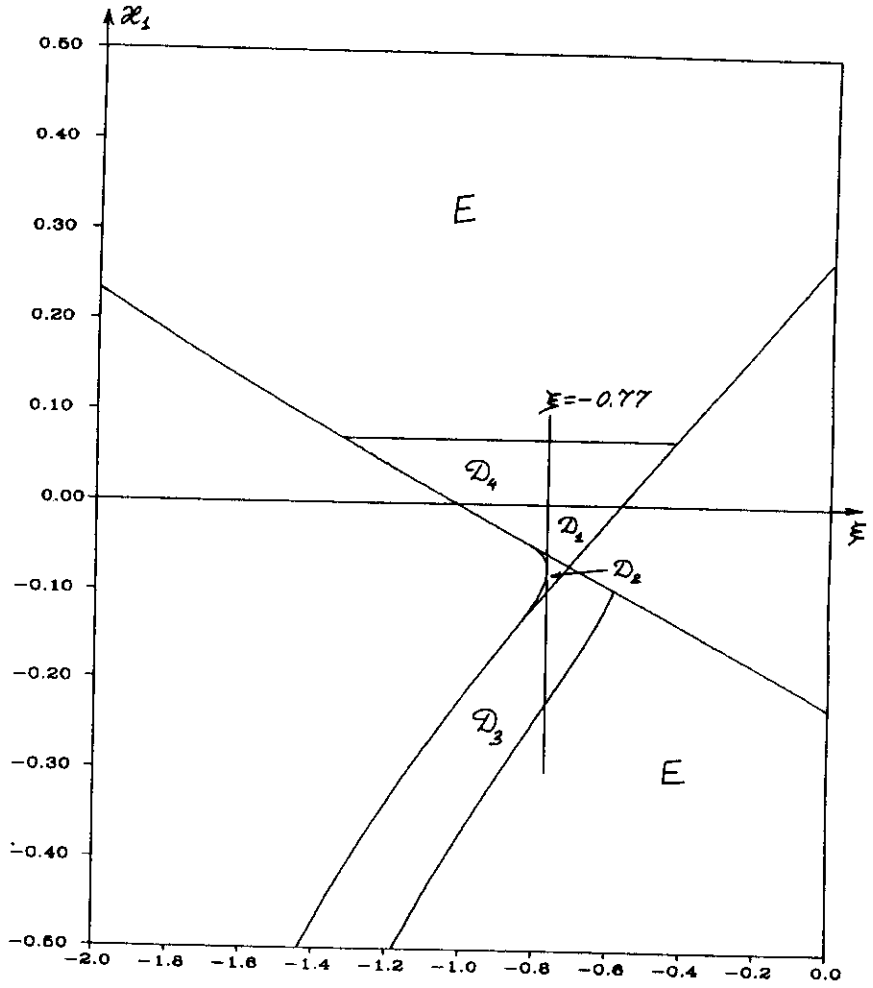

FIGURE 31. The regions D_1, D_2, D_3, D_4 and E on the plane ξ, κ_1 for $\eta = 0.75$.

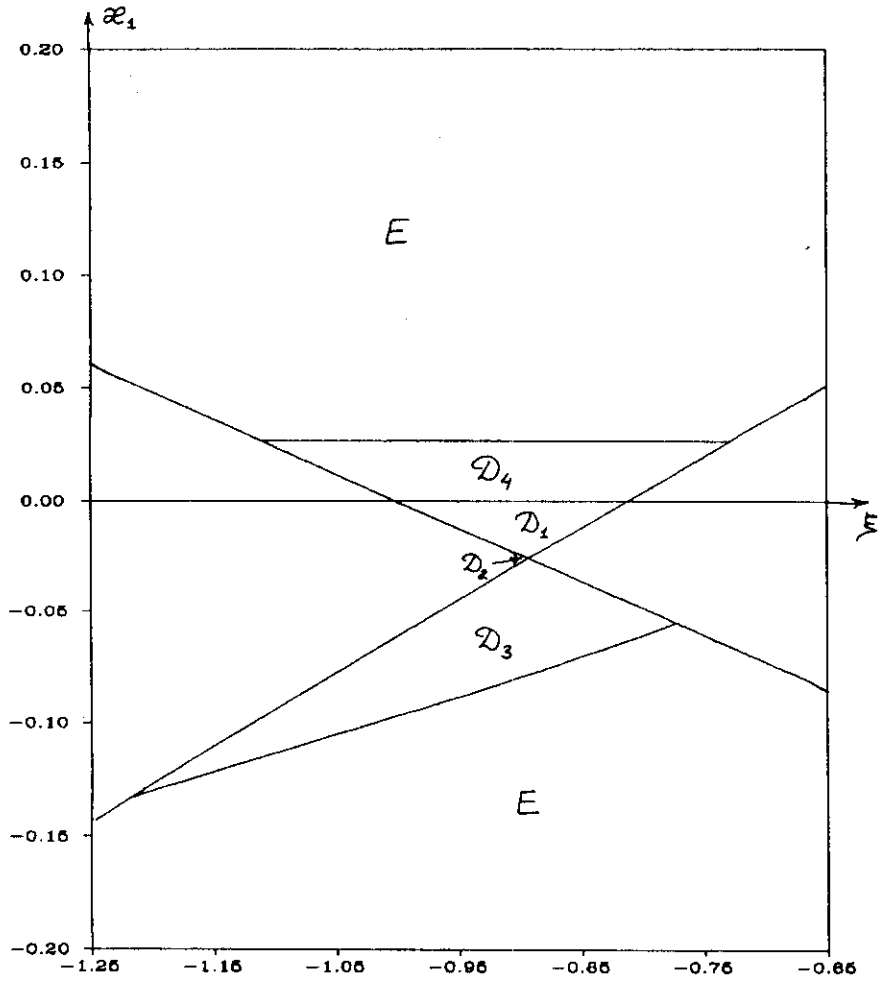

FIGURE 32. The regions D_1, D_2, D_3, D_4 and E on the plane ξ, κ_1 for $\eta = 0.9$.

$$\frac{d(\eta)}{2\ln\eta(1-\eta^2)} \le \kappa_1 \le \frac{3d(\eta)}{2\ln\eta(8\eta^2\ln\eta + 1 - \eta^2)} .$$

This case is realized for $\eta = 0.05$, 0.15, 0.25, 0.35, 0.5, and 0.75 (Figures 26-31). If $-\frac{1-\eta^2}{4\ln\eta} < \frac{2}{3}\eta^2$ then this interval consists of two unlimited parts:

$$\kappa_1 \le \frac{3d(\eta)}{2\ln\eta(8\eta^2\ln\eta + 1 - \eta^2)} , \quad \kappa_1 \ge \frac{d(\eta)}{2\ln\eta(1-\eta^2)} .$$

This case is realized for $\eta = 0.9$ (Figure 32). Note that while η increases the sizes of the regions D_1, D_2, D_3, and D_4 are reduced and the regions move to greater values of ξ for $\kappa_1 > 0$ or to smaller values of ξ for $\kappa_1 < 0$.

It follows from inequalities (66) and (67) that if root (65) belongs to the interval $[\eta, 1]$ then $\tau > \eta^2$ and $\sigma > \eta^4$. Then formula (111) leads to

$$\frac{\tau}{\sigma} r_0^2 - 1 < 0 \qquad (114)$$

and in accordance with formula (108) $\mathrm{sign} q_2 = \mathrm{sign}(nB) = \mathrm{sign}(\kappa n)$. As $C > 1$ only if $\frac{\tau}{\sigma} > 0$ so it follows from formula (112) for $\tau > 0$ that if $C > 1$ for root (68) then

$$\frac{\tau}{\sigma} r_0^2 - 1 > 0$$

and $\mathrm{sign} q_2 = -\mathrm{sign}(\kappa n)$. If $\tau < 0$ then formula (112) leads to inequality (114) and $\mathrm{sign} q_2 = \mathrm{sign}(\kappa n)$. Note that if expansion (74) is considered for the eigenvalue with the maximum real part then in the case when both roots (65) and (68) belong to the interval $[\eta, 1]$ and for each of them $C > 1$ the root for which the value of C is greater is chosen for calculating of p_0. It follows from formulas (109), (111), and (112) that this root is always defined by (65). For this root

$$\mathrm{sign} q_2 = \begin{cases} \mathrm{sign}(\kappa n), & \text{if } (\xi, \kappa_1) \in D_1 \cup D_2 \cup D_4 , \\ -\mathrm{sign}(\kappa n), & \text{if } (\xi, \kappa) \in D_3 . \end{cases} \qquad (115)$$

Formula (109) leads to

$$C = \begin{cases} \sqrt{\dfrac{|\tau|}{\sqrt{\tau^2-\sigma}}+1}\ , & \text{if } (\xi,\ \kappa_1) \in D_1 \cup D_2 \cup D_4\ , \\ \sqrt{\dfrac{\tau}{\sqrt{\tau^2-\sigma}}+1}\ , & \text{if } (\xi,\ \kappa_1) \in D_3\ . \end{cases} \tag{116}$$

Formulas (83) and (115) lead to

$$\zeta = \begin{cases} \mathrm{sign} n, & \text{if } (\xi,\ \kappa_1) \in D_1 \cup D_2 \cup D_4\ , \\ i\,\mathrm{sign} n, & \text{if } (\xi,\ \kappa\ ) \in D_3\ . \end{cases} \tag{117}$$

It follows from formulas (80), (83), (84), (115), and (117) that the choice $\psi = \mathrm{sign} n$ ensures the inequality $\mathrm{Re} p_0 > 0$ to be true. In accordance with formulas (80), (81), and (84) the maximum real part of p_0 is obtained for $m = 0$ in formula (84). For $\psi = \mathrm{sign} n$ and $m = 0$ formulas (80), (81), (84), (108), (111), (116), and (117) lead to

$$p_0 = \frac{1}{r_0^2}\sqrt{2\left|\frac{nB}{\sigma}\left(\sigma - \tau^2 + |\tau|\sqrt{\tau^2-\sigma}\right)\right|}\left[\sqrt{\frac{|\tau|}{\sqrt{\tau^2-\sigma}}+1} - 1\right](1 + i\,\mathrm{sign}(\kappa n))\ , \text{ if } (\xi,\ \kappa_1) \in D_1 \cup D_2 \cup D_4\ ,$$

$$p_0 = \frac{1}{r_0^2}\sqrt{2\left|\frac{nB}{\sigma}\left(\sigma - \tau^2 - \tau\sqrt{\tau^2-\sigma}\right)\right|}\left[\sqrt{\frac{\tau}{\sqrt{\tau^2-\sigma}}-1} - 1 + i\,\mathrm{sign}(\kappa n)\left(1+\sqrt{\frac{\tau}{\sqrt{\tau^2-\sigma}}-1}\right)\right],\ \text{if } (\xi,\ \kappa_1) \in D_3\ . \tag{118}$$

For $\psi = \mathrm{sign} n$ formulas (85), (91), (108), and (115) lead to the following formulas for the functions $R_0(r)$ and $\Phi_0(r)$:

If $(\xi,\ \kappa_1) \in D_1 \cup D_2 \cup D_4$ then

$$R_0(r) = K\exp\left[\frac{1}{r_0}\sqrt{\frac{|nB|\sqrt{\tau^2-\sigma}R_m}{2\left(|\tau|+\sqrt{\tau^2-\sigma}\right)}}(1+i\,\mathrm{sign}(\kappa n))(r-r_0)^2\right]\ , \tag{119}$$

$$\Phi_0(r) = K\sqrt{\frac{1}{2}\left|\frac{B}{n}\right|}(-\mathrm{sign}\kappa + i\,\mathrm{sign} n)\times$$

$$\times\exp\left[\frac{1}{r_0}\sqrt{\frac{|nB|\sqrt{\tau^2-\sigma}R_m}{2\left(|\tau|+\sqrt{\tau^2-\sigma}\right)}}(1+i\,\mathrm{sign}(\kappa n))(r-r_0)^2\right]\ . \tag{120}$$

If $(\xi,\ \kappa_1) \in D_3$ then

$$R_0(r) = K\exp\left[\frac{1}{r_0}\sqrt{\frac{|nB|\sqrt{\tau^2-\sigma}R_m}{2\left(\tau-\sqrt{\tau^2-\sigma}\right)}}(1-i\,\mathrm{sign}\kappa)(r-r_0)^2\right]\ , \tag{121}$$

$$\Phi_0(r) = K\sqrt{\frac{1}{2}\left|\frac{B}{n}\right|}(-\mathrm{sign}\kappa + i\,\mathrm{sign} n)\times$$

$$\times\exp\left[\frac{1}{r_0}\sqrt{\frac{|nB|\sqrt{\tau^2-\sigma}R_m}{2\left(\tau-\sqrt{\tau^2-\sigma}\right)}}(1-i\,\mathrm{sign}\kappa)(r-r_0)^2\right]\ . \tag{122}$$

The value of r_0 in formulas (118)-(122) is defined by formula (65) if $(\xi,\ \kappa_1) \in D_1 \cup D_2$ or by formula (68) if $(\xi,\ \kappa_1) \in D_3 \cup D_4$, K is an arbitrary complex constant.

Note that it follows from formula (116) that if the point (τ,σ) being inside the region O_2 approaches to its boundary $\sigma = \tau^2$ then $C \to \infty$. It means that in accordance with formulas (80), (81), and (84) it is possible that there is any amount of eigenvalues p_0 with $\mathrm{Re} p_0 > 0$ (for different values of m). However if $\sigma = \tau^2$ then in accordance with formulas (62), (77), and (108) $q_2 = 0$ and the given above procedure of solving of equation (78) is not applicable. If $q_2 = 0$, then only the solution $R_0(x) = 0$ of equation (78) satisfied to the formulated boundary conditions. The eigenvalue p_0 is obtained by solving of equation (94) for $R_1(x)$. Condition (98) for the function $R_1(x)$ is not considered in this case.

COMPARISON OF ASYMPTOTIC ANALYSIS WITH NUMERICAL RESULTS

The values of γ for $R_m \to \infty$ were calculated by the Galerkin method and were compared with those obtained by the asymptotic formulas. The calculations by the Galerkin method were made for $\Omega_2 = 0$, $n = 1$, and $\kappa_1 = 0$. The approximation γ^*_K was calculated for different values of K to estimate the closeness of $\gamma^*_{K_2}$ to the value of γ by the value of $\gamma^*_{K_1} - \gamma^*_{K_2}$ $(K_1 < K_2)$. The results obtained for the perfect conductor boundaries are given in Tables 9-11: for $\eta = 0.25$, $\alpha = -2$, $\kappa = 0.75$ (Table 9); for $\eta = 0.5$, $\alpha = -2$, $\kappa = 1$ (Table 10); for $\eta = 0.75$, $\alpha = -1.3$, $\kappa = 1$ (Table 11). Comparison of the values of γ^*_K given in the tables shows that in each line the value of γ^*_K calculated for the value of K which is maximum in this line approximates the value of γ well enough. Denote this value of γ^*_K by $\gamma_c(R_m)$. In accordance with relations (55) and (57) the attempt was made for each table to approximate the values of $\gamma_c(R_m)$ in the form

$$\gamma_c(R_m) \approx d_1 + d_2\sqrt{R_m} \,. \tag{123}$$

The coefficients d_1 and d_2 were obtained by the method of least squares, that is, to minimize the function

$$\sum_{i=1}^{15} \left(\gamma_c(R_m^{(i)}) - d_1 - d_2\sqrt{R_m^{(i)}} \right)^2 , \tag{124}$$

where $R_m^{(i)}$ is the value of R_m for the i-th line of the table. These values are: $d_1 = -7.4333$ and $d_2 = 0.6902$ (Table 9), $d_1 = -6.7802$ and $d_2 = 0.8713$ (Table 10), $d_1 = -7.5880$ and $d_2 = 1.2081$ (Table 11). The values of the approximation of $\gamma_c(R_m)$, calculated by formula (123) are given in the last columns of the tables. In Table 9 the

TABLE 9

R_m	γ^*_{13}	γ^*_{19}	γ^*_{29}	γ^*_{49}	γ^*_{69}	γ^*_{99}	$d_1 + d_2\sqrt{R_m}$
100	-0.9	-0.8					-0.5
200	2.5	2.5					2.3
400	6.5	6.5					6.4
800	12.1	12.1					12.1
1600	19.7	20.1					20.2
3200	32.5	31.6					31.6
6400	69.1	46.7	47.8				47.8
12800		69.6	70.7				70.7
25600		143.6	102.7	103.0			103.0
51200			139.2	148.7			148.8
102400			259.0	213.5	213.4		213.4
204800				303.9	304.9		304.9
409600				403.1	434.5		434.3
819200				768.3	613.6	617.1	617.3
1638400					813.5	876.1	876.0

TABLE 10

R_m	γ^*_{13}	γ^*_{19}	γ^*_{29}	γ^*_{49}	γ^*_{69}	γ^*_{99}	$d_1 + d_2\sqrt{R_m}$
100	-1.7						1.9
200	3.4						5.5
400	10.5						10.6
800	19.0						17.9
1600	29.4						28.1
3200	43.4	43.3					42.5
6400	60.8	63.5					62.9
12800	101.2	92.6	92.4				91.8
25600		127.3	133.2				132.6
51200			191.2	190.9			190.4
102400			267.4	272.5			272.0
204800				387.8	387.8		387.5
409600				552.2	551.0		550.9
819200				762.8	781.7		787.8
1638400					1111.2	1108.0	1108.5

approximation is well for all values of R_m. In Table 10 it is slightly worse for the small values of R_m ($R_m < 6000$) and it is bad for small values of R_m in Table 11. Through the last fact the values of the coefficients d_1 and d_2 were recalculated for Table 11 with considering only 11 items of sum (124) for $R_m > 1000$. The new

TABLE 11

R_m	γ^*_{13}	γ^*_{19}	γ^*_{29}	γ^*_{49}	γ^*_{69}	γ^*_{99}	$d_1 + d_2\sqrt{R_m}$	
100	-2.0						4.5	(9.6)
200	0.5						9.5	(14.5)
400	7.8						16.6	(21.6)
800	22.4						26.6	(31.5)
1600	43.6						40.7	(45.6)
3200	67.8	67.9					60.8	(65.5)
6400	95.1	95.0					89.1	(93.7)
12800	133.0	133.1					129.1	(133.5)
25600	189.7	189.3					185.7	(189.8)
51200	257.0	269.1					265.8	(269.4)
102400		382.8	381.8				379.0	(382.1)
204800		518.2	541.1	541.1			539.2	(541.3)
409600			767.5	766.4			765.6	(766.6)
819200			1069.6	1085.1	1085.1		1085.9	(1085.1)
1638400				1535.8	1535.8	1535.8	1538.8	(1535.6)

values of the coefficients are: $d_1 = -2.4445$, $d_2 = 1.2016$. The new values of approximation (123) are given in the last column of Table 11 in brackets. The accuracy of this approximation for $R_m > 10^4$ is not worse than in Table 9.

As a whole for Tables 9-11 the relative difference between $\gamma_c(R_m)$ and its approximation (123) is of the order 10^{-3} if $R_m > 10^4$. These approximations agree well with relation (57) derived above by asymptotic methods.

The imaginary parts δ^*_K of the eigenvalues which correspond to the real parts given in Tables 9-11 are given in Tables 12-14 respectively. Denote by $\delta_c(R_m)$ the last value of δ^*_K in a line of a table. In accordance with relation (57) the values of $\delta_c(R_m)$ are approximated in the form

$$\delta_c(R_m) \approx g_1\sqrt{R_m} + g_2 R_m \ . \qquad (125)$$

Here the coefficients g_1 and g_2 are obtained by the method of least squares, that is, to minimize the function

TABLE 12

R_m	δ^*_{13}	δ^*_{19}	δ^*_{29}	δ^*_{49}	δ^*_{69}	δ^*_{99}	$g_1\sqrt{R_m} + g_2 R_m$
100	51	51					50
200	96	96					96
400	186	186					186
800	364	364					364
1600	717	717					717
3200	1423	1418	1418				1418
6400		2813	2813				2813
12800		5604	5594	5594			5594
25600			11141	11142			11142
51200			22229	22220			22220
102400			44401	44348	44348		44348
204800				88563	88567		88567
409600				176985	176952		176952
819200				353801	353635	353645	353645
1638400					707007	706924	706924

TABLE 13

R_m	δ^*_{13}	δ^*_{19}	δ^*_{29}	δ^*_{49}	δ^*_{69}	δ^*_{99}	$g_1\sqrt{R_m} + g_2 R_m$
100	58						56
200	110						108
400	211						208
800	408						407
1600	799						799
3200	1577	1577					1578
6400	3128	3126					3126
12800	6230	6211	6212				6212
25600		12366	12365				12365
51200		24688	24649	24649			24649
102400			49179	49183			49183
204800			98257	98202	98202		98203
409600				196174	196174		196174
819200				392008	392022		392022
1638400					783582	783582	783582

$$\sum_{i=1}^{15} \left(\delta_c(R_m^{(i)}) - g_1\sqrt{R_m^{(i)}} - g_2 R_m^{(i)}\right)^2$$

where $R_m^{(i)}$ is the value of R_m for the i-th line of the table. The obtained values of the coefficients g_1 and g_2 are: $g_1 = 0.68995$ and $g_2 = 0.4309334$ (Table 12), $g_1 = 0.87081$ and $g_2 = 0.4775802$ (Table

TABLE 14

R_m	δ^*_{13}	δ^*_{19}	δ^*_{29}	δ^*_{49}	δ^*_{69}	δ^*_{99}	$g_1\sqrt{R_m} + g_2 R_m$
100	31						34
200	61						62
400	117						113
800	221						212
1600	413						404
3200	784	784					781
6400	1521	1521					1521
12800	2986	2986					2986
25600	5892	5893					5893
51200	11676	11672					11673
102400	23259	23184	23185				23186
204800		46145	46145				46145
409600		92123	91972	91972			91973
819200			183475	183493	183493		183494
1638400				366349	366349	366349	366349

13), $g_1 = 1.2044$ and $g_2 = 0.2226605$ (Table 14). The values of the approximation of $\delta_c(R_m)$ calculated by formula (125) are given in the last columns of the tables. Note that the obtained values of d_2 are close to the corresponding values of g_1. This fact is in accordance with relations (57), (74), and (89).

The calculations carried out for the dielectric boundaries conform that for $R_m \to \infty$ the values of γ are close to those obtained for the same values of parameters in the case of perfect conductor. For example if $\eta = 0.25$, $n = 1$, $\alpha = -2$, $\kappa = 0.75$, $\kappa_1 = 0$, and $\Omega_2 = 0$ (the same values as for Tables 9 and 12) then for the dielectric boundaries the following values of the coefficients in formulas (123) and (125) were obtained: $d_1 = -7.5958$, $d_2 = 0.6903$, $g_1 = 0.68926$, $g_2 = 0.4309340$. The values of d_2 and g_2 are practically coincide with those given above for the perfect conductor boundaries. Note that if $\Omega_2 \neq 0$ then in accordance with formulas (15) the value of g_1 is not changed and the value of g_2 is

replaced by $g_2 - \dfrac{nb\Omega_2}{(1-\eta)U_m}$.

According to (55), (74), and $p_1 = 0$ the coefficients in formulas (123) and (125) have to satisfy to the following relations

$$d_2 \approx \mathrm{Re}p_0, \quad d_1 \approx \mathrm{Re}p_2, \quad g_1 \approx \mathrm{Im}p_0, \quad g_2 \approx -q(r_0).$$

Table 15 lists the values of r_0, $-q(r_0)$, $\mathrm{Re}p_0$, $\mathrm{Im}p_0$, and $\mathrm{Re}p_2 = p_2$ calculated by formulas (15), (60), (89), and (107) for the same values of the parameters that were used for Tables 9-14. The values of d_1, d_2, g_1, and g_2 are also given in Table 15 for comparison. All these computations were made for $\Omega_2 = 0$, $n = 1$, and $\kappa_1 = 0$. Note that the values of $-q(r_0)$, $\mathrm{Re}p_0$, $\mathrm{Im}p_0$, and p_2 are close to the values of g_2, d_2, g_1, and d_1, respectively. According to (107), p_2 is real which agrees with (125) where the term of zero degree in R_m is not present.

Figure 33 illustrates the variation of the real and imaginary parts of the eigenfunction $R(r)$ of system (24) with boundary conditions (25). This eigenfunction is derived by the Galerkin

TABLE 15

	$\eta = 0.25$, $\alpha = -2$, $\kappa = 0.75$	$\eta = 0.5$, $\alpha = -2$, $\kappa = 1$	$\eta = 0.75$, $\alpha = -1.3$, $\kappa = 1$
r_0	0.52655	0.67978	0.87105
$-q(r_0)$	0.4309	0.4776	0.2227
g_2	0.4309	0.4776	0.2227
$\mathrm{Re}p_0$	0.6900	0.8704	1.2021
d_2	0.6902	0.8713	1.2016
$\mathrm{Im}p_0$	0.6900	0.8704	1.2021
g_1	0.6900	0.8708	1.2044
p_2	-7.3975	-6.0385	-2.9316
d_1	-7.4333	-6.7802	-2.4445

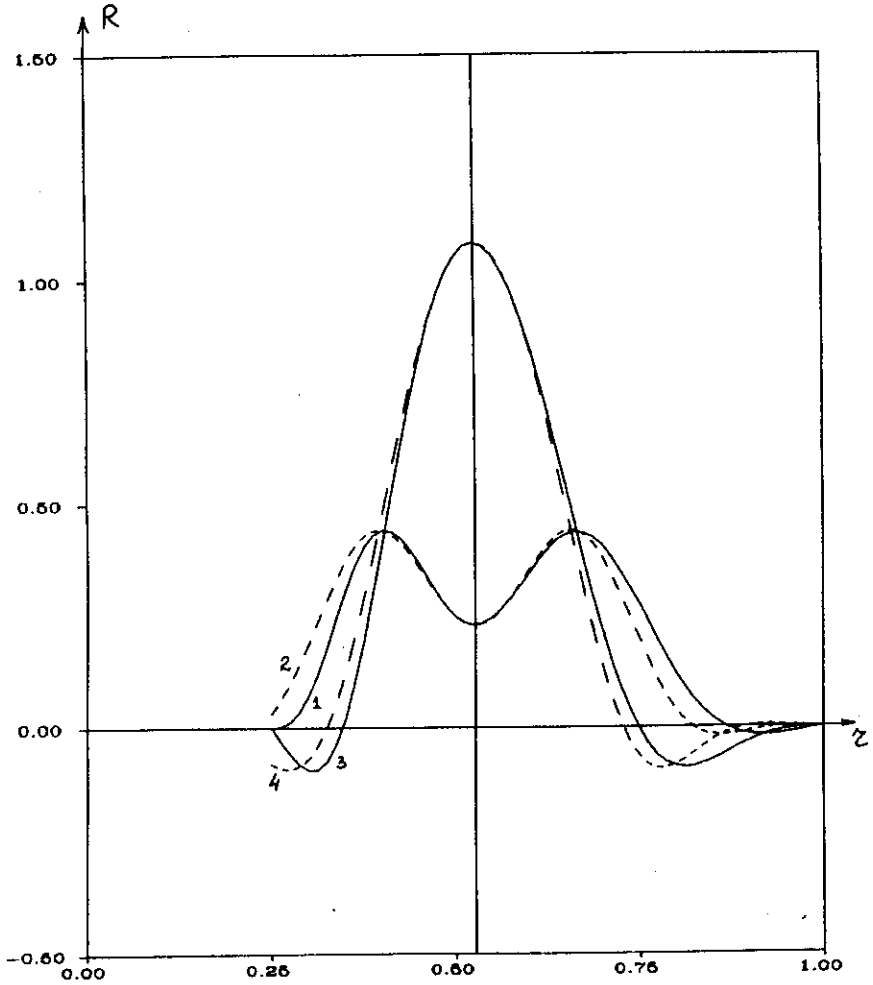

FIGURE 33. Variations of the function $R(r)$ (solid lines) and $R_0(r)$ (broken lines): 1, 3 - real parts, 2, 4 - imaginary parts.

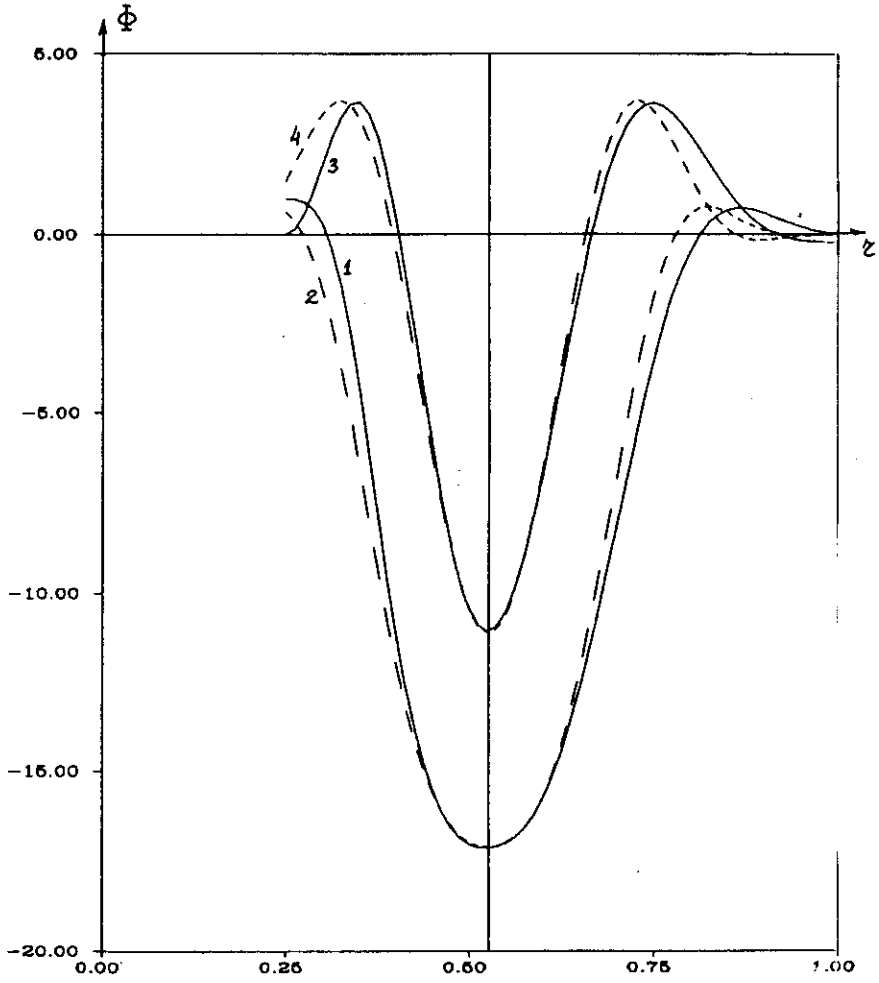

FIGURE 34. Variations of the function $\Phi(r)$ (solid lines) and $\sqrt{R_m}\Phi_0(r)$ (broken lines): 1, 3 - real parts; 2, 4 - imaginary parts.

method with $K = 29$ for the following values of the parameters: $R_m = 1600$, $\eta = 0.25$, $n = 1$, $\alpha = -2$, $\kappa = 0.75$, $\Omega_2 = 0$, and $\kappa_1 = U_p = 0$ (the same values of η, n, α, κ, Ω_2, and κ_1 that were used for Tables 9 and 12). Figure 34 illustrates the real and imaginary parts of $\Phi(r)$. The position of the point r_0 is marked in the figures. The tendency of the eigenfunctions to concentrate around the point r_0 is apparent. The figures also show, for comparison, the real and imaginary parts of $R_0(r)$ and $\sqrt{R_m}\Phi_0(r)$ calculated from (89) and (92). The value of K is chosen as

$$K = R(r_0) \ . \tag{126}$$

The vector function $(R(r), \Phi(r))$ in the figures is well approximated by $(R_0(r), \sqrt{R_m}\Phi_0(r))$ near r_0. The approximation is not valid in the vicinity of the boundaries, because these two vector functions do not satisfy the same boundary conditions. The calculations show that for the larger values of R_m, for example $R_m = 10^5$, the graphs of the real and imaginary parts of the functions $R(r)$ and $\Phi(r)$ practically coincide with those of the functions $R_0(r)$ and $\sqrt{R_m}\Phi_0(r)$.

The regions of the magnetic dynamo existence on the plane R_m, κ_1 are presented above for the following values of the parameters: $\eta = 0.25$, $\xi = -0.5$ (Figure 17); $\eta = 0.5$, $\xi = -0.6$ (Figure 18); $\eta = 0.75$, $\xi = -0.77$ (Figure 19); $\eta = 0.5$, $\xi = 0.6$ (Figure 20). For these values of η the regions D_1, D_2, D_3, and D_4 on the plane ξ, κ_1 are shown in Figures 28, 30, and 31. According to the asymptotic analysis the magnetic dynamo exists in these regions for $R_m \to \infty$. The sections of the conjunctions of the regions D_1, D_2, D_3, and D_4 by the lines $\xi = -0.5$ (Figure 28), $\xi = -0.6$ and $\xi = 0.6$ (Figure 30), and $\xi = -0.77$ (Figure 31) show the intervals of the values of κ_1 for which the magnetic dynamo exists for $R_m \to \infty$. These

intervals agree well with Figures 17-20. For $\eta = 0.5$ and $\xi = -0.6$ the interval $-0.2785 < \kappa_1 < -0.1185$ (Figure 30) is outside the conjunction of the regions D_1, D_2, D_3, and D_4 and the calculations by the Galerkin method show that the magnetic dynamo does not exist for $R_m \to \infty$ (for example, if $\kappa_1 = -0.2$ and $R_m = 505000$ then $\gamma^*_{69} = -2759.81$). However the part of the right branch of the neutral curve limited the region of the magnetic dynamo existence for these values of κ_1 is absent in Figure 18 because the magnetic dynamo vanishes for the values of R_m which considerably exceed 5000.

According to the definition of the region D_2 there are two roots of equation (64) with $\mathrm{Re}\, p_0 > 0$ for the points (ξ, κ_1) of this region. For example, if $\eta = 0.25$ (Figure 30), $n = 1$, $\kappa = 1$, $\alpha = 3$ $(\xi = 1/3)$, $U_c = 0$, $U_p > 0$ $(\kappa_1 = \infty)$ then root (65) is $r_0 = 0.3473932$ and root (68) is $r_0 = 0.46631493$. For $\Omega_2 = 0$ formulas (15) and (118) lead to

$$p_0 = 3.10416631(1 + i), \ -q(r_0) = -3.40602064$$

and

$$p_0 = 1.19619821 + 5.32582878i, \ -q(r_0) = -3.45928306$$

for roots (65) and (68) respectively. If $R_m = 250000$ then

$$-q(r_0)R_m + p_0\sqrt{R_m} = 1552.0832 - 849953.08i$$

and

$$-q(r_0)R_m + p_0\sqrt{R_m} = 598.09911 - 862157.85i$$

for roots (65) and (68) respectively. For the same values of the parameters the following two eigenvalues with maximum real parts were obtained by the Galerkin method with $K = 69$:

$$1536.9920 - 849954.63i \text{ and } 581.85305 - 862132.07i.$$

These eigenvalues are close to those calculated by the asymptotic formulas. The form of equation (73) leads to the assumption that the

value of p_2 has to be close to $-\alpha^2 - \frac{n^2}{r_0^2}$. Note that in accordance with formula (107) it is true for a helical Couette flow because $\left|\frac{53}{36} - \sqrt{2}\right| < 0.1$. If this rough value of p_2 is considered in the asymptotic formulas then

$$-q(r_0)R_m + p_0\sqrt{R_m} - \alpha^2 - \frac{n^2}{r_0^2} = 1534.7969 - 849953.08i$$

and

$$-q(r_0)R_m + p_0\sqrt{R_m} - \alpha^2 - \frac{n^2}{r_0^2} = 584.50034 - 862157.85i$$

for roots (65) and (68) respectively. These values are more close to the eigenvalues obtained by the Galerkin method than those given above without regard for the rough value of p_2.

If the point (ξ, κ_1) is in the region E then root (68) belongs to the interval $[\eta, 1]$ but $\mathrm{Re}p_0 < 0$ even if $m = 0$ in formula (84). However in this case the eigenvalue obtained by asymptotic formulas with $m = 0$ in (84) is close to that calculated by the Galerkin method. For example, if $\eta = 0.5$ (Figure 30), $n = 1$, $\kappa = 0.75$, $\alpha = -1.25$ ($\xi = -0.6$), $\kappa_1 = -8$, $\Omega_2 = 0$, and $R_m = 100000$ then the asymptotic formulas lead to

$$r_0 = 0.65962283,$$
$$-q(r_0)R_m + p_0\sqrt{R_m} - \alpha^2 - \frac{n^2}{r_0^2} = -154.36600 - 266705.06i\ .$$

The eigenvalue with the maximum real part calculated by the Galerkin method with $K = 69$ for the same values of the parameters is:

$$-156.92513 - 266701.64i\ .$$

CONCLUSION

The results of the calculations and the asymptotic analysis have proved that the Couette-Poiseuille flow of an electrically conducting fluid between two cylinders can lead to excitation of a magnetic field. Moreover the results derived by the numerical and asymptotic methods are in good agreement. This demonstrates the validity of the application of the methods developed by Ruzmaikin et al. (1987) to the Couette-Poiseuille low and the reliability of the numerical results.

The minimum threshold value of R_m for magnetic field generation is ~ 48. This value is reached in the following case: the ratio of the radii of the cylinders is ~ 0.32, the pressure gradient has an opposite direction to the velocity of the axial motion of the inner cylinder, the value of U_p is half that of U_c, and the product of the inner cylinder radius by the difference between the angular velocities of the cylinders is $\sim \pm 0.61 U_c$.

If $\gamma > 0$ then the corresponding solution of the magnetic induction equation (3) grows in time as $\exp(\gamma t)$ where t is the time measured in the units of b^2/λ. It means that the diffusive time scale is used (Soward, 1990). If t_c is the time measured in the units of b/U_m (the convective time scale) then the magnetic field grows in time as $\exp((1-\eta)\gamma t_c/R_m)$. Accordingly to (12), (57), and (74) if $R_m \to \infty$ then

$$\frac{(1-\eta)\gamma}{R_m} = (1-\eta)(\mathrm{Re}p_0 R_m^{-1/2} + O(R_m^{-1})) \to 0$$

and at the same time $\gamma \to \infty$. Therefore a fast dynamo is not possible for the Couette-Poiseuille flow of an electrically conducting fluid

but there is an intermediate dynamo (Soward, 1990).

In accordance with the definition of R_m (12) in the case when the sizes of the flow are not changed $R_m \to \infty$ either if $U_m \to \infty$ or if $\lambda \to 0$. In the case when $\lambda \to 0$ the electrical characteristics of the fluid approximate to those of the perfect conductor. If τ is the time measured in the standard units then the magnetic field grows in time as $\exp(\lambda\gamma\tau/b^2)$. If $\lambda \to 0$ then relations (57) and (74) lead to

$$\frac{\lambda\gamma}{b^2} = \frac{\mathrm{Re}p_0\sqrt{1-\eta}\sqrt{U_m}}{b^{3/2}}\sqrt{\lambda} + O(\lambda) .$$

It means that for $\lambda \to 0$ the factor by the time in the exponent which defines the growth of the magnetic field decreases as $\sqrt{\lambda}$. The time dependence of the solution of the magnetic induction equation (3) has the oscillatory nature which is defined by the factor $\exp(i\lambda\delta\tau/b^2)$ where δ is the imaginary part of the eigenvalue with the real part γ. For $\lambda \to 0$ formulas (57) and (74) lead to

$$\frac{\lambda\delta}{b^2} = -q(r_0)\frac{U_m(1-\eta)}{b} + \frac{\mathrm{Im}p_0\sqrt{1-\eta}\sqrt{U_m}}{b^{3/2}}\sqrt{\lambda} + O(\lambda) .$$

Thus the limit of the oscillation period is $\left|\frac{2\pi b}{q(r_0)U_m(1-\eta)}\right|$.

REFERENCES

Arnold,V.I. (1984). On the evolution of a magnetic field due to diffusion and transfer (in Russian), in *Some Questions of Modern Analysis*, MGU, Moscow, 8-21.

Arnold,V.I. and E.I.Korkina (1983). Growth of a magnetic field in a three-dimensional transient flow of an incompressible fluid (in Russian), *Vestnik MGU, ser 1, Matematica, mekhanika*, 3, 43-46.

Backus,G.E. (1958). A class of self-sustaining dissipative spherical dynamos, *Ann. Phys.*, 4, 372-447.

Bathaiah,D. and R.Venugopal (1982). Effect of porous lining on the MHD flow between two concentric rotating cylinders under the influence of a uniform magnetic field, *Acta mech.*, **44**, 3-4, 141-158.

Benton,E.R. (1983). Geomagnetism of Earth's core, *Rev. Geophys. and Space Phys.*, **21**, 3, 627-633.

Braginsky,S.I. (1964). Self-excitation of a magnetic field during the motion of a highly conducting fluid (in Russian), *Zh. Eksp. and Teor. Fiz.* (USSR), **47**, 3, 1084-1098 [English transl.: *Sov. Phys. JETP*, **20**, 726-735 (1965)].

Bullard,E.C. and H.Gellman (1954). Homogeneous dynamos and terrestrial magnetism, *Phil. Trans. Roy. Soc.*, A247, 213-278.

Busse,F.H. (1981). Dynamics of the Earth's core and the geodynamo, in *Evolv. Earth.*, Washington D.C.-Boulder Colo., 53-58.

Busse,F.H. (1982). Nonlinear dynamo oscillations, *Geophys. and Astrophys. Fluid Dyn.*, **21**, 1-2, 129-141.

Busse,F.H. (1983). Recent developments in the dynamo theory of planetary magnetism, in *Rev. Earth and Planet. Sci.*, **11**, Paolo Alto Calif., 241-268.

Childress,S. (1983). The macrodynamics of spherical dynamos, in *Stellar and Planetary Magnetism*, New York e.a., 245-257.

Childress,S. (1985). An introduction to dynamo theory, in *Proc. Int. Sch. Phys. Enrico Fermi. Course* 88: *Turbul. and Predict. Geophys. Fluid Dyn. and Clim. Dyn. Lect. Semin. Varenna on Lake Como* 14-24 *June*, 1983, *Bologna*, Amsterdam e.a., 200-225.

Chowdhury,S.K.R. (1983). A note on the steady hydromagnetic flow

between two porous concentric cylinders, *Indian J. Theor. Phys.*, **31**, 3, 137-143.

Cowling,T.G. (1934). The magnetic field of sunspots, *Mon. Not. Roy. Astr. Soc.*, 94, 39-48.

Cowling,T.G. (1981). The present status of dynamo theory, in *Annu. Rev. Astronomy and Astrophys*, **19**, Palo Alto Calif., 115-135.

Galloway,D. and V.Frisch (1984). A numerical investigation of magnetic field generation in a flow chaotic streamlines, *Geophys. Astrophys. Fluid Dynamics*, 29, 13-18.

Gubbins,D. (1984). The Earth's magnetic field, *Contemp. Phys.*, **23**, 3, 269-290.

Herzenberg,A. (1958). Geomagnetic dynamos, *Phyl. Trans. Roy. Soc.*, A250, 543-585.

Joseph,D.D. (1976). *Stability of Fluid Motions*, Springer, Berlin.

Korn,G.A. and T.M.Korn (1961). *Mathematical Handbook for Scientists and Engineers. Definitions, Theorems and Formulas for Reference and Review*, McGraw-Hill Book Company, INC., New York Toronto London.

Krause,F. and K.-H.Rädler (1980). *Mean-Field Magnetohydrodynamics and Dynamo Theory*, Academic-Verlag, Berlin.

Larmor,J. (1919). How could a rotating body such as the Sun become a magnet? *Rep. Brit. Assoc. Adv. Sci.*, 159-160.

Moffatt,H.K. (1978). *Magnetic Field Generation in Electrically Conducting Fluids*, Cambridge University Press.

Moffatt,H.K. (1983). Induction in turbulent conductors, in *Stellar and Planetary Magnetism*, New York e.a., 3-16.

Parker,E.N. (1955). Hydromagnetic dynamo models, *Astrophys. J.*, **122**, 293-314.

Parker,E.N. (1957). The solar hydromagnetic dynamo, *Proc. Nat. Acad. Sci. US*, **43**, 8-13.

Parker,E.N. (1979). *Cosmical Magnetic Fields*, Clarendon Press.

Ponomarenko,Y.B. (1973). On the theory of hydromagnetic dynamos (in Russian), *Zh. Prikl. Mekh. and Tekh. Fiz.* (USSR), 6, 47-51.

Rikitake,T. (1958). Oscillations of a system of disk dynamos, *Proc. Camb. Phil. Soc.*, **54**, 89-105.

Roberts,P.H. (1972). Kinematic dynamo models, *Phil. Trans. Roy. Soc. Lond.*, A272, 663-698.

Rutishauser,H. (1958). Solution of Eigenvalue Problems with LR-transformation, *Nat. Bur. Standards Appl. Math.*, Ser. 49, 47-81.

Ruzmaikin,A., D.Sokoloff, and A.Shukurov (1987). Hydromagnetic screw dynamo, *J. Fluid Mech.*, **197**, 39-56.

Sai,K.S. (1985). MHD flow between two rotating cylinders with porous lining, *Rev. Roum. Phys.*, **30**, 2, 119-125.

Soward,A.M. (1990). A unified approach to a class of slow dynamos, *Geophys. Astrophys. Fluid Dynamics*, **53**, 81-107.

Tabeling,P. (1982). Sequence of instabilities in electromagnetically driven flows between conducting cylinders, *Phys. Rev. Lett.*, **49**, 7, 460-463.

Zeldovich,Ya.B. (1956). A magnetic field during the two-dimensional motion of an electrically conducting turbulent fluid (in Russian), *Zh. Eksp. and Teor. Fiz.* (USSR), **31**, 1, 154-156.